FLUID QUANTITY GAGING
Final Report

5 December 1988

Allan J. Mord
Howard A. Snyder
Kathleen A. Kilpatrick
Lynn A. Hermanson
Richard A. Hopkins
Donald A. Van Gundy

Approved by:

Allan J. Mord
Program Manager

F8806102AG0-1

TABLE OF CONTENTS

PRECEDING PAGE BLANK NOT FILMED

TABLE OF CONTENTS (Continued)

TABLE OF CONTENTS (Continued)

ABSTRACT

A system for measuring the mass of liquid in a tank on orbit with 1 percent accuracy has been developed and demonstrated. An extensive tradeoff identified adiabatic compression as the only gaging technique that is independent of gravity or its orientation, and of the size and distribution of bubbles in the tank. This technique is applicable to all Earth-storable and cryogenic liquids of interest for Space Station use, except superfluid helium, and can be applied to tanks of any size, shape, or internal structure. Accuracy of 0.2 percent has been demonstrated in the laboratory, and a detailed analytical model has been developed and verified by testing. A flight system architecture is presented that allows meeting the needs of a broad range of space fluid systems without custom development for each user.

EXECUTIVE SUMMARY

EXECUTIVE SUMMARY

The Fluid Quantity Gaging program has selected, developed, and demonstrated the technology needed to measure the mass of liquids in tanks in space. The adiabatic compression gaging system has met its goal of one percent accuracy without relying on positioning the liquid repeatably in flight. A flight system architecture has also been developed that meets the needs of many different fluid systems with a limited number of standardized system components. This gaging system has minimal impact on the fluid systems and will require little or no custom development for each application.

The compression gaging technique is applicable to all Earth-storable and cryogenic two-phase liquid/gas systems of interest for Space Station, except superfluid helium. It can be applied to tanks of any size, shape, or internal structure, and can operate with or without a bladder separating the liquid from the pressurizing gas.

This development program was sponsored by NASA-Johnson Space Center, under the direction of Mr. Kenneth Kroll as the Technical Monitor. The tradeoff phase began in April 1986, and the demonstration and report phase was completed in December 1988.

Extensive analysis and study of the literature led to the realization that the requirement that the gaging accuracy must not depend on the location of the liquid in the tank ruled out many well-known gaging techniques. Imposing this ambitious requirement, however, was prudent because of NASA's need for a gaging system that will serve the long-term requirements of many different missions and tank configurations. We found that the only technique that could achieve ±1 percent accuracy without depending on the location of the liquid is adiabatic compression, and that it would work with all liquids except superfluid helium.

The compression gaging system determines the fluid mass by measuring the volume of the ullage bubble(s). Figure 1 shows the elements of the basic system. When a reading is to be made, a piston varies the tank volume cyclically by ΔV, which is less than 10^{-4} of the total tank volume. Because
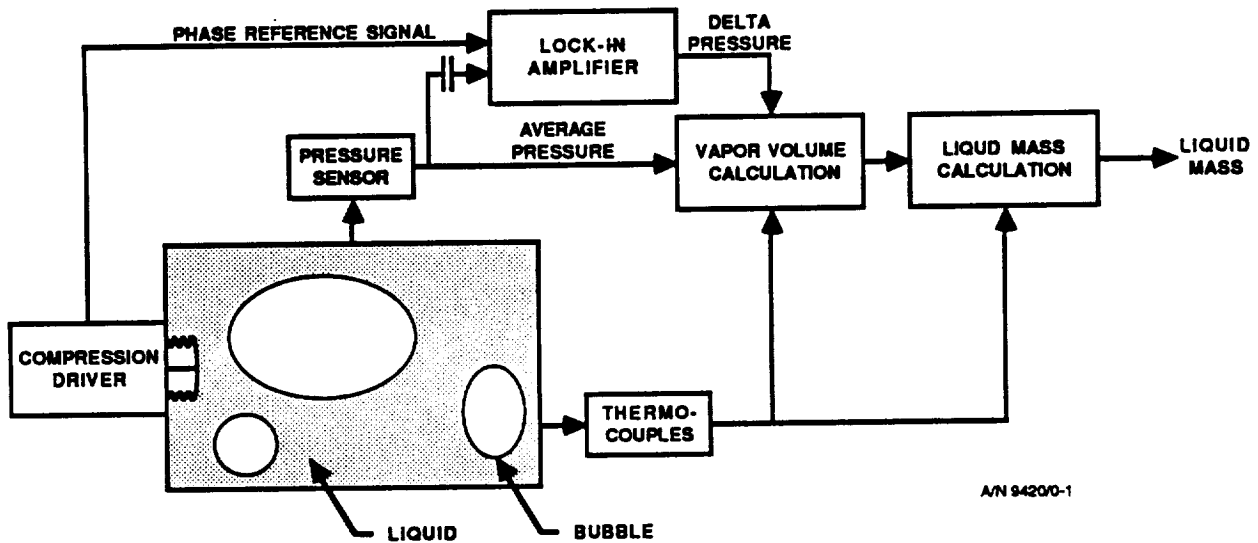
Figure 1. Compression gaging concept

the ullage bubble is much more compressible than the liquid, the gas is compressed. With the piston operating at about 1 Hz, there is little time for heat transfer between the gas and its surroundings. The compression is therefore nearly adiabatic, so the volume of the bubble can be computed from the pressure p and the pressure change Δp according to

$$V_{bubble} = -\gamma \, \Delta V \, (p/\Delta p), \tag{1}$$

where $\gamma = c_p/c_v$ is the ratio of the specific heats of the gas at constant pressure and at constant volume, respectively. The bubble volume is subtracted from the known tank volume, and the liquid density is used to compute the fluid mass. Temperatures are monitored to correct for variations in density and γ.

The adiabatic compression gaging technique developed on this contract differs in one key respect from other pressure-volume-temperature (PVT) gaging techniques that have been discussed in the past. The volume of the tank is modulated at a frequency that is:

- High enough to limit heat transfer between the gas and its surroundings, so that the compression is nearly adiabatic and evaporation and condensation are negligible

- Low enough so that errors introduced by fluid dynamic effects such as the inertia of liquid in contact with the pressure sensor or sloshing of liquid between bubbles are within the system error budget

Figure 2 shows that the flight system consists of two modules: a gage head mounted on the tank, plus a gage electronics module mounted remotely. The gage head will be built in different versions to suit broad groups of applications, while a single electronics module design is common to all of them. The compression driver and the pressure sensor are mounted together in a single pressure shell. The temperature sensors are included in the gage head so that the only interface with the tank is at a single mounting flange. The piston of the driver is sealed by a welded steel bellows. The bellows are readily available in cryogen-compatible steels, and preliminary testing indicates that a fatigue life adequate for 15 years of daily operation is obtainable.
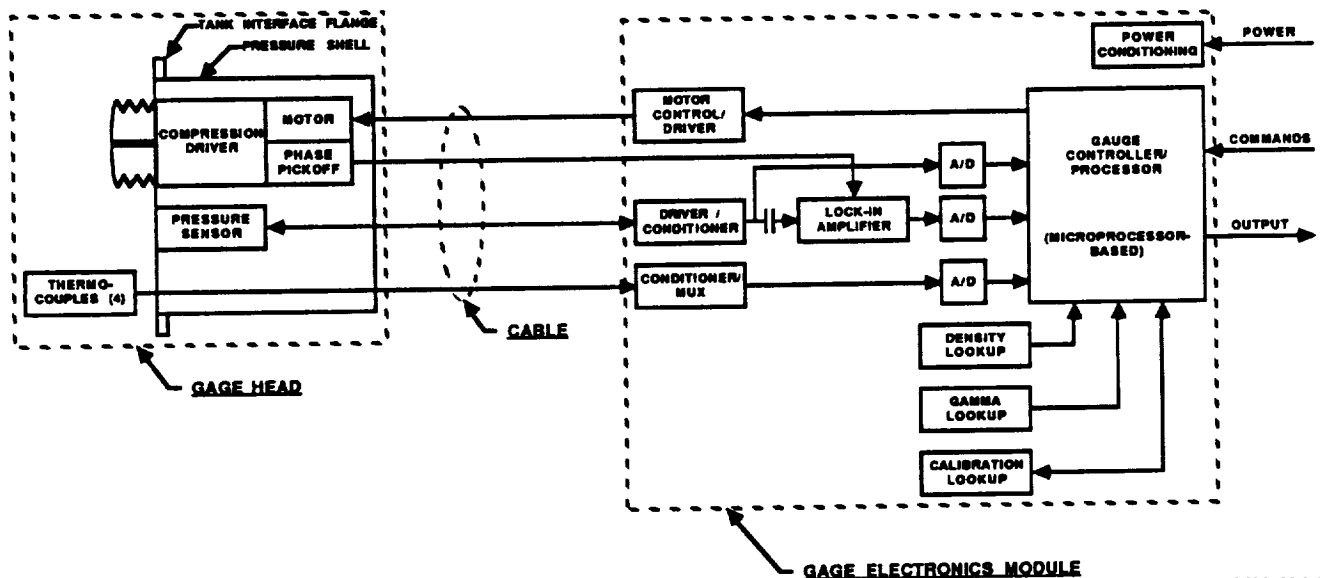
Figure 2. Flight system concept

The electronics module performs all of the functions necessary to operate the gage, process the data, and return a mass reading to the host vehicle. Liquid density data is stored permanently in read-only memory, and tank calibration data is stored in non-volatile memory where it can be updated if necessary.

A breadboard apparatus was constructed consisting of a 232-liter tank with a compression driver ΔV of 8×10^{-5} times the tank volume, plus two types of pressure sensor. This system was operated with water pressurized with air and with helium. A RMS error of 0.19 percent of capacity was demonstrated for 5 fill levels from 0 to 90 percent full.

In practical application, several physical processes can make the response of the gaging system more complex than the ideal behavior described by equation (1). We therefore developed a detailed analytical model of the system based on well-established physical principles, and verified its correctness and completeness through a carefully thought out test program. The close agreement ultimately obtained between the data and the model shows that the physical processes operating are now well understood.

Tests were directed toward several important practical issues or potential sources of gaging error. The most significant findings are as follows:

- Heat transfer between the gas and its surroundings will alter the compressibility of the gas. The mass gaging algorithm uses measurements of Δp at two frequencies to make this effect drop out of the equations.

- The inertia of liquid contacting the pressure sensor can degrade the system accuracy. A suitably non-confining sensor entrance geometry keeps this effect within the overall system error budget.

- Thermal stratification will alter the density of the liquid and the γ of the gas. Monitoring the average tank temperature allowed 0.22 percent accuracy to be achieved with temperature differences of over 20°

- The tank expands slightly in response to the Δp produced by the compression driver. This effect is incorporated in the mass gaging algorithm, and the 0.2 percent mass accuracy results demonstrate that it does not degrade the system performance.

- A new class of mechanical resonances was discovered that can occur when there are multiple bubbles in a sealed tank. Distortions caused by this effect are kept within the system error budget by keeping the operating frequency below 0.07 times the lowest resonance of the tank.

- It is important that the flight gaging system not impose constraints on the design of structures inside the tank. The complex structure and many baffles of the apparatus used to study multiple bubble effects was found not to degrade the system performance.

Because of the maturity and solid foundation of the compression gaging concept, and because of the significant long-term benefits that a versatile fluid gaging system offers for future space activities, we recommend proceeding toward developing an operational flight system. We present an orderly and low-risk development plan. The two principal hardware development items are the pressure sensor and the compression driver. The driver requires careful design, but does not entail significant development risk. The pressure sensor can be most easily developed by modification of the commercial unit used in the breadboard. The electronics module is very straightforward, and represents essentially no development risk.

Section 1

INTRODUCTION

Section 1
INTRODUCTION

The Fluid Quantity Gaging program is a development effort funded by NASA-Johnson Space Center (JSC) to define, develop, and demonstrate system concepts for gaging a variety of fluids required for Space Station operations. The work has been performed by Ball Electro-Optics and Cryogenics Division (BECD) in Boulder, Colorado, under the direction of Mr. Kenneth Kroll of the Propulsion Branch of NASA-JSC.

A gaging concept based on adiabatic compression has been successfully developed that meets the ±1 percent accuracy goal. A gaging system architecture has also been developed that meets the needs of many different Space Station fluid systems with a limited number of standardized system components. This gaging system will have minimal impact on the fluid systems and will require little or no custom development for each application.

This final report summarizes our findings and gives our recommendations regarding the further development of this gaging system concept for flight use. This introductory section states the objectives and accomplishments of the program and summarizes its evolution as the information was developed. We then discuss how the compression gaging concept developed here relates to previous work, and give a guide to the organization of this report.

1.1   PROGRAM GOALS AND ACCOMPLISHMENTS

The objective of this effort has been to identify and demonstrate a gaging concept or group of concepts that:

- Measures the mass of liquid in a tank to ±1 percent of capacity

- Operates with all tank sizes containing a variety of liquids, including both Earth-storables and cryogens

- Operates independently of gravity or its orientation, and of the configuration, location, or number of liquid/gas interfaces

- Is independent of internal tank structure, such as slosh baffles or liquid acquisition systems

- Generally meets the long-term needs of NASA and the Space Station for a reliable fluid gaging system that can be easily used as a component with a wide variety of fluids and fluid subsystems

In summary, this program accomplished the following:

- Demonstrated gaging accuracy of 0.2 percent of tank capacity in the laboratory

- Identified potential sources of gaging error, quantified them with laboratory testing, and developed solutions

- Developed a detailed analytical model of the system to serve as a system design tool

- Demonstrated sufficiently good agreement between the test data and the analytical model that development of the flight system can proceed with minimal risk

- Developed a flight gaging system architecture that offers modularity and flexibility in meeting the needs of a broad range of users

- Identified off-the-shelf system components that can be used with minimal modification

When it appeared that adiabatic compression would be the gaging method selected, NASA-JSC provided us with a list of flight system performance requirements and goals developed specifically in light of the characteristics

of this method. Table 1-1 lists these, and shows that the flight system described here meets all of the requirements and most of the goals.

1.2   PROGRAM SUMMARY

At the outset, we expected to find several candidate gaging concepts and to select two of them for demonstration, using mass, power, etc. as the selection criteria. We also expected to find that different fluids would be best measured by different techniques so that NASA would need two, three, or more different gaging systems to serve the broad range of fluids that will be needed on Space Station.

Extensive analysis and study of the literature led to the realization that the requirement that the gaging accuracy must not depend on the location of the liquid in the tank ruled out many well-known gaging techniques. Imposing this ambitious requirement, however, is prudent because of NASA's need for a gaging system that will serve the long-term requirements of many different missions and tank configurations. We found that the only technique that could achieve ±1 percent accuracy without depending on the location of the liquid is adiabatic compression, and that it would work with all liquids except superfluid helium.

Superfluid helium (liquid helium below 2.18 K) is unique because is has an effectively infinite thermal conductivity. This property prevents compression gaging from working, but permits a very simple heat capacity gaging technique to be used instead. Because testing at BECD and elsewhere had already demonstrated the heat capacity gaging of superfluid, NASA-JSC deleted superfluid from the list of fluids to be considered in this program.

At the conclusion of the concept selection phase, therefore, we found that we should concentrate the program resources on adiabatic compression alone. A laboratory breadboard system was built and tested on the ground in parallel with an extensive analysis of the underlying physics. Discrepancies between test results and theoretical predictions became clues that helped shed light on the physical processes taking place. At the end of the testing, the high level of agreement between the analytical model and the test data gave us

Table 1-1
DESIGN REQUIREMENTS AND GOALS

ISSUE	REQUIREMENT	GOAL	EXPECTED PERFORMANCE
Accuracy, including effect of liquid orientation and bubbles	5 percent	1 percent	1 percent or better
Accuracy not limited by:	Fluid mass or tank geometry		Independent of tank geometry, including internal structure. Can be sized for any tank size, but may be impractical for very small tanks.
	Error accumulation		Errors do not accumulate
When usable	Tank isolated	During fluid transfer	Probably not usable during transfer operations. Use flow meters instead.
Pressurant gas	N_2 or He for storables; own vapor for cryogens	Any gas	Compatible with any pressurant. Accuracy degraded if gas mixture is unknown.
Tank pressure range	Survive vacuum, operate over 5:1 range	Operate from 0 to 500 psi	No limitation in principle. Pressure sensor limitations may limit accuracy near bottom of 5:1 range. 500 psi may make design of compression driver difficult.
Calibration	Can recalibrate in place; initial calibration on ground	No recalibration needed over time. No calibration needed for replacement	Calibrated on ground, using substitute fluid if convenient. Calibration co-efficients can be reloaded from ground. Mechanical characteristics of pressure sensors generally stable; electronic calibration can be checked by injecting reference signals. Replacement unit calibrated on ground, loaded with tank parameters used by previous unit.

F8806102A00-1

Table 1-1

DESIGN REQUIREMENTS AND GOALS (Continued)

ISSUE	REQUIREMENT	GOAL	EXPECTED PERFORMANCE
Redundancy	Fail-safe	Fail-op, fail-safe	Inherently fail-safe. Architecture permits several fail-op options using multiple heads/electronics modules.
Repair	Modular replacement with tank empty; can tell when failed	Replacement with tank not empty	Gage electronics module replaceable with tank full. Gage head replacement when tank not empty TBD. Failure monitoring TBD, but doesn't seem difficult.
Life	5 years, 10 years with refurbishment.	30 years without refurbishment.	Fatigue life of bellows probably the limiting factor. Preliminary tests show 15 years life with operation once per day feasible.
Commonality	For all fluids; interchangeable among similar tanks	Common hardware for all tanks	Common for all fluids, interchangeable (with reloading of calibration coefficients). Electronics module common to all tanks and fluids; a few gage head designs needed for different size tanks.
Compatibility	With fluid, tank materials, space environment	With all fluids	No compatibility problems identified. Standard design precautions required to avoid hydrogen embrittlement of bellows.
		With tanks having fluid containment diaphragms	Compatible, provided there is no significant amount of gas on liquid side of diaphragm.
Mass	Less than 1 percent of fluid mass (water)	Minimized	Estimate 0.2 percent of 10,000 liter tank. TBD for smaller tanks.

F88061O2AD8-2

Table 1-1

DESIGN REQUIREMENTS AND GOALS (Concluded)

ISSUE	REQUIREMENT	GOAL	EXPECTED PERFORMANCE
Energy Input	Less than 1 percent cryogen boiloff over 90 days	Minimized	Estimate less than 0.1 percent for 10,000 liters of LN_2.
Power Usage	Less than 1 kW peak	Minimized	Estimate less than 100 W for 10,000 liter tank.
Tank Penetrations	Less than 2, with redundant seals to vacuum	One	Baseline is one penetration per gage head. Additional gage heads may be desired for redundancy, or additional internal or external temperature sensors may be desired for maximum accuracy in extreme thermal environments.
Safety	No limitations on other operations	No safety limitations on any operations	No safety problems identified.

F88Ø61Ø2ADØ-3

confidence that we truly understand the behavior of the system. The benefit of this understanding is confidence that the laboratory testing can be extended into flight development with little risk of ugly surprises.

No attempt was made during this program to design a flight gaging system, but in the course of building the breadboard system we learned a great deal about all of the critical components and how they function. In Section 5 we discuss what this insight implies for the flight system; the information presented there shows that this system concept is sufficiently mature to begin operational hardware development.

We have developed a system architecture in which a single electronics module design is used with a gage head which is selected to suit the tank. The two principal hardware development items are the pressure sensor and the compression driver (a piston compressor). The compression driver requires careful design, but does not entail significant development risk. The pressure sensor can be most easily developed by modification of a commercial unit used in the breadboard. The electronics module is very straightforward, and represents essentially no development risk.

1.3   RELATIONSHIP TO PREVIOUS WORK

The problem of gaging fluid in space has received considerable attention over the past 25 years. Although much has been learned and several useful techniques have been developed, the ambitious goals set for this project were not fully satisfied by any of the previous efforts.

Before beginning this program, and then again during the concept selection phase discussed in Section 3, we carefully studied the existing literature to gain maximum benefit from the previous work. Summarizing the technical history in this area would be a formidable task, so no attempt will be made to do so in this report. In Appendix A we present the bibliography we developed, in which the references are organized according to the principal topic addressed.

The adiabatic compression gaging technique developed here differs in one key respect from other pressure-volume-temperature (PVT) gaging techniques that have been discussed. The volume of the tank is modulated at a frequency that is:

- High enough to limit heat transfer between the gas and its surroundings, so that the compression is nearly adiabatic and evaporation and condensation are negligible

- Low enough so that errors introduced by fluid dynamic effects such as the inertia of liquid in contact with the pressure sensor or sloshing of liquid between bubbles are within the system error budget

The simplest PVT system involves pressurizing a tank containing a known amount of liquid prior to launch and monitoring its pressure and temperature as liquid is withdrawn. The inevitable difficulties of long-term dc measurements have limited its useful accuracy to around 10 percent; and this scheme is not applicable to tanks which will be refilled or topped off on orbit, or to cryogen tanks whose pressure is determined by their temperature. Schemes which involve adding known quantities of backfill gas suffer from requiring a large reference gas volume to overcome the sensitivity limitations of dc measurements and from the eventual exhaustion of their gas supply, and can not be used with cryogens.

The Resonant Infrasonic Gaging System (RIGS) developed by TRW and others depends on the same adiabatic compression principle used by this project, but measures a signal frequency instead of amplitude; this can therefore be viewed as an alternative implementation of the same basic concept. We explored this alternative in depth, as discussed in Section 3 and Appendix B, and rejected it in favor of the amplitude measurement because its large development risk is not offset by any significant advantages.

1.4   ORGANIZATION OF THIS REPORT

This report has been organized so that most readers will find an adequate overview of the compression gaging system in Section 2, which explains the underlying concept and describes the characteristics of the flight system. Section 3 discusses the analysis that led to the selection of compression gaging, and lays the logic out in sufficient detail that the impact of any future technology changes or new requirements can be assessed.

Section 4 discusses the development of compression gaging in detail, and addresses both the laboratory testing and analytical model. Section 5 describes the flight system in detail and discusses the insight gained from our experience with the breadboard system hardware. Section 6 gives our recommendations for the development of the flight system, and the appendices contain many of the analytical and data analysis details.

OVERVIEW
of
COMPRESSION GAGING

Section 2

OVERVIEW OF COMPRESSION GAGING

The basic principles of fluid quantity gaging in zero gravity by adiabatic compression are now well understood, that understanding has been verified by testing, and the hardware required to implement it in flight applications is well enough defined to begin its development. This section explains the basic principle and how it has been verified, describes the baseline hardware concept and its operation, and then assesses the performance that we expect to be achievable in flight. Finally, we discuss the overall maturity of this concept and the development work that remains to be done.

2.1 COMPRESSION GAGING CONCEPT

The compression gaging system determines the fluid mass in a tank by measuring the volume of the ullage bubble, and then computing the fluid mass from the known tank volume and liquid density. The reasons for selecting this two-step approach are discussed in detail in Section 4, but basically boil down to these:

- This is the only technique found that can achieve ±1 percent accuracy without depending on controlling or knowing the location of the liquid.

- The programmatic risk of developing a gaging system that will satisfy the needs of a wide variety of Space Station fluid systems can be minimized because the principles underlying its operation are well understood.

Figure 2-1 shows the elements of the basic system. When a reading is to be made, a piston varies the tank volume cyclically by ΔV, which is something less than 10^{-4} of the total tank volume. Because the gas in the ullage volume is much more compressible than the liquid, it is compressed. With the piston operating at about 1 Hz there is little time for heat transfer between the gas and its surroundings. The compression is therefore nearly adiabatic,
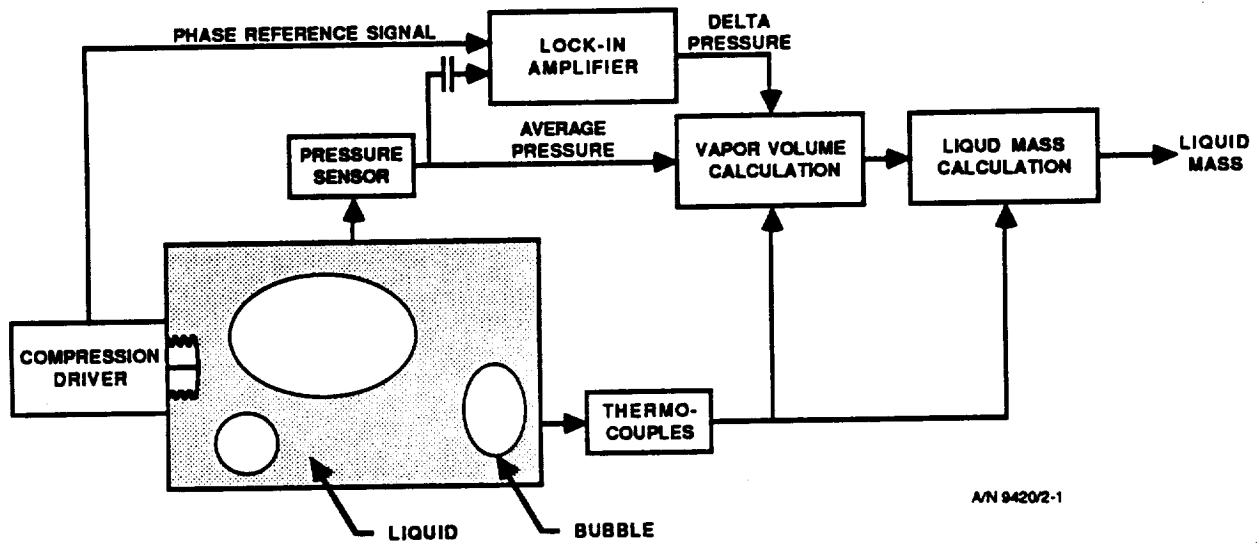
Figure 2-1 Compression gaging concept

so the volume of the bubble can be computed from the pressure p and the pressure change Δp according to

$$V_{bubble} = -\gamma \, \Delta V \, (p/\Delta p), \tag{2-1}$$

where $\gamma = c_p/c_v$ is the ratio of the specific heats of the gas at constant pressure and at constant volume, respectively. In order to achieve adequate signal-to-noise ratio in Δp with a small ΔV, a lock-in amplifier is used to measure the ac component of the p signal that is synchronous with the motion of the compression driver piston. The bubble volume is subtracted from the known tank volume, and the liquid density is used to compute the mass. Temperatures are monitored to correct for variations in density and γ.

2.2   CONCEPT VERIFICATION

In practical application, several physical processes can make the response of the gaging system more complex than the ideal behavior described by equation (2-1). We therefore developed a detailed analytical model of the system (discussed in Section 4.2) based on well-established physical principles, and verified its correctness and completeness through a carefully thought out test program.

This approach amounts to adopting the scientific method of close interplay between theory and experiment. The test data was held to a higher standard than repeatability in reporting liquid mass; the absolute values of all measured quantities were compared to the theoretical predictions. Discrepancies between them were used as clues to identify defects in the experiment or omissions from the model. The close agreement ultimately obtained between the data and the model shows that the physical processes operating are now well understood.

Tests using water pressurized with air and with helium were directed toward several important practical issues or potential sources of gaging error. Section 4.3 and the appendices discuss these tests in detail, but some of the most significant findings are summarized here.

<u>Compression that is not perfectly adiabatic</u>. Any heat transfer between the gas and its surroundings will cause the compressibility κ of the gas to drop below the value γ used in equation (2-1). The testing with both air and helium discussed in Section 4.3.3.1 confirmed the accuracy of our analytical model of this effect. We developed a mass gaging algorithm that uses measurements of Δp at two frequencies to make this effect drop out of the problem. The validity of the algorithm is confirmed by the fact that the breadboard system demonstrated an average error of 0.2 percent over five fill levels, as discussed in Section 4.3.2.

<u>Liquid contacting the pressure sensor</u>. Liquid in contact with the diaphragm of the pressure sensor will dramatically increase the effective mass of the diaphragm, altering its dynamic behavior and potentially degrading the response of the gaging system. The testing discussed in Section 4.3.3.3 with a commercial pressure sensor showed that the mass of the water confined in the long, narrow lead-in tube reduced the resonant frequency of the sensor from a few kHz to 40 Hz, and that the resulting shift in amplitude and phase of the Δp signal matched the predictions of the analytical model. The model shows that a less confining entrance geometry will allow the sensor resonance to remain far enough above the operating frequency that the resulting distortion can be kept well within the overall system error budget discussed in Section 2.3.4.

<u>Thermal stratification</u>. Both the liquid density and γ of the gas depend on temperature, so thermal stratification in flight could cause gaging errors. Tests discussed in Section 4.3.3.2 showed that monitoring the average tank temperature allowed 0.22 percent accuracy to be achieved with temperature differences of over $20^{\circ}C$ in either the air or the water.

<u>Tank expansion stiffness</u>. The tank will expand slightly in response to the Δp produced by the compression driver, and the increase in tank volume would distort the mass computed from equation (2-1). This effect is easily incorporated in the mass gaging algorithm, as discussed in Section 4.2.1.5, and the 0.2 percent mass accuracy results demonstrate that it does not degrade the system performance.

<u>Multiple bubbles in the tank</u>. We discovered a new class of mechanical resonances (Section 4.3.3.4) that can occur when there are multiple bubbles in a sealed tank, and showed that the Δp signal is effected in amplitude and phase in exactly the way predicted by the analytical model developed. The model shows that any distortions caused by this effect can be kept within the system error budget by keeping the operating frequency below 0.07 times the lowest resonance of the tank.

<u>Sensitivity to structure inside the tank</u>. It is important that the flight gaging system not impose constraints on the design of baffles, liquid acquisition systems, or other structure inside the tank, or be sensitive to variations in the structure inside different tanks. Adiabatic compression at low frequencies is expected to be independent of such structure, and the close agreement between the test data and the analytical model during the testing with the multiple bubble apparatus installed demonstrates that this structure indeed had no measurable effect.

We also studied the following effects and showed through the analysis in Section 4.2.3 that the errors introduced in any practical application will be negligible:

- Vapor condensation with cryogens or other liquids stored at their saturation temperature

- Solubility of the pressurant gas in the liquid

- Compressibility of the liquid, including hydrogen

- Non-ideal behavior of the gas

- Surface tension effects

2.3   FLIGHT SYSTEM

This section describes the flight system concept that was developed and the performance that can be expected from it. Section 5 describes more fully our present insight into the flight system and the design options that must be considered.

2.3.1   Baseline Hardware Concept

Figure 2-2 shows that the flight gaging system consists of two modules: a gage head mounted on the tank, and a gage electronics module mounted remotely. The gage head will be built in different versions to suit different groups of applications, while a single electronics module design is common to all of them.

The compression driver and the pressure sensor are mounted together in a single pressure shell that is designed to meet the fault tolerance requirements of the tank. An optical pickoff generates a phase reference pulse once per revolution of the driver. The thermocouples (or other temperature sensors) for monitoring the tank temperature are included with the gage head so that the only interface with the tank is at a single mounting flange. Additional temperature sensors may be mounted independently if desired.

The compression driver shown in Figure 2-3 is a piston driven by a simple crankshaft and sealed by a welded steel bellows. The bellows are readily available in cryogen-compatible steels, and preliminary life testing with a non-optimized bellows design indicates that fatigue life adequate for 15
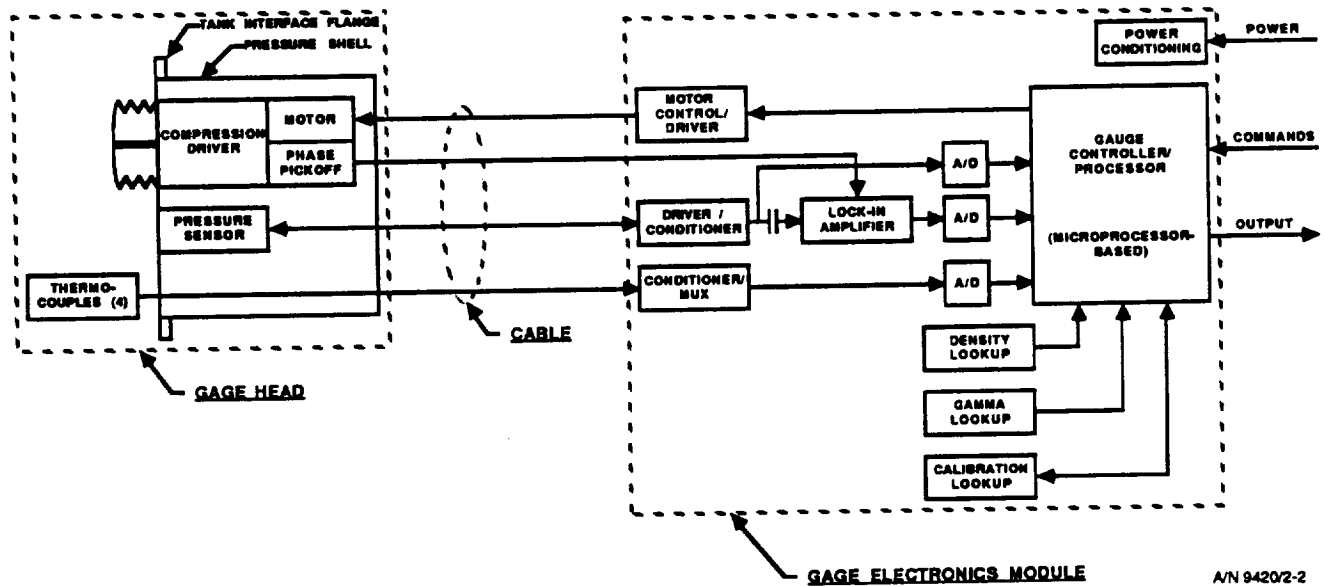
Figure 2-2 Flight system concept
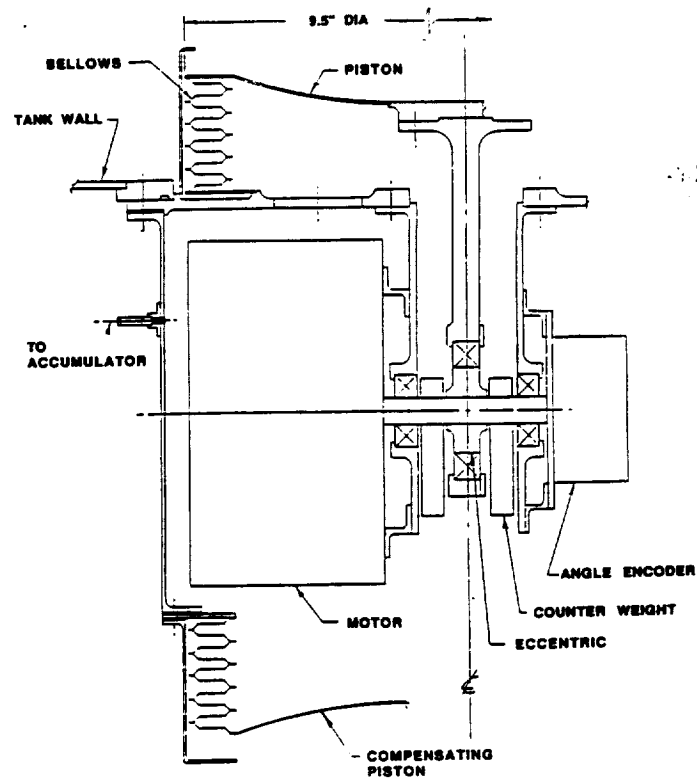
Figure 2-3 Compression driver concept

years of daily operation is obtainable. Many design details remain to be worked out, but our experience with cryogenic mechanisms and with dry lubrication indicates that developing a high-reliability driver will be straightforward.

The electronics module performs all of the functions necessary to operate the gage, process the data, and return a mass reading to the host vehicle. This unit is built around a microprocessor that interprets commands, controls the driver, and processes the data from the pressure sensor and thermocouples. Liquid density and thermocouple calibration data is stored permanently in read-only memories (ROMs), and calibration data (volume, expansion stiffness, and electronic gain) is stored in non-volatile RAM where it can be updated if necessary.

The lock-in amplifier is a key component in achieving high sensitivity in measuring Δp. This circuit, which is also called a phaselock amplifier or synchronous demodulator, can isolate a small ac signal in an exceedingly narrow frequency band centered on the operating frequency of the compression driver. By rejecting all signals that are not synchronous with the driver, it allows measuring Δp with a high signal-to-noise ratio.

This gaging system architecture is designed to serve the needs of the full range of Space Station fluid systems with minimum redevelopment or customizing for each specific application. A family of gage heads with different displacements will be developed to fit different tank volumes. One series of gage heads could be designed to work with all Earth-storable (i.e. room temperature) fluids and another with all cryogenic fluids, or it may be more cost-effective to develop a single cryogen-compatible series for application to all users. The gage electronics module will be adapted to different applications by loading the appropriate fluid and calibration data into the memories. The output stage of the motor controller will be sized to suit the different drivers.

2.3.2   Operation and Impact on User

This gaging system is designed to have minimum design and operational impact on the user fluid system. In its simplest form, the gage head attaches to

the tank at a single bolted or welded flange, with a single cable connecting it to the electronics module. The operation of the gage is independent of any internal structure (e.g. slosh baffles or liquid acquisition systems) in the tank, so changes in the tank configuration details will not impact the gaging system. Flexibility in the choice of ΔV and in the number and locations of the thermocouples allows optimizing the tradeoff between weight and complexity vs. accuracy for each application. These tradeoffs are discussed in Section 5.3.

It is assumed that the gaging system will be used intermittently (e.g. once per day) in orbit as needed to monitor the mass of fluid in the tank. The measurement will take from 1 to 5 minutes, depending on the frequencies and integration times used. The anticipated duty cycle will be a factor in the detailed design tradeoff for each application. For example, if a cryogen tank is to be monitored only once per several days, it may be preferable to mount the driver motor directly on the cold tank instead of accepting the boiloff due to heat leakage along the insulated drive shaft from a motor on the warm shell of the tank.

The two known limitations of this gaging system are its sensitivity to mixed pressurizing gas and to large-scale fluid motion. Because the pressure rise Δp depends on γ of the gas, the gas species or mixture must be known. A liquid oxygen tank, for instance, that is pressurized with helium will have an average γ that changes when helium ($\gamma = 1.67$) is added and has not had time to re-establish thermal equilibrium with the oxygen vapor ($\gamma = 1.40$). NASA-JSC informed us that it is likely that many or all of the future Space Station cryogenic systems will be pressurized with their own vapor.

Also, measurements made when the liquid is moving violently (e.g. during fluid transfer operations or during vehicle maneuvers) may be degraded by pressure surges. While it would be ideal to have a mass gage that functions well under these conditions, flow gaging is available during transfer operations, and routine mass measurements would normally be performed under quiescent conditions.

2.3.3   Mass Gaging Algorithm

The algorithm for computing fluid mass from the sensor signals is a simple algebraic expression that does not impose a significant computational load on the electronics module. When the compression is nearly adiabatic, it is easy to show from equation (2-1) that the liquid mass M is

$$M = \rho\{V + \gamma p[\alpha + \Delta V/\Delta p]\} \tag{2-2}$$

where ρ is the liquid density, V is the tank volume, γ is c_p/c_v, ΔV is the driver displacement, Δp is the measured peak-to-peak pressure change, and α is the tank expansion coefficient (volume increase per torr change in pressure). Note that since p goes down when V goes up, $\Delta V/\Delta p < 0$, so the term in the {} is just $V - V_{bubble}$.

ρ (and in some cases γ) depends on temperature, so it is stored in a lookup table, probably as a function of thermocouple voltage rather than of temperature as such. The only two adjustable parameters, other than the gains required to compute p and Δp from the sensor voltage, are V and α, which are determined during calibration.

Equation (2-1) describes perfectly adiabatic compression, but heat transfer produces an acoustic boundary layer in which the behavior is somewhere between adiabatic and isothermal. The analysis and test results in Section 4 and the appendices show that equation (2-1) then becomes

$$V_{bubble} = -\kappa \, \Delta V \, (p/\Delta p), \tag{2-3}$$

where to first order

$$\kappa = \gamma \, (1 + Cf^{-1/2})^{-1} \tag{2-4}$$

where f is the frequency and C is a constant than can be determined by two or more measurements. Therefore, to compensate for non-adiabatic compression, measurements of Δp_1 and Δp_2 are made at frequencies f_1 and f_2. The algorithm for computing mass can then be written as

$$M = \rho(V - \gamma p Z) \tag{2-5}$$

where

$$Z = \alpha + \frac{\Delta V}{\Delta P_1} \left[1 + \frac{(\Delta p_2 - \Delta p_1)\, f_2^{1/2}}{\Delta p_2\, (f_2^{1/2} - f_1^{1/2})} \right] \tag{2-6}$$

As with equation (2-2), the only parameters to be determined during calibration are the gains, V and α.

2.3.4   Expected Performance

Table 2-1 shows the system error budget presently baselined for the flight system. The numbers shown are believed to be readily achievable, and our laboratory experience indicates that the Δp and calibration error allowances may be unnecessarily conservative. After detailed analysis during the flight hardware development, it may be possible to reallocate the error budget so that $\Delta V/V$ can be reduced from the 10^{-4} level used in our mass and power estimates to something closer to 10^{-5}.

2.4   CONCEPT MATURITY

The adiabatic compression technique is sufficiently mature to permit flight hardware development to begin. The analytical model discussed in Section 4.2 is based on well-understood physics and has been thoroughly validated by the test results. This model constitutes the basic system design tool, and forms the basis for confidence that development risk will be minimal.

Table 2-1

SYSTEM ERROR BUDGET

CONTRIBUTOR	BUDGET (PERCENT)	COMMENTS
Δp Noise, Error	0.5	Determines ΔV needed
p Noise, Error	0.3	Limited principally by long-term drift
ΔV Variation	0.2	Set by mechanical clearances
ρ and γ Variation	0.3	Determine temperature monitoring needed
Resonance Distortion	0.5	Determines maximum operating frequency
Calibration Error	0.5	End-to-end calibration on ground will probably be better than this
RSS Total	$\overline{1.0}$ percent of capacity	

The two principal components needing development are the pressure sensor and the compression driver. The commercial pressure sensor used in the bread-board apparatus has been flown in space, and can be used for gaging earth-storable fluids by simply opening up the entrance aperture. (This is a standard catalog option.) Detailed discussions with the vendor lead us to believe that electronic modifications of a type familiar to BECD would permit it to be used with cryogens as well.

The compression driver is a straightforward mechanism design problem with little development risk. The welded bellows technology is available commercially, and preliminary testing with a highly non-optimum bellows indicates that a fatigue life of 15 years of daily use is feasible. Our experience with cryogenic mechanisms leads us to believe that it may be cost-effective to develop cryogen-compatible drivers and use them with earth-storable fluid systems as well.

The gage electronics module has very modest requirements, and presents no significant development risk. The principal question is what redundancy or multiple-gage capabilities to build into the common design at the outset.

Testing will be a necessary part of this development effort. The sensitivity of the system to violent large-scale liquid motion may limit the usefulness of low-g aircraft testing. Ground testing with a cryogen and on-orbit testing will therefore be high priorities.

SELECTION

of

COMPRESSION GAGING

Section 3
SELECTION OF COMPRESSION GAGING

We describe here the process by which compression gaging was selected for breadboard hardware development, and go through the logic in detail. This way it will be possible for the reader to see how our conclusions were drawn and how they would need to be modified in light of evolving technology or in light of different overall gaging system requirements.

3.1   SELECTION CRITERIA

The criteria for selecting the gaging concept or concepts fall into two categories: the primary functional requirements describing the job to be done, and secondary compatibility requirements describing the characteristics a gaging system based on the selected concept should have. Because there had been no well-established satisfactory solution to the primary requirements, the compatibility requirements had to be treated as design goals and adjusted in light of what was found to be possible.

Because tolerance of unconstrained bubbles is one of the fundamental requirements, our understanding of the behavior of liquid/gas bubbles in zero gravity is implicitly part of the selection criteria. We therefore also summarize what is known about bubble behavior.

3.1.1   Primary Functional Requirements

The basic requirement given by NASA-JSC for the gaging method selected was to measure the mass of liquid in a two-phase storage tank. (That is, this technique will not be applied to supercritical, solid, or liquid/solid slush storage systems.) The accuracy was to be 1 percent of full scale, with 5 percent as a fallback position if 1 percent were not achievable.

The fluids to be addressed are listed in Table 3-1, and were given in four priority groupings. Six of the ten fluids listed are cryogens. Liquid oxygen and hydrogen were given lowest priority because they are being addressed

separately under NASA-JSC contract NAS9-17378 which is currently being completed at BECD. Our analysis does show that the compression gaging technique developed here is applicable to oxygen and hydrogen.

Table 3-1
FLUIDS SPECIFIED IN CONTRACT

PRIORITY 1	PRIORITY 2	PRIORITY 3	PRIORITY 4
Monomethyl Hydrazine	Water	Freon*	Oxygen*
Nitrogen Tetroxide	Hydrazine	Ammonia*	Hydrogen*
Nitrogen*			
Argon*			

* Stored at saturation pressure.

Superfluid helium was initially included as a Priority 2 fluid. The uniquely high thermal conductivity of superfluid helium turns out to make the compression technique impossible, but makes it the only fluid for which the heat capacity method is practical. Because of this lack of commonality with any other fluid, and because tests at NASA-GSFC and at BECD have demonstrated that the heat capacity method does work, superfluid helium was dropped from consideration by this program.

Figure 3-1 shows that there are several possible ways of approaching the gaging problem. Using active techniques to make the position of the liquid repeatable on orbit, or to mix the liquid and the bubble so thoroughly that the tank contents are nearly homogeneous, would permit many common gaging techniques to be used.

Because the goal of NASA is to develop fluid gaging technology for Space Station that has the widest possible applicability and highest possible reliability, we were directed to develop techniques that do not rely on active manipulation of the fluid in the tank, or on knowledge of its location. This additional requirement dramatically increased the difficulty of our task.

The only options open to us are therefore those which meet this fundamental requirement: the gage reading must not depend on the location of the fluid
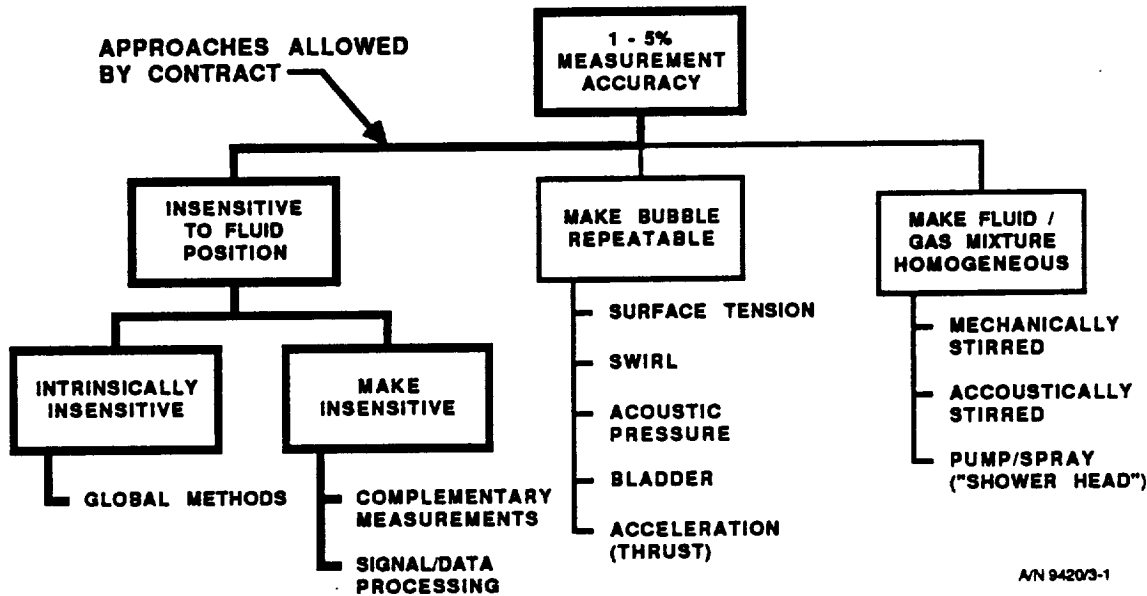
Figure 3-1 Possible approaches to zero-G gaging

<u>in the tank.</u> This could be satisfied either by a gaging concept which is intrinsically insensitive to the liquid location, or by using multiple measurements with signal processing techniques to make the computed reading position insensitive.

3.1.2   <u>Compatibility Requirements</u>

Once the accuracy and position independence requirements have been met, many secondary compatibility requirements and design goals come into play. The need to provide gaging for a wide variety of Space Station users results in the following selection criteria:

- Compatibility with as many fluids as possible

- Compatibility with as many tanks as possible, including:
    - Different volumes and shapes
    - Minimum impact on tank design
    - Ease of accommodating small design/manufacturing differences between specimens

- Minimum custom design or modification required for each application

- Minimum impact on the vehicle in terms of weight, power (peak and average) consumption, bulk, etc.

- Maximum safety, reliability, and maintainability

- Maximum confidence that there will be no significant surprises when going from ground testing to on-orbit testing and use

As the concept selection process progressed and it appeared that adiabatic compression was the only viable candidate, NASA-JSC provided us with a list of performance and compatibility requirements and goals developed specifically in light of the characteristics of this gaging concept. Table 1-1 in Section 1.1 lists them and shows that the gaging system concept developed here satisfies all of the requirements and many of the goals.

Two limitations of this concept were identified, and were discussed with NASA-JSC for guidance. These limitations and JSC's responses are as follow:

- Accuracy during fluid transfer operations. The violent fluid motion would probably cause pressure surges at the sensor that would overwhelm the lock-in amplifier. JSC advised us that this was not a major problem because flow meters would be available to measure the mass transferred, and the error accumulation problem inherent in mass estimating from flow measurements would not be a problem over the short period involved.

- Accuracy when cryogens are pressurized with helium gas. When helium ($\gamma=1.67$) is added to a cryogen ($\gamma=1.4$ for N_2), the average γ for the gas mixture changes until thermal equilibrium is re-

established, degrading the gaging accuracy during this period. JSC advised us to proceed because Space Station cryogenic systems would probably be pressurized with their own vapor for long-term logistic reasons.

We have made no attempt to develop the full set of design requirements and goals in detail during this program. This will be an important part of the flight hardware development effort.

3.1.3 Bubble Behavior in Zero Gravity

The basic physics of bubble dynamics and thermodynamics in low gravity is known for individual bubbles. It is difficult to estimate the precise number and distribution of sizes when a large number of interacting bubbles is involved. However for the storage conditions anticipated, some general statements may be made. Enough is known to permit the design of a fluid gaging system that will function under most conditions.

The following conclusions are based on an extensive study of the literature. One of the authors (H.A.S.) has followed this topic since 1974 when he attended several NASA planning sessions to select experiments for the Shuttle program on fluid mechanics in low g. He edited the proceedings of the Second National Conference on Drops and Bubbles sponsored by NASA, and is presently a member of or a consultant on low g fluid mechanics to three NASA-sponsored research centers at the University of Colorado:

- Center for Space Construction
- Center for Low g Fluid Mechanics and Transport Processes
- Bioserve

There are processes which break up large bubbles into smaller bubbles; other processes cause small bubbles to coalesce or dissolve in the liquid and lead to growth of larger bubbles. If the breakup and growth processsses occur simultaneously and at a relatively constant rate, a dynamic equilibrium is established between the competing processes. It is unlikely however that this situation will occur for space storage. Usually, it is expected that

the large bubbles will be broken up by an infrequent and intense disturbance. This is followed by a quiet period when the small bubbles decay and the large bubbles grow. In the latter case, the important quantities are the time constants of the growth process and the time between major disturbances.

Bubbles are produced during storage in space by the breaking of surface waves when the tank is shaken, by filling and emptying, and in the case of cryogens, by boiling. It is estimated that docking will cause accelerations of 10^{-2} g on Space Station; this will move the tank less than 0.25 mm. Calculations indicate that this is insufficient to cause any appreciable breakup of large bubbles. The heat influx to a well-designed cryogen storage tank of about 2000 L is about 10 W, producing about 4 L of bubbles per day. The largest source of bubbles will probably be the filling and emptying processes. The filling jet of liquid breaks up large bubbles, and the pressure jet during transfer is entrapped by the liquid to form bubbles. These filling and emptying processes occur at infrequent intervals.

There are several processes which cause small bubbles to disappear. In saturated storage small bubbles become part of a big bubble through a thermodynamic process driven by the excess pressure in the small bubble. An analogous process occurs when a liquid is stored with a backfill gas, in which the gas dissolves in the liquid at the small bubble and comes out of solution at the large bubble. Both of these processes are very slow, with a time constant for bubbles larger than 1 mm of weeks if no mixing occurs. Tank motion due to the background g level and emptying cause mixing which can speed up the thermodynamic processes by one or two orders of magnitude.

Small bubbles also disappear by coalescence in both saturated and non-saturated storage. The coalescence mechanisms of significant magnitude for the present application are the acoustic field and the thermal gradient.

The acoustic pressure field induced by the compressor makes the bubbles oscillate in radius. This oscillation sets up a velocity field around each bubble which interacts with that of each other bubble. The detailed analysis shows that oscillating bubbles attract each other if they are in phase and repel when out of phase. This method is used to clear bubbles from bubble

chambers used to detect ionizing radiation. The coalescence rate is propor-
tional to the radius cubed of the larger bubble, and proportional to the
square of the frequency. The radii of the bubbles produced in bubble
chambers are less than 1 mm; the frequency used is in the kilohertz range and
the chamber is cleared in a few minutes. For the larger bubbles found in
space storage the calculations indicate that a 10 Hz signal from the
compression driver could clear the chamber in a few minutes if desirable.

The acoustic force also applies to bubbles attached to a wall but the calcul-
ations indicate that it is insufficient to dislodge a bubble from a wall.
For unsaturated storage of a liquid which wets the tank wall, the bubbles
will therefore coalesce with those attached to the wall or to internal struc-
tures by surface tension. When the liquid/gas/wall system is sufficiently
non-wetting, one large bubble will form that is free of the wall.

The fluids that are stored at saturation are primarily cryogens; in that case
there is a thermal gradient between the wall and the location of the vent. A
bubble in a thermal gradient experiences a force because the surface tension
on the warmer side of the bubble is less than on the other side; this is
known as the Marangoni force. The drift velocity of a bubble is directly
proportional to the radius and the thermal gradient. For liquid nitrogen
with a thermal gradient of 1 K/m, a bubble of radius 1 cm will drift toward
the higher temperature at 1.04 cm/sec. The bubbles which are formed by
boiling will therefore remain in the vicinity where they are produced and
will coalesce when they touch each other to form a sheath in the vicinity of
the wall of the dewar. The drift rate is sufficient to keep up with the
boiling rate during steady state storage.

The qualitative picture that emerges therefore is as follows: The major
sources of bubbles are operations associated with filling and emptying the
tank. These bubbles can be coalesced by operating the gage at 10 Hz for a
few minutes. The location of large bubbles formed by coalescence depends on
whether the liquid wets the walls and internal structure. If wetting occurs
the bubbles stick to the walls and internal structure; otherwise, the large

bubbles are spheres floating freely. For cryogens the thermal gradient makes the bubbles formed by boiling stay near the wall where they will tend to coalesce.

3.2   SELECTION METHODOLOGY

The past history of efforts to develop on-orbit gaging technology showed us that we must be extremely careful in selecting the one or two techniques to focus on in this program. We therefore adopted a methodology designed to enable us to consider all conceivable techniques, and to choose between them without expending our resources on unnecessary detailed analysis.

The most fundamental decision was to focus first on the principles underlying each candidate technique, and to assess whether or not the laws of physics would permit it to meet the fundamental performance requirements. The next step was to address the practical requirements of implementation and impact on the host vehicle. This way we could avoid the pitfall of spending our resources analyzing hardware details of techniques that were doomed for more fundamental reasons.

The selection was made using the multistep process shown in Figure 3-2. First, all possible gaging methods were identified and classified in a design option tree. Then a first cut selection was made, based on the fundamental performance criteria. The potential accuracy of the members of this much smaller list of design options was then analyzed to identify the acceptably accurate methods. At this point the issues of ease of implementation and impact on the vehicle were to be used in a tradeoff to select one or two techniques for breadboard development. As it turned out, only the compression technique survived the second cut as fundamentally capable of delivering the required accuracy under the conditions specified by NASA-JSC. This greatly simplified the tradeoff step.

The selection process began with an exhaustive review of previous efforts on this problem. All techniques previously suggested, plus all others that we could identify, were tested against the fundamental requirement that they be capable of giving an output that is independent of the fluid location in the
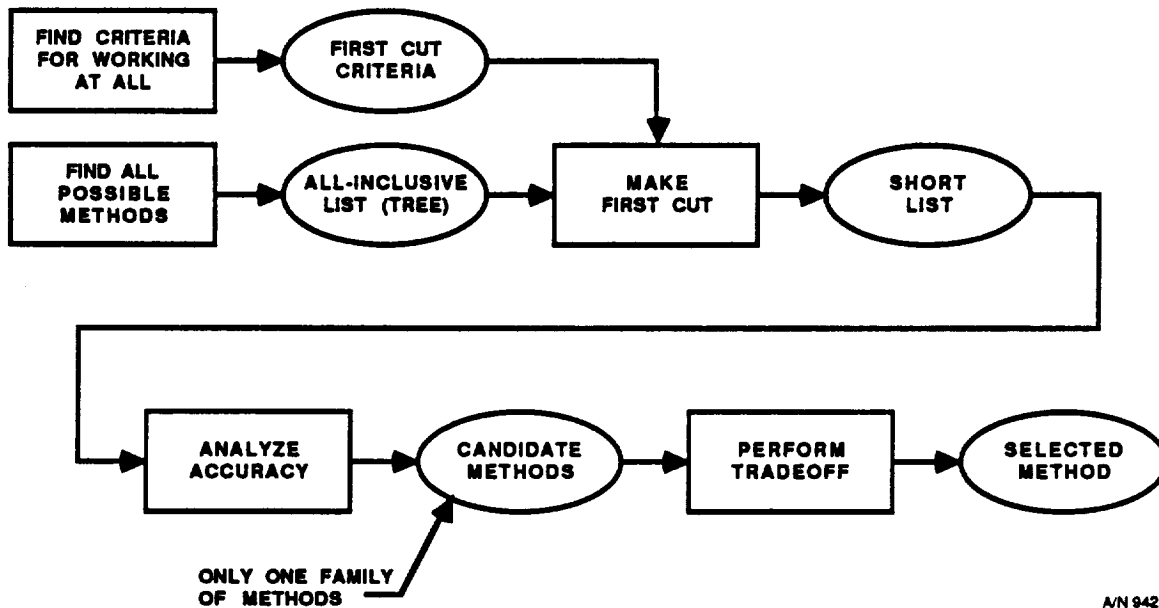
Figure 3-2 Concept selection process

tank, at least in concept. Of 41 distinct candidates initially identified, 9 survived this first cut.

Because of the enormous number of conceivable ways of gaging fluid quantity, and because none of the previous development efforts had produced a truly satisfactory solution to our particular requirements, it was necessary to use an analysis tool that would organize and impose discipline on the process of identifying the design options. This tool had to satisfy several goals:

- Include all possible options, so that no good ones are overlooked.

- Organize the options to permit efficient but logically correct analysis.

- Provide an understandable visual summary of very many details.

Figure 3-3 shows the tree diagram that was developed. Visually, this looks like an organization chart, but its logical structure is different. It is an OR tree, in the sense that each block can be satisfied by any one of the blocks below it, and in no other possible way. This structure gives us a way of being certain that no possible options are overlooked, because when the tree is complete anything not listed explicitly will be a variation or subset of one that is.

The entries in Figure 3-3 are organized to facilitate rapid convergence on the feasible ones. The various possibilities are grouped with so that any suspected weak links common to several entries appear high in the tree, so that one calculation can "prune" a large section at once. In this case, the inventory methods, those applicable specifically to superfluid helium, and those that involve constraining the position of the liquid were immediately ruled out by NASA-JSC as inconsistent with the goals of this contract. The first-cut analysis further narrowed it down to the entries highlighted with heavy lines.

The potential techniques for gaging with the liquid position unconstrained were classified as either sensing the liquid directly, or sensing the gas and then inferring the liquid mass from the known tank volume. Because of the primary requirement that the gage reading be independent of the spatial distribution of the liquid in the tank, the next level of classification was by the spatial sampling scheme used. Finally, the candidates were classified by the physical phenomenon used, and the techniques themselves were listed.

When Figure 3-3 was developed, we concentrated on being sure that nothing was overlooked. In some cases we knew of no clear scheme for making an entry work, or it looked silly, but we included it for completeness. This was fortunate, because it seemed "obvious" to us at the beginning that compression gaging was impractical. The discipline of constructing a truly all-inclusive option tree forced us to analyze it objectively.

LIQUID
POSITION
UNCONSTRAINED

SENSE
LIQUID

SPATIAL
SAMPLING

GLOBAL

POINT
SENSING

LINE
SAMPLING

FIELD
SAMPLING

PHENOMENON

MECHANICAL

THERMAL

INTERFACE
SHAPE

PHYSICAL
PROBE

BEAM
PROBE

CAPACI-
TANCE

RF

OPTICAL
ABSORBTION

RESONANT
FREQUENCY
(LINEAR /
ROTATIONAL)

AVERAGE
VISCOSITY

HEAT
CAPACITY

OPTICAL
FIBER

HEAT
CAPACITY

HOT WIRE

OPTICAL
FIBER

TORSIONAL
WAVE

GAMMA
RAY

OPTICAL

ULTRASONIC

NEUTRON
SCATTERING

CONVEN-
TIONAL

UNIFORM
FIELD

MODE
COUNTING

MODE
FREQUENCY
ANALYSIS

RESONANCE
WIDTH

INTEGRAT
CAVITY

/ FOLDOUT FRAME

F8806112AC0-11

Figure 3-3 All-inclusive method tree

3.3 FIRST CUT SELECTION

We now summarize the first-cut analysis that pruned the tree of options to those branches shown with bold lines. The options rejected at this point were judged to have no chance of meeting the fundamental requirement of 1 percent accuracy with the position of the liquid unconstrained.

The gas bubble, rather than the liquid, can be viewed as the localized "object" in the tank. We therefore sometimes speak in terms of imaging or measuring the bubble.

3.3.1 Mechanical Resonant Frequency

This is a global sampling method that consists of measuring the inertia of the tank plus liquid by shaking it. One way would be to suspend the tank from the main vehicle on a compliant mount, then perturb it and measure its natural resonant frequency.

The problem is making sure the liquid moves with the tank. Some sort of mesh would be required to effectively tie the liquid to the tank at the resonant frequency. This structure would act like a sponge, and prevent draining the liquid without leaving an unacceptable fraction behind.

3.3.2 Average Viscosity

This scheme would measure the power or torque required to stir the entire contents of the tank. This was rejected for two reasons:

- The weight of the stirring mechanism and the constraints imposed on the design of the tank would be unacceptable.

- There is no good analytical model for the behavior of such a system, so on-orbit calibration would be required.

3.3.3   Heat Capacity

In this concept, a heater adds a known amount of energy to the tank, and the mass is inferred from the measured temperature rise and the known heat capacity of the liquid. For this to work well, the liquid must come close to thermal equilibrium within the measurement period. Unfortunately, the thermal conductivity of all normal liquids is extremely low in the absence of gravity-driven convection. For example, a temperature change takes about two days to propagate 10 cm in water. (As we noted above, the situation is dramatically different for superfluid helium, and this becomes the easiest technique to use.) We therefore rejected this technique for all fluids other than superfluid helium.

3.3.4   Point Sampling Techniques

In point sampling, the presence of liquid is sensed locally at N points distributed on a suitably designed sampling grid. These N measurements can in principle be used to form an image of the bubble(s), and then used to calculate its volume. This is a binary 3-dimensional image, as opposed to the usual 2-dimensional continuous gray tone image, but the same concepts of sampling theory apply: our knowledge of the bubble volume is limited by the accuracy of the "image" that can be reconstructed from the output of the N sensors. It is easy to see that more than 100 sensors are required to achieve ±1 percent accuracy, no matter what physical principle is used by the sensor.

We identified two sensors capable of sensing liquid at a point:

- Heater/thermometer units to measure the local heat capacity

- Optical fibers with flat ends to measure the local index of refraction by the fraction of light reflected

These are both physical probes placed at the sample point, with support structure and cabling running to each sensor. We found two fatal flaws with this concept:

- The impact on the tank design and fabrication due to the number of penetrations and the amount of internal support structure required would be unacceptable.

- Liquid drops are likely to be retained on the sensors by surface tension, so that sensors inside gas bubbles would report a "wet" reading. A non-wetting coating would just reverse the problem, so that bubbles are retained.

We therefore rejected all point sampling methods using physical probes. If a non-contact point probe is found, this option could be reopened, provided that the number of tank penetrations is acceptable.

3.3.5   Line Sampling with Physical Probes

This group of methods uses a physical object to sense the liquid density or location along each of many lines through the tank. Even before addressing the sampling theory issues, we rejected these three candidates for the following reasons:

- Hot wire sensors have been used to measure liquid depth on earth, but they can not sense the position of the liquid along the wire, and are likely to be misled by droplets clinging to the wires.

- Thin, flat rods have been used to measure water depth in nuclear reactors by exciting a torsional wave and measuring its resonant frequency, thereby determining the moment of inertia of the rod plus the liquid in contact with it. In zero gravity, droplets could cling to the rod inside large a gas bubble, or the oscillation could cause local bubble formation inside a large glob of liquid.

- It was suggested that some sort of line sensing scheme using optical fibers could be found, but it never was. Again, any sort of physical probe would be subject to errors due to droplets clinging to it.

3.3.6 Neutron Scattering

Neutrons differ from the other possible beam probes in that they <u>scatter</u> from the liquid atoms, losing energy at each collision until they reach the temperature of the liquid, and scatter through large angles as they slow down. We checked to see if this behavior would help somehow and found that it did not. To a detector on or in the tank, the liquid would look like a "source" of thermal neutrons, and the count rate would depend on the square of the distance between the detector and each element of the liquid. This method therefore could not give a reading that is independent of the location of the liquid.

3.3.7 Optical Integrating Cavity

This scheme would shine light into the tank in such a way that it takes random paths in reaching the detector(s), so that the amount of light absorbed would measure the average amount of liquid throughout the tank. This method was rejected because:

- It would be extremely difficult to manufacture a tank with highly reflective walls.

- While the detector output would depend "somehow" on the total amount of liquid inside, there is no analytical guide to finding a data processing algorithm what would produce an output that is independent of the liquid position.

3.3.8 Backfill with Gas

This method consists of adding a known amount of gas to the tank and measuring the resulting pressure rise. This is a close cousin of the adiabatic compression technique that was eventually selected, and differs from it basically by operating for a single cycle at a very much lower frequency. This technique was not pursued for the following reasons:

- Significantly better sensitivity (i.e. achievable accuracy for a given gas volume displacement or addition) would be expected for the cyclic adiabatic compression technique than for this DC technique because of the 1/f noise typically found in sensors and amplifiers.

- This technique would not be usable with cryogens because the pressure rise would cause vapor condensation. If the backfill gas is of the same species as the liquid, the pressure rise would decay to zero. If the backfill gas were helium (i.e. non-condensible), the pressure rise would decay by an amount depending on the ratio of cryogen vapor to helium in the gas space.

- The supply of backfill gas would eventually be consumed.

- There is no apparent advantage of this technique over adiabatic compression.

3.3.9   Relaxation Oscillator

This is a technique that was explored at NASA-Langley Research Center for use in normal gravity, and which is closely related to the backfill method. Gas is added to the tank at a known rate until the pressure has risen by a preset amount, and is then allowed to bleed out at the same rate until the pressure returns to its original level. The system therefore constitutes a relaxation oscillator whose frequency is related to the volume of the gas bubble in the tank. This technique was not pursued for the reasons given above for the backfill method, plus the difficulty of venting only gas from a tank in zero gravity.

3.3.10   X-Ray Photo

An X-ray source would be used to form a continuous image on film or other medium, and this image would be processed on board to infer the bubble volume. This scheme would bypass the sampling theory issues, but images from more than one perspective would be needed to infer a unique value for the

bubble volume, especially if there is more than one bubble. No implementation could be found, however, that would not require unacceptably bulky and heavy hardware.

3.3.11 Acoustic Field Sampling Methods

The field sampling methods are those which sense the liquid or gas by means of some continuous field that may (or may not) extend throughout the tank. Somewhat arbitrarily, we have classified the electrical field sampling methods (RF and capacitance techniques) as sensing the liquid, and acoustical methods as sensing the gas.

Acoustic candidates include analyzing the behavior of the tank as a resonant cavity by measuring the resonant frequency(ies), counting the modes observed in a certain frequency band, or measuring the response to an impulse or more complex stimulus. These are all analogous to RF techniques that have been studied, and they all depend fundamentally on the different wave propagation velocities in the gas and the liquid.

Efforts to date to develop RF gaging have been frustrated by the fact that the location of the liquid affects the resonant modes in complicated ways. For electromagnetic waves in oxygen, the propagation velocity differs by only a factor of 1.2 between the liquid and the gas, while the velocity of sound differs by a factor of 5.1. This means that the position-dependent effects are far worse for the acoustic field. Since there is no obvious advantage to the hardware implementation of an acoustic system over an RF system, we rejected acoustic field sampling. If a clear solution to the problems of RF gaging is found, it may be worthwhile to reexamine these acoustic methods.

3.4 SECOND CUT SELECTION

Figure 3-4 shows the survivors of the first cut selection, and breaks the beam probe methods down into beam attenuation and ranging techniques. We set up straw man designs and gathered information from manufacturers and the

FLUID
GAGING

SENSE
LIQUID

SENSE
GAS

LINE
SAMPLING

FIELD
SAMPLING

GLOBAL

BEAM
ATTEN.

RANGING

CAPACI-
TANCE

R. F.

COMPRESS-
IBILITY

- GAMMA
  RAY

- ULTRASONIC

- CONVEN-
  TIONAL

- MODE COUNTING

- AMPLITUDE

- OPTICAL

- UNIFORM
  FIELD

- MODE
  FREQUENCY
  ANALYSIS

- RESONANCE
  (RIGS)

- RESONANCE
  WIDTH

A/N 9420/3-4
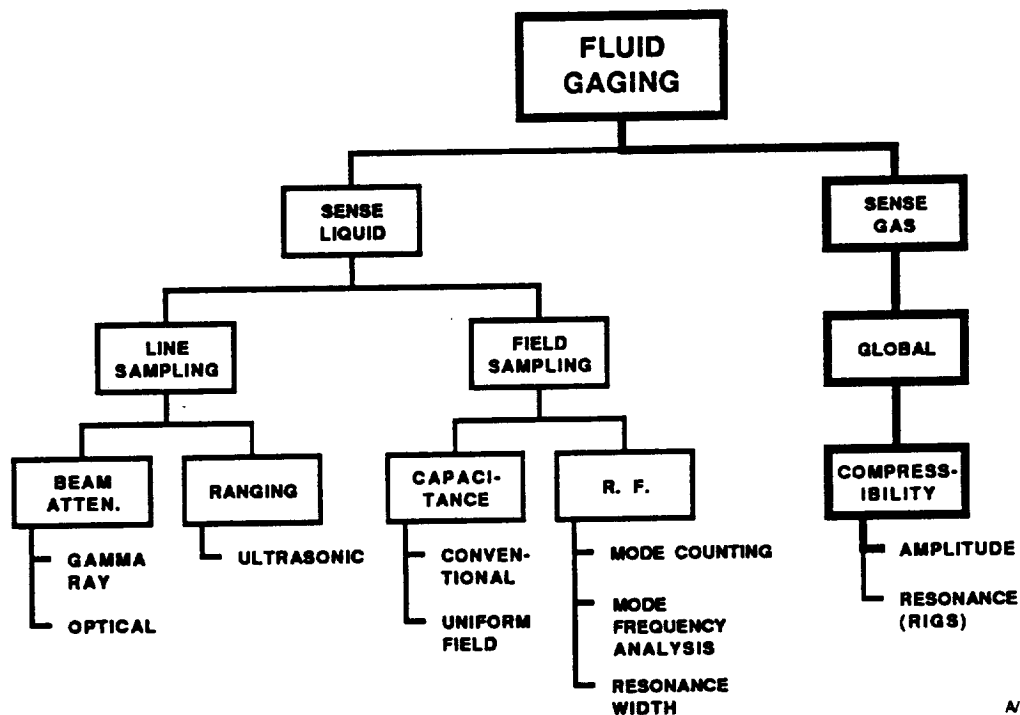
Figure 3-4 Methods surviving first cut

literature as necessary to assess the practicality and accuracy potential of
each candidate. The paragraphs below summarize our findings.

As we went through this process we also looked for ways of combining measure-
ments to reduce or eliminate the position sensitivity of the readings. The
only candidates for complimentary measurements we found were variations on
the capacitance and radio frequency gaging techniques, and are discussed in
those sections below.

3.4.1   Line Sampling Methods

Line sampling techniques for sensing the liquid include gamma ray or optical
beam attenuation, which measure the total density along the sample line, and
ultrasonic ranging, which can measure the distance from the transducer to
liquid/gas interface(s). Gamma ray attenuation, which is frequently referred
to as nucleonic gaging, has been used in flight. Ultrasonic techniques are
commonly used in inspection and medical imaging.

Two basic gaging strategies using line sampling can be considered:

- True imaging of the bubble(s), followed by image processing to infer the bubble volume

- Model fitting, in which N suitably chosen measurements are used to determine N coefficients of an *a priori* model of the bubble(s)

As discussed below, the true imaging approach turns out not to be feasible for reasons unique to each of the three technologies, and the model fitting approach is ruled out by the basic requirement that the gage be independent of the location of the liquid.

Imaging by gamma ray attenuation. To build up an image requires many sample beams. The number of beams required increases as the resolution of the image (i.e. the complexity of the bubble structure that the system must be able to deal with) increases. In the familiar medical X-ray tomography technique, a single source plus detector array is rotated about the subject to record samples along lines in many different orientations in succession.

Eliminating the mechanical scanning apparatus would require either having all beams share a common source at the center with multiple detectors on the outside, or having multiple source/detector pairs on the outside. A system with a single source at the center would be incapable of distinguishing between a small bubble near the center and a larger one near the tank wall. The photon energy required to penetrate large tanks (>0.5 MeV) is impractical to generate with X-ray tubes in space, so radioisotope sources that can not be turned on and off must be used. The confusion generated by crosstalk between the different source/detector combination was judged to be too complex to sort out.

Model fitting with gamma ray attenuation. Nucleonic gages which have been used successfully on aircraft and on small satellite tanks have used a single detector with a distributed source, usually Kr^{85} gas in a small tube molded to the tank. The presumption is that the resulting weighted average limits

the sensitivity of the gage to the location of the liquid. Still, the technique depends on assuming that at each fill level the distribution of the liquid is approximately repeatable. We studied reports of past work and examined new multiple-detector schemes, but could not find a reliable procedure for designing a system that would deliver 1 percent accuracy with unconstrained liquid location.

<u>Optical beams</u>. Measuring the absorption of optical beams for use with either imaging or model fitting was examined. Dyes could be used to get significant absorption in the visible spectrum, or the wavelength could be chosen to lie on the wing of a spectral absorption feature of the liquid. The optical beam approach was found to be impractical because of refraction at the liquid/gas interfaces. Random bubble positions would cause the optical path to vary widely, hopelessly confusing the data interpretation.

<u>Ultrasonic beams</u>. The successful use of ultrasonic beams in medical imaging, plus the convenient transducer technology, made this technology look attractive for either imaging or model fitting. The phenomenon sensed is the reflection caused by the change in the speed of sound at the interface between two media.

The large difference in density between gas and liquid causes essentially total reflection at each bubble surface, so the transducer can not "see" past the first interface encountered. Also, the fact that the bubble surface is smooth causes the reflection to be specular, so each transducer would get a return signal from only the point where the bubble surface is perpendicular to the beam. With a scanning beam transducer, the image of a collection of bubbles would look like shiny ball bearings illuminated by a flashlight held by the observer's eye; all that would be seen is one bright point for each bubble, independently of the bubble size. Using the range information from the signal round-trip time, it would take nine transducers to model a single ellipsoidal bubble. Dealing with many bubbles therefore would require an unacceptable number of transducers.

3.4.2   Capacitance Gaging

Capacitance sensors are routinely used in aircraft to gage liquids and in spacecraft to gage supercritical (single-phase) fluids. The sensors are usually slender coaxial assemblies extending through the tank, and measure the average dielectric constant of the fluid between the electrodes inside the sensor assembly. These amount to line sampling sensors, and work well for measuring depth in 1 g or during vehicle acceleration, or for measuring the average density of supercritical fluid in 0 g. If applied to liquids in 0 g, the limitations of line sampling would be further complicated by the tendency of liquid to be retained inside the sensor by surface tension even though the sensor is surrounded by gas.

We examined various schemes for using capacitance sensing as a field sampling method in which the electric field extends throughout the tank. We found that these schemes fell into two broad categories: those in which the field is nearly uniform over the entire volume, and those in which it is not. For example, the electric field between a rod in the center of a tank and its walls falls off as 1/r, where r is the distance from the center. In corners between the tank wall and any internal structure like slosh baffles, the field will be close to zero. This means that capacitance gaging with non-uniform electric fields will be highly sensitive to the liquid location.

A non-uniform electric field exerts a force on a dielectric, so a capacitance gage using a rod along the tank center would tend to pull the liquid to the electrode. We checked to see if this effect could be strong enough to localize the fluid when the gage is turned on, thereby giving repeatable readings. We found that the force produced is too weak. In the presence of accelerations of 10^{-3} g, an electrode at 100 V with respect to the tank walls would retain liquid (with dielectric constant $\epsilon=2$) only out to a radius of 10 cm.

We also examined the possibility of using suitably designed electrode arrays operating at different voltages on the inside of the tank walls to create an

approximately uniform field. Because of dielectric shielding, the capacitance is a strong function of the distribution of the liquid. For example, in an ideal parallel-plate geometry 1/3 full of liquid with $\epsilon=2$, rotating a rectangular block of fluid by 90° changes the capacitance by 10 percent. This effect becomes a factor of 2 for hydrazine ($\epsilon=5$), and is enormous for water ($\epsilon=80$).

This location sensitivity can be reduced by measuring the capacitance with the field in two or more directions and averaging. We explored one technique (A.H. Dammig, A.E. Sherburne, and R.A. Brooks, US Patent 3,639,835, February 1, 1972) for this and found that even in an idealized geometry the errors were 4 percent for $\epsilon=2$, and 22 percent for $\epsilon=5$.

The final factors that led us to reject uniform field capacitance gaging were manufacturing complexity and risk, plus repairability. Electrode designs can be found that give reasonably uniform fields in two directions in cylindrical or spherical tanks, but those electrodes resemble printed circuit patterns applied to the inner surface of the tank walls before assembly. Long-term compatibility of the electrodes, insulators, and bonding with the fluids, especially cryogens, would require significant technology development. Any metallic internal structure (slosh baffles, tubing, etc.) would seriously perturb the field uniformity unless numerous compensating electrodes were added. All of the electrodes, leads, and electrical feedthroughs would have to be installed before the tank is assembled, and any repair would require cutting it apart.

3.4.3   Radio Frequency Gaging

Fluid gaging using radio frequency (RF) techniques has been addressed by several development efforts over a span of 25 years. The three techniques that have been studied are

- Analyzing the frequency of one or more resonant modes

- Counting the number of resonant modes in a specified bandwidth

- Measuring the width of one or more resonant modes

The first two are based on the fact that the reduced speed of propagation in the liquid causes the frequency of each resonant mode to decrease as the tank is filled. The third is based on the fact that energy absorption by the liquid causes the width of the resonance to increase.

The hardware required for RF gaging is straightforward, and the fact that only one small antenna (or possibly a few) need be attached to the tank make it seem very attractive. The difficulties lie in the details of the way the liquid location affects the signal, and the lack of any clear signal processing scheme that will give a gage output that is sufficiently independent of the liquid location. It is also true that the properties of a resonant RF cavity depend very strongly on the details of any metallic structure inside, so the calibration and possibly the gross behavior of an RF gage are likely to vary significantly from specimen to specimen of tanks built for Space Station.

The theory of resonant cavities is well-understood, and experiments with the lowest resonances of simple tank geometries agree with the theory rather well. The electromagnetic field pattern is different for each mode and is highly nonuniform, falling to zero at metallic surfaces. One would therefor expect the behavior of any single mode to depend on the location of the liquid, since liquid located in regions of low field (e.g. at the wall where it is expected to stick due to surface tension) would be "seen" less efficiently than liquid in regions of high field. A suitable signal processing algorithm based on the frequencies of several modes with complimentary field distributions might, however be found that would give a position-independent measurement of the liquid mass.

If the liquid were distributed homogeneously throughout the tank as a froth or mist, its net effect would be to increase the average dielectric constant slightly, thereby reducing the wave propagation speed and all resonant frequencies. The fact that the liquid is concentrated in certain places distorts the electromagnetic field, and shifts each resonance by an amount that depends in complicated ways on which mode it is and where the liquid is.

Tests in which the tank was tipped at several angles have confirmed this, although computational difficulties have made detailed comparison with theory impractical.

Mode Counting. One approach to avoiding the position dependence and the difficulties of analyzing a few of the lowest modes (around 200-500 MHz) has been to count the number of higher order modes in a specified bandwidth (say 1-3 GHz). The hope has been to average over the complications statistically. Typically several thousand modes must be counted, and counting accurately is difficult in the presence of mode crossing and varying resonance width. The theory behind this approach is quite complex, and matches the measured data only under certain conditions of tank geometry and fluids. We are not optimistic about the practicality of applying this technique to tanks with internal structure and non-ideal geometries.

Mode frequency analysis. The most recent and thorough attempt to remove the position dependence of the frequency measurement technique is currently in progress at BECD. This effort (NASA-JSC contract NAS9-17378 begun under Beech Aircraft, Boulder Division) is directed specifically towards oxygen and hydrogen, but the findings will be applicable to a broader range of fluids. The approach is to measure the frequencies of the three lowest modes and to apply an empirically developed algorithm to calculate a fluid mass that is independent of liquid position. This algorithm is presently based on a calibration using paraffin models to simulate many possible liquid distributions at several fill levels. We did not select this technique for the present study because to do so would be redundant with the contract then in progress at Beech.

Resonance width. Using the electromagnetic energy absorption by the liquid as a fluid gage is a new technique under study by R.J. Hansman at MIT. The RF generator is tuned to one of the low-order resonances and the width of the resonance is measured; this width is then related to the quantity of absorbing fluid in the tank. This scheme avoids the complications of the dependence of the frequency on the liquid location, but the amount of energy absorption (and therefore the resonance broadening) still depends on whether

the liquid is in a low-field or high-field region. The intention is to control the position sensitivity by combining measurements of several modes as necessary.

We did not select this technique for the present study because we did not see any clear advantage over the frequency analysis method. As with all of the RF techniques, the electromagnetic field will be weakest in those regions most likely to contain liquid: the corners around baffles, liquid acquisition devices, and other internal structures. The theory of the field patterns is computationally intractable in many practical geometries, and does not constitute a useful design tool. In addition, this technique will be highly sensitive to contamination of the fluid.

3.4.4   Adiabatic Compression Gaging

Before any attempt was made to evaluate different implementations of compression gaging, we checked to see if there were fundamental limitations due to the thermodynamics involved. In particular, we were concerned about the effects of temperature nonuniformities, surface tension, and vapor condensation in the case of cryogens. Detailed analysis (see Section 4.2) showed that the errors introduced could be kept below *1 percent. We did find, however, that these techniques are sensitive to $\gamma = c_p / c_v$ of the gas, where c_p and c_v are the specific heats at constant volume and constant pressure. This means that in situations in which the gas composition is varying or unknown (e.g. with a cryogen partially pressurized with helium gas), accuracy would be degraded. When we discussed this limitation with NASA-JSC, we were told to proceed, since many or all of the future space cryogenic systems planned for Space Station would be pressurized with their own vapor.

It is important to distinguish between the classical "PVT" technique of measuring the temperature and pressure of the tank pressurant and the adiabatic compression gaging approach considered here. Adiabatic compression differs from the PVT method in two key respects:

- Varying the volume cyclically allows ac signal processing tech- nqiues to achieve much higher sensitivity than is possible with dc techniques.

- Varying the volume at a frequency such that the compression is nearly adiabatic rather than isothermal avoids problems with con- densation of the vapor, thereby allowing the method to be used with cryogens.

The PVT method has been used with some success in flight systems that are pressurized before launch and simply "blow down" as the tank contents are consumed, but was not considered by this program because it is not applicable to Space Station systems that will be refilled in flight.

3.5   CHOICE OF COMPRESSION IMPLEMENTATION

Fluid gaging by measuring the compressibility of the ullage bubble can be implemented in two fundamentally different ways:

- By measuring the amplitude of the compressibility

- By measuring the frequency of a mechanical resonance that depends on the compressibility.

We used the amplitude implementation as the strawman when evaluating the compressibility techniques during the first and second cuts at concept selec- tion because it was the simpler of the two to analyze. Once we had confirmed that the underlying physics permitted compressibility to achieve the required accuracy independently of the liquid location, we performed the tradeoff between the two implementations.

We developed a new resonant gaging concept that works well in theory, but found that the "driver" (the actuator/sensor attached to the tank) is fairly large, and that it presents severe and probably fatal mechanical design re- quirements. Preliminary work on the amplitude approach revealed that the

size and power required by the compressor are quite acceptable, so we have chosen to pursue the amplitude scheme on this program.

After settling on amplitude measurement as the concept to pursue, we had to choose a specific configuration for the breadboard test hardware. Section 3.5.6 presents the options we identified, and shows why we adopted a simple crankshaft mechanism for the compression driver. We were focusing on our short-term testing needs, but it is likely that a thorough tradeoff for flight application would reach the same conclusion because of the inherent simplicity and low risk of this approach.

3.5.1   Resonance Gaging Concept

The basic idea behind the resonance approach to compression gaging is to measure frequency instead of signal amplitude. Because this is frequently easier, it was thought to offer the possibility of achieving adequate accuracy with a smaller change in the bubble volume, and therefore smaller and lighter driving mechanisms for large storage tanks.

Our resonance gaging system concept is shown schematically in Figure 3-5. A flexible diaphragm is connected to an actuator which applies a known force and measures the position of the diaphragm. The control system operates in such a way that the "spring constant" of the system and its effective inertia are measured separately. (The damping of the system may or may not be measured.) Since the bubble volume computation depends only on the spring constant, it is independent of the variable inertia.

In concept, this could be done by driving the diaphragm with a known force at three or more frequencies near resonance, and mapping out the "tuning curve" of its amplitude response. This would give us three equations in three unknowns (mass, spring constant, and damping), and we could solve them. An alternative used here applies a variable amount of electrical feedback to alter the effective spring constant, thereby shifting the resonance. This eliminates any need to measure the magnitude of the force applied.
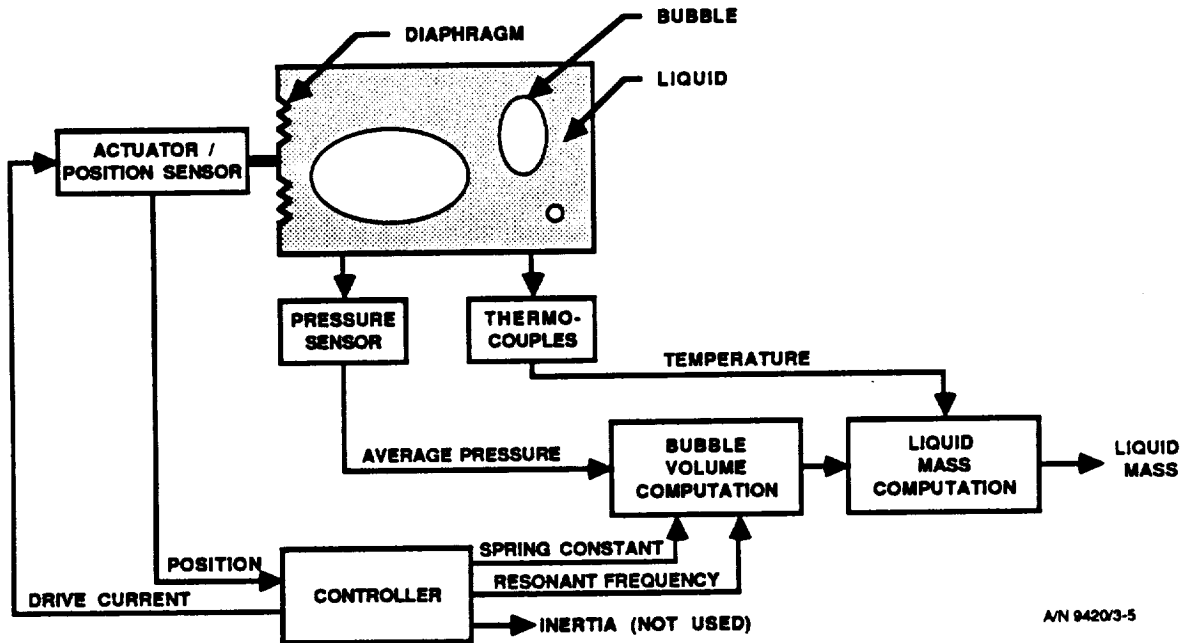
Figure 3-5 Resonance gaging concept

The fundamental difference between this approach and the Resonant Infrasonic Gaging System (RIGS) approach developed by TRW is that we use a control system and multiple measurements to separate the bubble compressibility (and hence volume) out from the diaphragm inertia. This is critical because the effective inertia of the diaphragm is higher when liquid is in contact with it than when it is not. This is a potentially fatal source of variability in zero g. TRW's approach to eliminating this "wet vs. dry" variability was to use a flexible bag to keep the liquid away from the diaphragm. This presents a serious materials problem when trying to apply the system to cryogens.

Further details and discussion of this concept are given in Appendix B. When the governing equations were worked out to permit sizing the driver, we did not take into account the cooperative bubble resonances later discovered during our testing of the amplitude measurement method. These same multiple bubble resonances would occur with resonance gaging. What their impact would be on this technique is unknown, but that may not matter since is appears to be impossible to build an acceptable resonance gaging driver.

3.5.2 Tradeoff Strategy

As we explored the resonance gaging concept, it became clear that might not have any size/mass advantage over the amplitude method. In order to complete the tradeoff between the two techniques as efficiently as possible, we therefore adopted the following strategy: We hypothesized that the amplitude method would win the tradeoff, and biased each piece of analysis in favor of resonance. This meant that we could use optimistic estimates for power and weight for resonance, and pessimistic ones for amplitude. Since the amplitude method won despite these biases, we knew that it would win for sure. Detailed designs were therefore not needed at this stage to complete the tradeoff.

3.5.3 Resonance Driver Requirements and Sizing

For purposes of this tradeoff, we examined the sizing and design requirements for the resonance driver, and we established that it must meet the following:

- Minimum resonant frequency not less than 1 Hz. This allows analog electronics to be used, and keeps the measurement time reasonably short.

- Maximum resonant frequency less than 0.9 times the minimum bubble resonance. This is necessary to prevent the gage resonance from being distorted by the bubble resonance. (This requirement may be too weak if there is significant damping of the bubble resonance.)

- Diaphragm area large enough that the "spring rate" of the largest bubble is no less than the spring rate of the diaphragm. This prevents the accuracy of the system from being degraded by uncertainties in the diaphragm spring rate.

- Variations in the thickness of the liquid layer contacting the diaphragm due to movement of the liquid shifts the resonant frequency by no more than a factor of four. This prevents the accuracy from being degraded by uncertainties in the amount of electrical feedback applied.

The governing equations then tell us the minimum diaphragm area and mass required, plus the maximum acceptable spring constant. We then made the following optimistic assumptions to get a lower limit bound on the driver size and mass:

- Diameter of the driver assembly is 1.1 times the diaphragm diameter.

- Depth of the assembly is 0.25 times the assembly diameter.

- Mass is the diaphragm mass plus 3 mm aluminum walls and end caps for the assembly (6 mm for the largest one).

Table 3-2 shows the results for a range of tank sizes.

Table 3-2

RESONANCE DRIVER SIZING

Tank Volume (liters)	DIAPHRAGM		DRIVER ASSEMBLY			
	Area (cm^2)	Mass (g)	Diameter (cm)	Depth (cm)	Volume (cc)	Mass (Kg)
100	45	5	8.3	2.1	110	0.1
300	77	12	10.9	2.7	250	0.2
1,000	141	28	14.7	3.7	630	0.3
3,000	244	64	19.4	4.8	1,400	0.6
10,000	662	288	31.9	8.0	6,400	1.7
30,000	5730	7350	94.0	23.5	160,000	30.3

These constraints conflict with other requirements on the diaphragm. The diaphragm must be able to support the maximum pressure in the tank (a minimum of one atmosphere). Gas pressure on the outside can not be used to support this load because the spring rate of the trapped volume would dominate the resonance of the system. The largest diaphragm would therefore have to support a load of 5.8×10^9 dynes (13,000 lb), but can have a mechanical spring rate no higher than 3×10^6 dynes/cm (18 lb/in). This conflict in requirements has no solution that we have found.

3.5.4 Compression Driver Requirements and Sizing

For purposes of this tradeoff, a preliminary estimate was made of the size, mass, and power consumption of the amplitude method hardware required for a 30,000 liter tank. A first-cut error analysis showed that ΔV of one liter would provide one percent accuracy, so a preliminary layout was made of a driver of this displacement. The mass estimate of 10 Kg was doubled to account for the pressure sensor and electronics. The power dissipation of the driver was estimated to be 79 W on the basis of viscous drag at 10 Hz (the highest frequency anticipated) and using an off-the-shelf motor. The 5 W power consumption of the Stanford Lambda Point Experiment flight computer was quadrupled to arrive at 20 W as an upper limit to the dissipation of the pressure sensor electronics and digital signal processor.

3.5.5 Tradeoff Between Amplitude and Frequency Measurement

Table 3-3 summarizes the tradeoff between these two implementations of compression gaging. The issues listed on the left are the driving ones, and their relative importance for our purposes is indicated by the number of stars. Both methods are taken to be capable of delivering the required one percent accuracy independently of the location of the liquid. All numbers given are for the largest tank considered.

Contrary to our initial expectations, the amplitude driver is slightly smaller than the resonance driver, although physical size is not believed to be critical for what amounts to a small accessory to the tank. The masses are comparable, although both are far less than the "threshold of pain" corresponding to the mass of one percent of the fluid specified by NASA-JSC. Following our tradeoff strategy, the power dissipation of the resonance system was taken to be negligible, but the pessimistic limit on power consumption for the amplitude method also is well below the 1 KW threshold defined by JSC.

The principal discriminators between the two candidates turn out to be design complexity and development risk. The design of the amplitude method is straightforward, especially if a driver based on a simple crankshaft is used.

Table 3-3
AMPLITUDE VS. RESONANCE TECHNIQUE TRADEOFF

ISSUE	CRITICALITY	AMPLITUDE METHOD[6]	RESONANCE METHOD[7]
Accuracy		Meets requirements	Meets requirements
Size[1]	*	33 cm dia. x 36 cm	85 cm dia x 21 cm
Mass[2]	**	20 Kg	30 Kg
Peak power[3]	***	Less than 100 W	Assumed negligible
Design complexity[4]	***	Low. Straightforward for crankshaft version. TBD for linear motor version.	Medium. Non-standard control system. Driver complexity is TBD.
Development risk[5]	****	Low. All components have some track record.	Extremely high. Driver is totally new. Spring constant required for given area may make this impossible.

Notes:

1. All numbers given for 30,000 liter tank, the largest considered.

2. Threshold of pain is one percent of mass of liquid in full tank, or 300 Kg.

3. Threshold of pain given by JSC is 1 KW. Important to minimize power delivered to fluid for cryogens.

4. Drives development cost. Limited development budget turns this into risk of not completing development successfully.

5. This is risk of doing a lot of work and having it not work in the end. Includes possibility of being able to design for one size tank, but not others.

6. Pessimistic limits.

7. Optimistic limits.

The control system required for the resonance gage is feasible, but is non-standard and possibly complex. Design complexity is taken to be of high criticality for this tradeoff because it will drive the cost and the risk of cost growth in developing a family of gaging systems for different Space Station applications.

Development risk was taken to be the most critical discriminator because it represents the risk of not having flight units ready when expected, with potentially large cost and schedule impacts on larger Space Station systems. All of the components of the amplitude method have enough prior history, and the overall configuration is sufficiently straightforward, that the development risk is taken to be small. The resonance driver, however, is a totally new device. The fact that our analysis revealed a conflict in design requirements that we could not resolve in a short time does not prove that a solution is impossible, but the fact that the difficulty spanned several orders of magnitude leads us to assess its development risk as extremely high.

The issues of reliability, safety, life expectancy, maintainability, and impact on tank design do not appear to be primary discriminators between these two implementations, since it appears that either one could satisfy these requirements. We therefore judged the amplitude method to be the clear winner for the following reasons:

- Resonance offers no size or mass advantage.

- The control system needed for resonance is complex, and would add to the development cost.

- The mechanical design of the resonance driver is at least difficult, and may be impossible. This constitutes unacceptable design risk.

If later on an acceptable solution is found to the resonance driver design problems, it may be worthwhile to revisit this tradeoff. The power required for the resonance method is almost certainly less than what will be needed to

drive the compressor. But the <u>physics</u> of compression gaging is common to both implementations, so using the simpler implementation for this concept development/demonstration program is certainly the right thing to do.

3.5.6   Compression Driver Configuration

There are several possible configurations for an amplitude measurement system, as shown in Figure 3-6. A simple crankshaft mechanism giving a fixed ΔV had been baselined for purposes of analyzing compression gaging and trading amplitude versus frequency measurement techniques. But it is tempting to explore a compression driver that uses a linear actuator to give a more compact and lighter package.
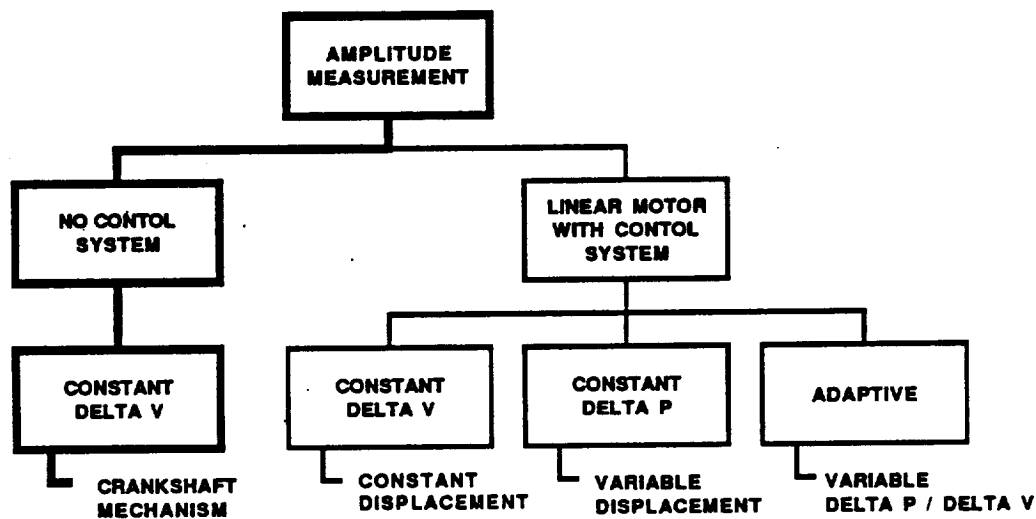
A/N 9420/3-6

Figure 3-6 Amplitude measurement options

We assumed that any linear actuator system would use a closed-loop servo system to control the piston stroke instead of mechanical stops for the sake of mechanical reliability. An electronic control system would then permit flexibility not possible with a crankshaft. The system could be set up for any of the following:

- Constant displacement, holding ΔV constant and measuring Δp

- Variable displacement, holding Δp constant and measuring ΔV

- Variable displacement to balance Δp and ΔV for maximum measurement accuracy, and measuring both of them

For the breadboard test program it was obvious that the control system development would consume resources without adding to our understanding of the compression gaging concept. When we explored the flight hardware issues, we became aware that this configuration tradeoff must be reanalyzed using the flight design selection criteria. We note, however, that the force requirement may lead to large windings or large currents for the linear motor, especially to provide the force required for a non-pressure-equalized design, thereby reducing any potential mass advantage of the linear system. Also, the control system adds considerably to the parts count, mass, and design cost of the electronics module, even though there is little design risk involved. The rotating crankshaft configuration offers simplicity, high reliability in controlling the non-repeatability in ΔV through bearing clearances, and the reliability of rotating bearings instead of reciprocating linear ones.

Section 4

DEVELOPMENT
of
COMPRESSION GAGING

Section 4

DEVELOPMENT OF COMPRESSION GAGING

In this section we describe the analysis and breadboard testing used to lay the foundation for flight hardware development. We outline the strategy used, and then present the theoretical analysis followed by the experimental results and their interpretation. For the sake of readability, many of the details are presented in the appendices cited.

4.1   DEVELOPMENT STRATEGY

In the concept selection process we used rigorous logic to find the gaging concept that is fundamentally capable of meeting the program requirements. The adiabatic compression technique selected had no prior spaceflight or development history, but is based on simple and well-understood physics. This allowed us to adopt the following development strategy:

- Quickly verify the correctness of the basic concept with preliminary tests.

- Build a detailed analytical model based on first principles, including all physical effects expected to be significant.

- Test the behavior of the system under conditions expected to stress its performance, comparing the output to the model predictions.

- Resolve all discrepancies between the observed behavior and the analytical model, refining the model and/or the measurements until no mysteries are left.

By emphasizing the correctness and completeness of the analytical model, we were hoping to develop maximum confidence that all physical processes relevant to the gaging system operation are accounted for, and thereby minimize technical and programmatic risk in developing the flight gaging system. The

data presented in Section 4.3 and in the appendices show that this goal was successfully met.

This approach amounts to adopting the scientific method of close interplay between theory and experiment. The test data was held to a higher standard than repeatability in reporting liquid mass; the absolute values of all measured quantities were compared to the theoretical predictions. Discrepancies were used as clues to help identify omissions from the analytical model or experiment defects. The close agreement ultimately obtained between the data and the model shows that the physical processes operating are now well understood.

The analysis from the concept selection process shows that the physics of adiabatic compression is essentially the same for all liquid/gas systems, with the differences between them being predictable from their known physical properties. The liquid/gas systems of practical interest for Space Station fall into two major classes:

- Ullage filled primarily with non-condensible gas (e.g., hydrazine/helium or water/air)

- Ullage filled primarily with condensible vapor of the liquid (e.g., cryogens or refrigerants stored at their vapor pressure)

The resources available for this program were adequate to do a thorough job studying one example of the first group, but would not permit studying the second group properly as well. We therefore settled on the water/air and water/helium systems for our breadboard testing. This allowed us to examine all of the thermodynamic and dynamic effects that are accessible in ground testing with the exception of vapor condensation, which is expected to be negligible. Additional testing with condensible vapor should be performed to confirm the analytical model for this case, but the maturity of understanding of the physics involved makes it unlikely that these experiments will produce significant surprises.

The breadboard testing began with table-top testing of system components on a small scale. Once this initial testing had established the validity of the basic compression gaging principle and the sensitivity achievable with the commercial pressure sensors, a 230-liter test system was built. Testing with this unit went through three phases:

- Operation at several fill levels to refine the mass calculation algorithm and to establish the achievable accuracy

- Operation under perturbed conditions to establish the effects of

  - Thermal properties of the ullage gas
  - Thermal stratification of the liquid and the ullage
  - Liquid in contact with the pressure sensor at various depths and orientations

- Detailed investigation of the effects of multiple bubbles

The first phase demonstrated the operation of the gaging system, and the last two refined and validated the analytical model.

4.2   ANALYTICAL MODEL

An extensive analysis of the physical processes associated with compression gauging was carried out as part of this study. There are three general conclusions:

- The signal depends weakly on bubble size and number. Accordingly, the method must be implemented in such a way that these size effects lead to errors smaller than the specified value.

- The system may have resonances which could distort the measurements and lead to appreciable errors. The compressor frequency must be chosen to avoid these resonant frequencies.

• It is possible to design the equipment and an algorithm for data reduction which avoids the problems associated with resonance and bubble size to achieve a 0.5 percent accuracy level.

This section contains an outline of the analysis on which these conclusions are based.

The equations which relate the measured variables of the compression method of gauging to the ullage volume are based on an analytic model of the system. The accuracy of our knowledge of the ullage volume is determined by the accuracy of both the experimental data and the model. The purpose of this section is to describe the model and to explain the various physical effects which are included in it.

The pressure rise accompanying compression of the ullage volume is the one primary physical effect which makes the compression method work. There are several secondary effects which must be included in the model to obtain results of a specified accuracy. Secondary effects are those which produce a small correction to the primary effect - roughly 10 percent or less. For the present application it is desired to build a model with an accuracy of better than 0.5 percent of tank capacity. All secondary effects which have been identified and which can have an effect larger than 0.5 percent of tank capacity for any anticipated fluid and any anticipated flight design will be discussed.

For an ideal gas which is confined and is undergoing adiabatic compression/expansion, the bubble volume V is related to the change in pressure Δp and the change in volume ΔV as:

$$V = -\gamma p \Delta V/\Delta p \qquad (4-1)$$

where p is the average pressure in the ullage and γ is the ratio of specific heats c_p/c_v. This formula results from combining the ideal gas law for an adiabatic process and the definition of compressibility. Equation (4-1) is the basic idealized formula of the compression method. This formula is independent of bubble size, shape and number; whether the bubbles are free or

attached to the wall or the interior structure of the tank; the distribution of bubble sizes; and the frequency of the compressor.

When the total volume of the bubbles is known from (4-1) the fluid mass, M, can be calculated from:

$$M = \rho_1(V_t - V) + \rho_g V \qquad (4\text{-}2)$$

where ρ_1 is the average density of the liquid, ρ_g is the density of the gas and V_t is the volume of the tank. Usually the second term in (4-2) is negligible.

The model consists of modifying equations (4-1) and (4-2) to include the significant secondary effects. These effects are classified into three categories:

- Appreciable thermodynamic effects
- Appreciable dynamic effects
- Negligible effects

4.2.1   Appreciable Thermodynamic Effects

Here we discuss those secondary effects in which temperature plays a role but the fluid dynamic effects which depend on the inertia of the liquid do not.

4.2.1.1   Acoustic Boundary Layers

The ullage volume has interfaces with the liquid and/or the structure of the tank. Equation (4-1) is based on the assumption that no energy or mass is transferred across the interfaces. It also assumes that the interfaces do not move during measurement; these conditions are not satisfied exactly.

When the ullage is compressed it gets warmer and heat is transferred to its surroundings. At a gas-liquid boundary, the interface moves as the gas is compressed; there is a flow of heat and an exchange of mass due to diffusion of dissolved gases and condensation/evaporation of the stored fluid. When

the compression is driven sinusoidally, boundary layers with nonuniform temperature and/or composition form. At a solid surface there is a thermal boundary layer in both the gas and the solid. At a gas-liquid interface there are thermal and concentration boundary layers in both the gas and the liquid. The boundary layers in the latter case are not referenced to a fixed surface in space since the interface moves under dynamic pressure unbalance and condensation/evaporation.

The objective, then, is to incorporate these physical processes into the model. The analysis is simpler when the boundary layers do not overlap. For air and water at a compression frequency of 1 Hz the boundary layer lengths are of order 1 mm. For practical applications the smallest bubbles which contribute significantly to the total volume are much larger than a few millimeters. In that situation a theory without overlap is sufficient. This case will be modeled first and the more general case will be considered later.

The compressibility $\Delta V/V\Delta p$ of the gas inside the boundary layers is not equal to the adiabatic value of $1/\gamma p$ used in equation (4-1). It varies exponentially from a value $1/\kappa_i p$ at the interface to $1/\gamma p$ at the outer edge of the layer. With ideal heat transfer, the compressibility would approach the isothermal value $1/p$ at the interface. The dependence is exponential because the equations governing all the thermodynamic variables at the interface are of the constant coefficient diffusive type. Each boundary layer is characterized by two parameters: the boundary layer length, d, and the value of κ_i at the interface. If we represent the compressibility of the gas as $1/\kappa p$ then κ goes from κ_i at the wall to γ at a distance $\gg$ d. In fact:

$$1/\kappa = 1/\gamma + (1/\kappa_i - 1/\gamma) \exp[(i-1)y/d] \qquad (4-3)$$

where y is the distance from the interface.

The compressibility measured by Δp is a volume average over the entire ullage. A volume average of κ over a flat interface gives:

$$\kappa_{av} = \frac{\gamma}{1 + \dfrac{(1+i)}{2V}\left[(\gamma/_{\kappa_{i1}} - 1)A_1 d_1 + (\gamma/_{\kappa_{i2}} - 1)A_2 d_2 + \dots\right]} \qquad (4\text{-}4)$$

where A_j is the area of an interface and d_j is the boundary layer distance for that boundary layer. The solid/gas interface has one term in equation (4-4) and the liquid/gas interface has two terms. Since under most circumstances both types of interface occur in the same tank, three terms are necessary. Note that $1 < \kappa_{av} < \gamma < 5/3$.

The boundary layer distances d_j all vary with the compressor frequency, f, as $d = d_o/f^{1/2}$ where d_o is a constant. Then κ_{av} can be written:

$$\kappa_{av} = \frac{\gamma}{1 + \dfrac{(1+i)C}{2\,f^{1/2}}} \qquad (4\text{-}5)$$

and the basic formula (4-1) is modified to:

$$V = \frac{-p\gamma\Delta V}{\Delta p\left[1 + \dfrac{(1+i)C}{2\,f^{1/2}}\right]} \qquad (4\text{-}6)$$

Comparing (4-4) and (4-5):

$$\frac{(1+i)C}{2\,f^{1/2}} = \left[(\gamma/_{\kappa_{i1}} - 1)\frac{A_1 d_1}{V} + (\gamma/_{\kappa_{i2}} - 1)\frac{A_2 d_2}{V} + \dots\right] \qquad (4\text{-}7)$$

The physical significance of C is the fraction of the ullage volume in the boundary layer multiplied by the deviation of the compressibility from adiabatic.

It is not necessary to know the A_j, κ_{ij}, and d_j to find C, since C can be measured by the apparatus. If two measurements are made at different frequencies, the value of V will not change. Equating V at f_1 and f_2 in equation (4-6) results in an equation for C in terms of f_1, f_2, Δp_1, and Δp_2. Accordingly, the boundary layer effect will drop out of the problem if measurements are made at two frequencies.

In discussing the boundary layers so far, we have assumed a flat interface. At a corner the boundary layers from each surface overlap and the volume in the boundary layer is overestimated by a factor proportional to d^2. This adds a term to κ_{av}:

$$\kappa_{av} = \frac{\gamma}{1 + \frac{(1+i)C}{2\ f^{1/2}} - \frac{D}{f}} \qquad (4\text{-}8)$$

When a detailed analysis of a curved surface is made, the curvature introduces three terms into κ_{av}. For the most complicated interface shape:

$$\kappa_{av} = \frac{\gamma}{1 + \frac{(1+i)C}{2f^{1/2}} - \frac{D}{f} + \frac{E}{f^{3/2}}} \qquad (4\text{-}9)$$

The measuring formula (4-6) then has the same denominator as (4-9). In this case measurements at four frequencies would be are necessary to evaluate C, D, and E. However, in practice it is only necessary to find C because C << D << E. In our experiments at 90 percent full and f = 1 Hz, where these effects are the largest, C produces a 6 percent correction in bubble volume, $D \simeq 0.1\ C$, and $E \simeq 0.1\ D$. In a later section experimental data will be presented to show that C and D agree well with the theoretical values. A more detailed discussion of the boundary layer theory is found in Appendix C.

The significance of this analysis is that it shows that it is not necessary to know the boundary layer parameters and the interface areas to make accurate liquid mass measurements. The unknowns are found as part of the measuring process. When this theory applies, the dependence on bubble size is made a part of the measuring formula (4-6) and does not cause an error.

This theory only applies when the boundary layers from opposite sides of the ullage envelope do not overlap. A rough estimate of the thickness of the thermal boundary layer can be made by studying the case where the thermal boundary dominates. Then $d_t = (D_t/2\pi f)^{1/2}$ where D_t is the thermal diffusivity and f the frequency. The diffusive boundary layer thickness $d_d = (D_d/2\pi f)^{1/2}$ where D_d is the diffusion constant of the vapor in the backfill gas. For the fluids studied here D_t varies from 10^{-2} to 10^{-1} cm^2/sec, and D_d

from 10^{-1} to 6×10^{-1} cm^2/sec. At 1 Hz the boundary layer lengths are both about 1 mm.

4.2.1.2 Property Variations

The basic formulas (4-1) and (4-2) contain variables which are not measured directly: γ, ρ_1 and ρ_g. These parameters change with pressure, temperature and ullage composition. Since ρ_g is so small compared with ρ_1, variations in ρ_g may be neglected at the 0.5 percent accuracy level. Likewise, the pressure dependence of γ and ρ_1 is sufficiently weak so that it can be neglected. The model must include thermal and compositional variations of γ and thermal variations of ρ_1. The basic formulas do not require a change of form to model the property variations. It is only necessary to use the volume averaged values of the parameters.

The pressure p is measured, but for ground-based testing it must be corrected for any pressure head difference between the gauge and the ullage volume. This correction is not necessary for space operation and will not be included in the model as shown here.

4.2.1.3 Composition Variations

The composition of the ullage volume for unsaturated storage depends on the vapor pressure of the stored liquid. The partial pressure of the stored vapor in the ullage gas equals the vapor pressure of the liquid at the temperature of the gas-liquid interface. If the value of γ for the vapor, γ_v, differs from that of the backfill gas, γ_b, the effective average value of γ is:

$$\gamma = \frac{\gamma_v \, p_v}{p_o} + \frac{\gamma_b \, (p_o - p_v)}{p_o} \tag{4-10}$$

where p_v is the vapor pressure and p_o is the total pressure which is measured. Since this is usually a small correction, a rough measurement of the ullage temperature is all that is required to look up p_v.

4.2.1.4   Thermal Stratification

When the ullage consists of several bubbles and each bubble is surrounded by liquid at a different temperature, it is not obvious what temperature to use to look up γ. For an ideal monatomic gas like helium or argon, the only internal motions are electron transitions. These occur at very high temperatures (>1000 K), so both c_p and c_v are independent of temperature at the anticipated storage temperature. A very weak dependence of γ on temperature occurs because all gases are nonideal. But unless the storage conditions are near the critical point, the correction for monatomic gases is less than 0.5 percent for an expected maximum thermal stratification of 10K.

For polyatomic gases, dc_v/dT can become appreciable if there are internal energy levels of the molecule close to kT, the Boltzman constant times the storage temperature. If there are no levels within $\pm 2kT$, then γ is constant to within 0.5 percent for a worst case stratification of 10K and again the correction can be neglected. The problem remains for some polyatomic gases.

The error in the measured ullage volume ΔV_e for a maximum ΔT is:

$$\frac{\Delta V_e}{V} = \frac{-\Delta c_v}{c_v} = \frac{-\Delta \gamma}{\gamma} \qquad (4-11)$$

Experimental data on $\Delta \gamma / \Delta T$ are usually derived from measurements of the speed of sound in the gas, c. A thermodynamic identity for an ideal gas states:

$$\frac{\Delta \gamma}{\gamma} = \left[\frac{2\Delta c}{c\Delta T} - \frac{1}{T} \right] \Delta T \qquad (4-12)$$

For each application it is necessary to find $\Delta \gamma / \Delta T$ at the storage condition, estimate the maximum thermal contrast and calculate $\Delta V_e/V$.

Thermal stratification also causes an error in equation (4-2) because $d\rho_1/dT \neq 0$. In most cases $d\rho_1/(\rho_1 dT) < 10^{-3}/K$. A 5 K thermal contrast in the tank then causes an error of less than 0.5 percent in equation (4-2). If the thermal expansion coefficient is large and the thermal stratification is also

large, a thermometer array may be necessary to achieve the desired 0.5 percent accuracy.

4.2.1.5   Tank Compressibility

When the tank and/or the liquid have a compressibility that is larger than 0.5 percent that of the gas, equation (4-1) must be modified. The displacement of the compressor ΔV_c, the change in the volume of the ullage ΔV, the tank expansion ΔV_t, and the liquid compression ΔV_l are related as:

$$\Delta V_c = \Delta V + \Delta V_l + \Delta V_t \tag{4-13}$$

The compressibility of the tank is normally a constant:

$$\frac{\Delta V_t}{\Delta p V_t} = K_t \tag{4-14}$$

Also, the compressibility of the liquid is constant:

$$\frac{\Delta V_t}{\Delta p V_l} = K_l = \frac{1}{\rho_l c_l^2} \tag{4-15}$$

where ρ_l is the density of the liquid and c_l is the speed of sound in the liquid. Solve (4-14) for ΔV_t and (4-15) for ΔV_l, replace in (4-13), solve for ΔV and insert the result in equation (4-1):

$$V = \frac{p\gamma \left[\dfrac{\Delta V_c}{\Delta p} - (K_t + K_l)V_t \right]}{1 - p\gamma K_l} \tag{4-16}$$

Since for all the liquids considered here, including hydrogen, the correction due to K_l is much less than 0.5 percent, equation (4-2) can simplify (4-16) and combining with (4-9) with $E = 0$:

$$V = \frac{p\gamma \left[\dfrac{\Delta V_c}{\Delta p} - K_t V_t \right]}{1 + \dfrac{(1+i)C}{2\,f^{1/2}} - \dfrac{D}{f}} \tag{4-17}$$

4.2.2   Appreciable Fluid Dynamic Effects

Here we discuss those secondary fluid dynamic effects which depend on the inertia of the liquid.

4.2.2.1   Resonances

There are two resonance effects associated with the ullage bubbles which require significant modifications of the basic formulas. The compressor forces the bubbles to oscillate in radius; the mass of the liquid that oscillates is restrained by the compressibility of the bubble. This constitutes a mass-spring system, and is referred to as single-bubble resonance. Another similar resonance occurs when two or more bubbles oscillate out of phase, with one expanding while the other contracts. This is similar to a coupled set of masses and springs, and is called a cooperative bubble resonance. The effects of resonances in general on compression gaging are discussed in detail in Appendix E.

Single-Bubble Resonances

The resonant frequency for a single bubble f_r is well known:

$$f_r = \left[\frac{3\gamma p}{\rho_1}\right]^{1/2} \left[\frac{1}{6\pi^2 V_o}\right]^{1/3} \qquad (4\text{-}18)$$

where V_o is the volume of the bubble. For large bubbles f_r can be close to the driving frequency, f. When this occurs equation (4-17) must be multiplied by the resonance factor and becomes:

$$V = \frac{p\gamma \left[\frac{\Delta V_c}{\Delta p} - K_t V_t\right]}{\left[1 + \frac{(1+i)C}{2\,f^{1/2}} - \frac{D}{f}\right]} \cdot \frac{f_r^2}{(f_r^2 - f^2 + 2if\epsilon)} \qquad (4\text{-}19)$$

where ϵ is the damping factor of the resonance. The unknowns C, D, f_r and ϵ can be found by the equating V measured at four different frequencies.

Cooperative Resonance

It is impossible to have a single-bubble resonance in a closed tank because the bubble must stay in phase with the compressor because of mass conservation. It is therefore necessary to have at least two bubbles in a tank for resonance. The cooperative resonance was not reported in the literature prior our observations, and its theory has been worked out here to explain the data of this study. The detailed theories for multiple spherical bubbles, spherical segments, and cylindrical bubbles are found in Appendices F and G.

With two or more bubbles in the tank, the volume change of all the bubbles must add to the compressor displacement. Consider spherical bubbles of radius $R_i = R_{oi}(1 + X_i)$ where X_i is the fractional amplitude of the radial oscillation of the bubble i. Then,

$$4\pi \sum_i R_{oi}^3 X_i = \Delta V_c \qquad (4\text{-}20)$$

The equation of motion for x_i for an individual bubble is well known:

$$\rho_1 R_{oi}^2 \ddot{X}_i + 4\mu \dot{X}_i + (3\kappa_i p_{oi} - 2\sigma/R_{oi})X_i = P \qquad (4\text{-}21)$$

where μ is the viscosity of the liquid, p_{oi} is the equilibrium pressure in the bubble, σ is the surface tension and P is the instantaneous pressure in the liquid. Each bubble oscillates according to (4-21) and equation (4-20) couples the oscillations of all the bubbles to cause a cooperative resonance. If we assume a sinusoidal driving force of angular frequency ω, (4-21) can be written as:

$$L_i X_i \equiv [-\rho_1 R_{oi}^2 \omega^2 + 4i\mu\omega + (3\kappa_i p_{oi} - 2\sigma/R_{oi})]X_i = P \qquad (4\text{-}22)$$

The coupled equations, if the pressure transducer is in bubble i = 1, are:

$$L_1 X_1 - L_i X_i = 0 \qquad i = 2,3 \cdots n$$

$$\qquad (4\text{-}23)$$

$$R_{o1}^3 X_1 + R_{o2}^3 X_2 + \cdots = \Delta V_c/4\pi$$

The resonance occurs when the determinant of this set equals zero.

The lowest resonance occurs when the ullage volume is concentrated in two bubbles of nearly the same size. In that case the resonant frequency is:

$$\omega_r = (3p\gamma/\rho_1)^{1/2} /R_o \tag{4-24}$$

If most of the ullage is in two large bubbles, the response curve is:

$$X_1 = \frac{L_2\Delta V}{V_1L_2 + V_2L_1} \tag{4-25}$$

where V_i is the volume of bubble i. The measured pressure depends on whether the pressure transducer is connected to bubble number 1, bubble number 2, or the liquid.

In order to correct the measurement formula for the cooperative resonance, it would be necessary to know the L_i of the large bubbles, plus where the transducer is connected in relation to the bubbles. It would be possible in theory to find this information by measuring a frequency response curve. However, since each L_i has two parameters and the number of L_i which are important is not known, it appears impractical to correct for the cooperative resonance. It is therefore necessary to use the theory to calculate the lowest resonance and to operate at a frequency about one decade below the resonance. The gage operation will then not be affected by bubble resonance, but the potential for resonance imposes a limit on the range of frequencies that can be used.

The acceptable frequency range has an upper and lower bound. The lowest acceptable frequency is that for which the boundary layers begin to overlap; the upper bound is that for which the resonance factor is 1.005, that is 0.07 f_r. The lowest cooperative resonance can be estimated from equation (4-24). In the worst case: $V_i \simeq V_2 \simeq V_t/3$; $p_1 \simeq p_2$ and $R_1 \simeq R_2$. Then (4-24) reduces to:

$$f_r = (3p\gamma/\rho_1)^{1/2} \frac{0.23}{R_t} \tag{4-26}$$

where R_t is the radius of the tank. For air and water at STP, $f_r \simeq 4.7 \times 10^2 / R_t$ with R_t in cm. A tank of 2 m diameter should be operated at a frequency below about 0.33 Hz and above about 0.01 Hz when it is nearly empty. Higher frequencies could be used at higher fill levels.

4.2.2.2   Tank Acceleration

The storage tank will move in response to the random acceleration of the space structure to which it is attached. Motion of the tank does not produce radial oscillations of the ullage volume because the volume of the tank does not change; this driving force is therefore dipole or higher. The compressor which does produce bubble compression is a monopole driver. Tank motion causes motion of the bubble as a whole and distortion of the bubble from the usual spherical surface. These motions do not produce pressure changes in the bubble; they do produce a hydrostatic head in the liquid in the direction of the acceleration. If the pressure gauge is in line with the tank acceleration, it will record an additional pressure of $\rho a h$, where h is the height of the liquid "above" the gage in the direction of acceleration, and a is the acceleration.

For a 3 m tank the pressure resulting from an acceleration of 10^{-3}g (typically experienced on the Space Shuttle) can reach 0.2 torr for fluids with a density close to that of water. The Δp compression gaging signal for a nitrogen tank 90 percent full would be about 1 torr. Random tank motion can therefore generate a noise signal comparable to the Δp generated by the compression driver.

This noise signal is not coherent with the signal generated by the compressor. Therefore, the lock-in amplifier will integrate the noise disturbance to zero eventually. However, the data acquisition time may need to be longer in a random acceleration environment than on earth. The tank motion does not change the model equation, but it must be considered when choosing the integration time.

An acceleration can also be caused by an unbalanced compression driver. If the tank and compressor apparatus are not properly designed, the tank could

move measurably in response to the compressor. A tank acceleration of 10^{-3}g, which corresponds to a displacement of 0.25 mm at 1 Hz, causes a Δp of 0.08 torr in a tank of 1 m diameter. This signal is about 1/3 of the compression signal from a tank 50 percent full. A compressor-induced acceleration pressure is coherent with the compressor and is not removed by signal processing. Careful design of the system can control this effect.

4.2.2.3   Pressure Transducer Resonance

For the breadboard test unit the commercial pressure transducer consists of a metallic diaphragm connected to the tank by a long, narrow lead-in tube. The pressure measured by the gauge will match that in the tank only at zero frequency because the diaphragm is a mass-spring resonant system. The resonance curve has been calculated for three situations: gas in the lead-in tube, liquid in the tube, and liquid with a bubble in the tube. The calculations are given in Appendix H.

When the gauge and lead-in tube contain gas, the resonant frequency of any practical pressure gage is very high compared to the compressor frequency. When the gauge is filled with liquid, the mass which resonates is much greater and the resonant frequency is much lower. The natural frequency and damping constant for a gauge filled with liquid is found to be:

$$\omega_n = (\pi R^2 k / \rho L)^{1/2} \; ; \qquad \varsigma = \nu D / 2 \omega_n \qquad (4\text{-}27)$$

where

$$D = \frac{2 \, (C/R) \, [J_1(CR)/J_o(CR)]}{1/2 - (1/RC) \, [J_1(CR)/J_o(CR)]} \; ; \qquad C^2 = -i\omega/\nu$$

where L is the length of the lead-in tube, R the radius of the lead-in tube, ρ the density of the liquid, ν the kinematic viscosity of the liquid, and k = Δp/ΔV of the diaphragm chamber.

The effect is to add a resonance term to the right hand side of equation (4-17) like that in (4-19). To avoid significant errors, it is therefore necessary to design the pressure transducer to keep the wet resonance at

least 15 times the highest frequency at which the gaging system will be operated. Appendix H shows that this is easily done by enlarging the lead-in tube and keeping it short, or by eliminating it altogether.

4.2.3   Negligible Effects

There are several effects that produce errors in V of less than 0.5 percent for any well thought out design. The purpose of this section is to document the calculations that have been made to verify that these effects are small.

4.2.3.1   Vapor Condensation

At first glance it would seem that compression gaging would be difficult to apply to cryogens or other fluids stored at saturation pressure because of vapor condensation. Indeed, compressing the bubble isothermally would cause condensation with no pressure rise. The fact that the compression is done at a frequency such that it is nearly adiabatic causes three things to happen:

- Condensation occurs on the decompression stroke instead of the compression stroke because dT/dp is larger for adiabatic compression than for the liquid/gas saturation line.

- The maximum fraction of the vapor that can condense is limited by the fact that the total entropy of the system does not change.

- The actual condensation will be less than this upper limit because the rate of condensation is limited by nucleation processes and by the fact that the heat of vaporization liberated at each droplet will create a local hot spot until it can diffuse away.

For $\Delta V/V = 1 \times 10^{-4}$, the upper limit on the fractional error introduced is 2×10^{-5} for hydrogen, the worst case, and 1×10^{-5} for nitrogen.

4.2.3.2 Tank Leakage

Tanks fabricated for use in space will have a negligible leak rate, but prototypes and ground test equipment may not be leak tight. It is therefore useful for diagnostic purposes to know how leaks affect the data. The analysis is similar to that for tank compression. From conservation of mass:

$$\frac{dV_c}{dt} = \frac{dV}{dt} + \frac{dV_1}{dt} + \frac{dV_t}{dt} + Q \qquad (4\text{-}28)$$

where Q is the leak rate. Recall that the compressor is driven sinusoidally so that $dV_c/dt = i\omega\Delta V_c$. Solving for V and neglecting compression of the tank and liquid:

$$V = \gamma p\left[\frac{\Delta V_c}{\Delta p} + \frac{Q}{i\omega\Delta p}\right] \qquad (4\text{-}29)$$

This shows that $\Delta V_c/\Delta p$ alone underestimates the ullage volume and that the error increases as the frequency gets lower. $Q/\Delta p$ is a constant divided by the length of the slit for laminar viscous flow, which is what would be anticipated for a leak. The details of the calculation are found in Appendix I.

4.2.3.3 Transport Effects at Liquid-Gas Interfaces

If the liquid contains a dissolved impurity gas or if a backfill gas is used which dissolves in the liquid, the concentration in the bubble will depend on the pressure amplitude. As a bubble oscillates the pressure swings from $+\Delta p$ to $-\Delta p$ and the pressure is positive for the same time interval as it is negative. The radius of the bubble changes from $R-\Delta R$ to $R+\Delta R$; the area therefore is larger when the pressure is negative than when it is positive. Therefore there is a net diffusion of dissolved gas into the bubble, and this must be balanced by an increase in the transport out of the bubble by diffusion. This is called "rectified pumping by the acoustic field."

Rectified pumping of heat also occurs for the same reason. An equilibrium is reached at a concentration or temperature above that when the acoustic field is not present. The excess above the zero frequency values of C_o and T_o is:

$$C = C_o \left[1 + \frac{2}{3}\left(\frac{\Delta p}{p}\right)^2\right] \quad ; \qquad T = T_o \left[1 + \frac{2}{3}\left(\frac{\Delta p}{p}\right)^2\right] \qquad (4\text{-}30)$$

Both of these variables affect the value of γ. Since the gaging system operates with $\Delta p/p$ in the range 10^{-4} to 10^{-3} these effects are negligible.

4.2.3.4 Surface Tension and Viscosity Effects

The p in the various formulas above refers to the average pressure in the ullage volume. When the pressure transducer is in contact with the liquid it measures the liquid pressure. The two pressures differ due to surface tension σ and the viscosity of the liquid μ_1. If the bubble surface is nearly spherical of radius R:

$$p = p_1 + \frac{2\sigma}{R} + \frac{4\mu_1}{R}\frac{dR}{dt} \qquad (4\text{-}31)$$

For an oscillating bubble it is easy to show that the last term is $(4/3)\mu_1(\Delta V/V)2\pi f$. For the liquids considered, hydrazine has the largest σ at 92 cgs and nearly the largest μ_1. In this case the correction terms are less than 0.1 percent at 1 Hz for $R > 2$ mm.

The effective compressibility is a volume average over bubble sizes. The total volume of bubbles with $R < 2$ mm is very small. For all anticipated applications the pressure jump across the bubble interface is therefore negligible.

Motion of the tank and other disturbances may generate surface waves at the ullage interfaces. These perturbations will cause the curvature of the surface to deviate from the spherical shape. The curvature from point to point will vary, but an average over the entire bubble will be very close to $2/R$. Thus, the distortion will not change the pressure. When a bubble touches a solid surface, the part of the bubble in contact with liquid will be spherical; the correction is therefore the same as that for a spherical bubble.

For ground testing it might be desirable to simulate the ullage geometry found in space by using balloons tethered in the test tank. (Note: We do not recommend this; when we tried it, we found that the "bubble" geometry and

F88061Ø2AC4-19

conditions were far less controlled than with rigid cups.) In this case the balloon acts like an interface with large surface tension. It is easy to show, using equation (4-31), that equation (4-1) can be written in terms of p_1 instead of p as:

$$V = -p_1 \gamma \frac{\Delta V}{\Delta p_1} \left[1 + \frac{2\sigma}{Rp_1} \left(1 - \frac{1}{3\gamma} \right) \right] \tag{4-32}$$

There is no correction if the pressure transducer is in the bubble. The derivation of (4-32) is found in Appendix J.

4.2.3.5 Property Variations Due to Impurities

It was noted above that variations in γ and ρ_1 can affect the measurements significantly. The anticipated temperature variations can under some circumstances produce changes in both parameters at the 0.5 percent level. Impurities cause composition changes which may be larger than 0.5 percent if sufficient impurities are present. It does not appear practical to measure the impurity concentration at each fluid transfer and to correct γ and ρ_1; it is better to specify the purity level for the fluid. Since the two parameters each enter the measuring formulas as first order factors, the fractional errors add. If the values of the parameters of the impurities are close to those of the stored fluid, the concentration of impurities can be fairly high. The mixture values depend linearly on the mole fraction, x, of the contaminants:

$$\gamma = \gamma_1 + (\gamma_2 - \gamma_1)x_2 \tag{4-33}$$

For most of the anticipated combinations of stored fluid and impurities and for large bubbles, a 2 percent mole fraction of impurity produces a negligible effect.

Impurities affect saturated systems in a different fashion. For a saturated system, small bubbles will collapse and the main large bubble will expand because of the excess pressure in small bubbles. However, if an impurity gas is present, only the vapor of the saturated liquid can condense. As the bubble shrinks the concentration of the impurity will increase and the bubble

will reach an equilibrium when it contains mostly the impurity. The equilibrium radius is determined by a balance between the bubble pressure $p = p_1 + 2\sigma/R$ and the solubility of the impurity in the liquid $c_a a p$, where a is Henry's constant. Then, $R = 2\sigma/(c_a/a - p_1)$ for a saturated solution. Collapse of the saturated bubbles creates small bubbles consisting entirely of impurities. By this mechanism impurity gases which are soluble in the liquid are removed from solution.

Impurities can also have a strong effect on surface tension. A layer two or three molecules thick at the interface can increase the surface tension by a factor of ten. In the last section it was shown that an error in the pressure results from a pressure jump of $2\sigma/R$ across the interface. It was stated that for most fluids a 0.1 percent error occurs if $R < 2$ mm. If σ increases by a factor of 10, the limiting radius is $R < 2$ cm. It is then quite possible that an appreciable fraction of the ullage might be in bubble smaller than this size and an appreciable error could occur.

Another effect of impurities is the modification of evaporation rates. This is important only for saturated systems. Surface acting substances in very small concentration can impede evaporation by a factor of 100 or more. Evaporation restores levels an out-of-equilibrium vapor pressure with the speed of sound. Accordingly, all theoretical work on bubble dynamics assumes that the vapor pressure in the bubble follows the changes in the liquid pressure immediately. If an impurity slows down the evaporation rate by a factor of 100, the departure from the ideal behavior of (4-1) becomes smaller.

4.2.3.6   Liquid Compressibility

The compressibility of the liquid was considered above in section 4.2.1.6 along with the compressibility of the tank. There it was shown that the fractional error in neglecting the liquid compressibility is $V_t p \gamma / V \rho_1 c_1^2$. Even for hydrogen, the most compressive liquid considered here, the error is negligible until the tank is about 99 percent full. A more thorough discussion of the effect of the compressibility of hydrogen on gauging is found in Appendix K.

4.2.3.7   Nonideal Gas Behavior

The model assumes that the gas is ideal. For most gases this is a good assumption at the 0.5 percent error level for the usual storage temperatures, or until the pressure gets above about 75 percent of the critical pressure. When the gas is closer to the critical point, other forms of the gas law have to be used. There are several approximate formulas which give good agreement with experiment; the most popular is the Van der Waals formula, for which equation (4-1) becomes:

$$V - bM = -\gamma p \ \Delta V/\Delta p \tag{4-34}$$

where b is the second Van der Waals constant per gram for the gas considered. Only the left hand side of the equation is affected. The corrections which appear on the right hand side, such as equation (4-19), are not changed to first order by the nonideal behavior of the gas.

Also, when considering thermal stratification with a Van der Waals gas:

$$c_p - c_v = R \left[1 + \frac{a \ (v - b)^2}{v^3 RT} \right] \tag{4-35}$$

where a is the first Van der Waals constant for the gas. In this case c_v is still constant but γ has a slight thermal dependence.

When the storage condition is not close to the critical point, these effects are negligible. If desired, the nonideal effects could be included in the measuring formula to remove this source of error.

4.2.3.8   Finite Driving Force Amplitude

It has been assumed above that any nonlinear equations used in the analysis can be linearized. Nonlinear effects can occur when $\Delta p/p > 0.1$. For strong driving forces, the radius change becomes comparable to the radius since $\Delta R/R = -(1/3K)\Delta p/p$, and the full nonlinear equations must be used.

Table-Top Test Apparatus

As soon as adiabatic compression was selected, we assembled the Table-Top Test Apparatus shown in Figure 4-1. This unit consists of a miniature tank and compression driver mated to a pressure sensor head designed to fit directly on the larger Breadboard Apparatus. The tank consists of any of three different lengths of 6 in aluminum pipe sandwiched between end plates. The compression driver is a 0.5 in diameter steel dowel sealed by an o-ring in the base plate and driven through a lever with 4 possible pivot positions. This combination of variable tank volume and variable piston stroke gives 12 different $\Delta V/V$ ratios from 5×10^{-4} to 8×10^{-6}. This unit is usable dry or with water, with air or helium gas. Because of the stiff tank walls, it can also be operated significantly above or below atmospheric pressure, unlike the larger Breadboard Apparatus.
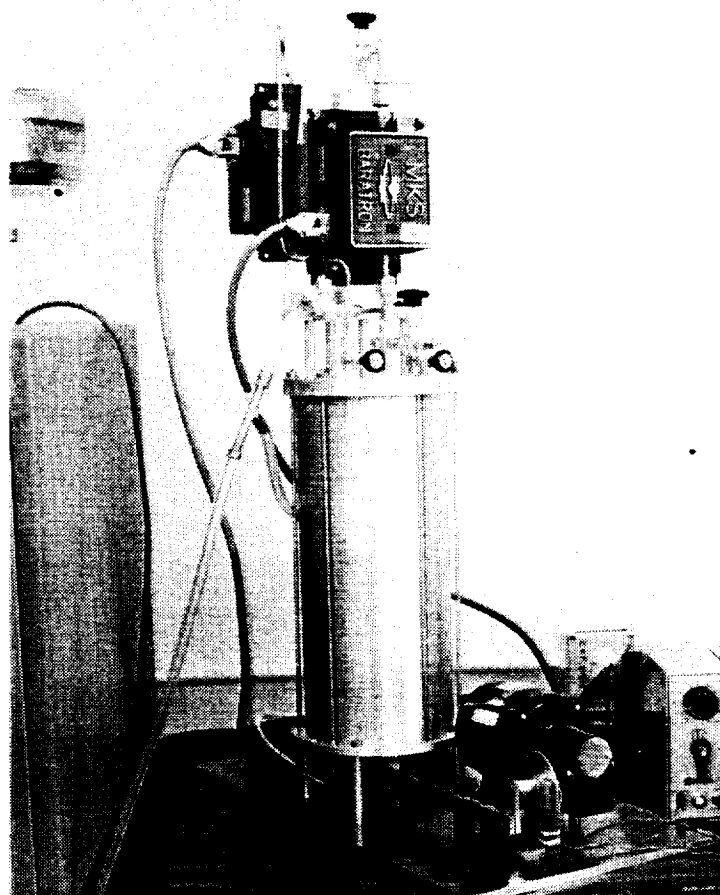
Figure 4-1 Table-top test apparatus

Initial tests were done with this unit to confirm the broad outlines of our starting-point analytical model of compression gaging. These tests revealed the following:

- The behavior of the system followed the analytical model as closely as expected, given the state of development of the acoustic boundary layer model at the time.

- The sensitivity of the absolute pressure sensor used to measure p was more than adequate to measure Δp as well. The noise level was such that we selected a $\Delta V/V$ ratio of 8×10^{-5} for the Breadboard Apparatus as sufficiently conservative that we would not be limited by pressure sensor noise.

- The 1-torr differential pressure sensor we initially included to assure adequate sensitivity was not needed. Furthermore, analysis showed that the reference pressure chamber required to use it presented difficulties that would probably be insurmountable in a flight system. We therefore adopted the single-sensor concept presented in this report.

This apparatus served its function and allowed us to proceed with developing the Breadboard. The data taken with it were superseded by more complete testing with the larger apparatus, so they are not presented here.

Breadboard Tank

A commercial 210-liter process drum (a seamless stainless steel 55-gallon drum with a removable head) was modified for the project's needs. It was configured for maximum flexibility in testing by adding six 8 in Conflat-style flanges, three 3 in flanges, and two air bleed ports. The flanges are interchangeable, so the pressure sensor head and the compression driver can be mounted in many different positions. The flanges not used for the sensor head or the driver are equipped with glass viewports, as shown in Figure 4-2. After the modifications, the total volume of the tank was measured to be 232.4 liters.
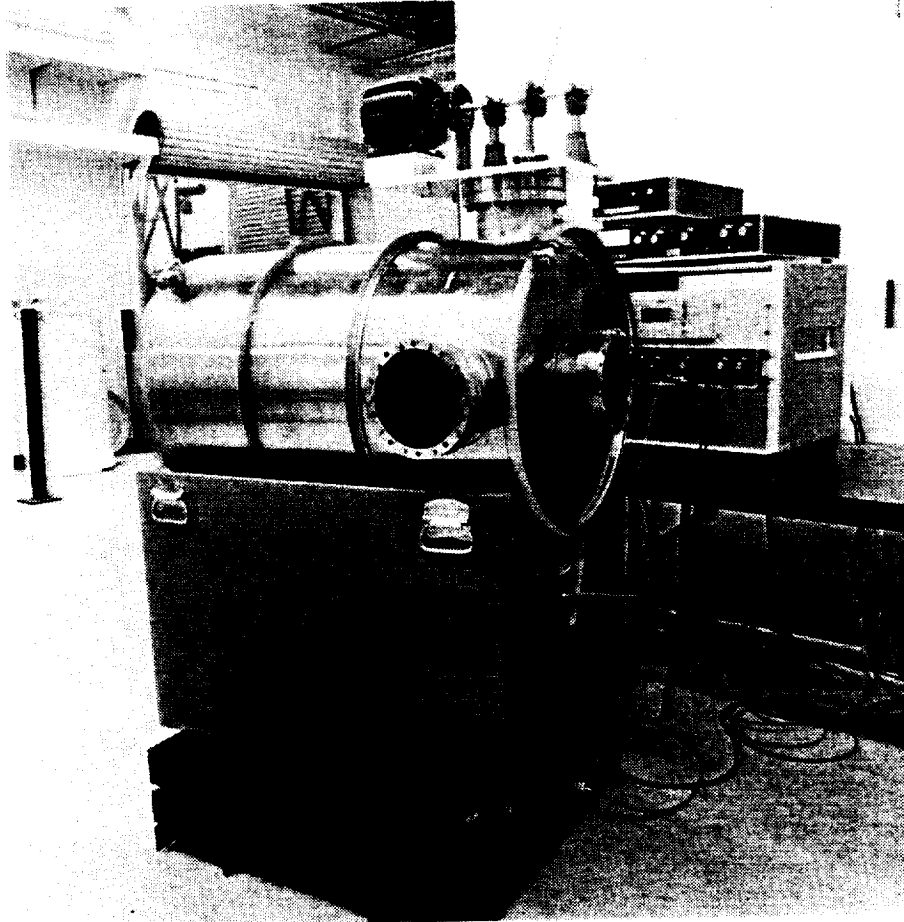
Figure 4-2 Breadboard test apparatus

The tank expansion coefficient (compressive stiffness) is an important factor
to consider in the test chamber because it effects the Δp signal. Too much
tank expansion can cause nonlinearity of $\gamma p/\Delta p$. The compressibility of a
flight tank is expected to be about 0.005 percent per psi, but the flat ends
of the process drum were very much softer (0.8 percent per psi). Staybolts
running between the heads were therefore installed inside to stiffen the tank
to about 0.02 percent per psi. These staybolts also provide a mounting
structure for equipment inside the tank, including a thermocouple "rake."

Compression Driver

The compression driver uses a welded stainless-steel bellows operated by an
eccentric, as discussed in Section 3.5.6. It is based on a commercial com-
pressor manufactured by Metal Bellows Corporation of Sharon, Massachusetts.

ORIGINAL PAGE
BLACK AND WHITE PHOTOGRAPH

We used the replacement drive assembly for a model MB-111 gas compressor, which included the bellows, piston and connecting rod, bearing, eccentric, and counter weight. After performing life testing on a standard unit, we obtained one modified for free liquid flow to use in the Breadboard. The displacement ΔV is 18.05 cc.

The drive shaft is mounted in adjustable-height bearings to vary the bellows extension. The assembly uses a simple variable-speed motor, and is attached to a plate that fits any of the 8-inch ports. An optical pickoff provides pulses that are converted into a square wave to serve as the reference signal for the lock-in amplifier.

Sensors

The MKS model 390 1000-torr absolute pressure sensor is used, and is attached to the mounting plate via flex tubing. It is supported structurally by a plate, as shown in Figure 4-1. A model 270B Signal Conditioner provides direct digital readout of the average pressure p and an analog output is routed to the lock-in amplifier to measure Δp. This sensor is specified by the manufacturer to be accurate to 0.08 percent of reading, to be able to resolve 0.001 torr, and to have a response time of 25 ms.

A Validyne model DP-1000 1000-torr sensor was also used with a model CD-15 Sine Wave Carrier Demodulator for some measurements. Section 5.1.3 discusses the differences between this sensor and the MKS unit. The MKS sensor was used in most measurements because of its lower electrical noise.

Eight type E Constantan-Chromel thermocouples are attached to a threaded rod which is supported near the edge of the tank. The thermocouples are connected to a multiplexer that has its own reference junction, and are read by the programmable multimeter.

Electronics and Data Acquisition System

The electronics and data acquisition system are arranged as shown in Figure 4-3. An Ithaco model 393 Dynatrac (R) lock-in amplifier converts the ac
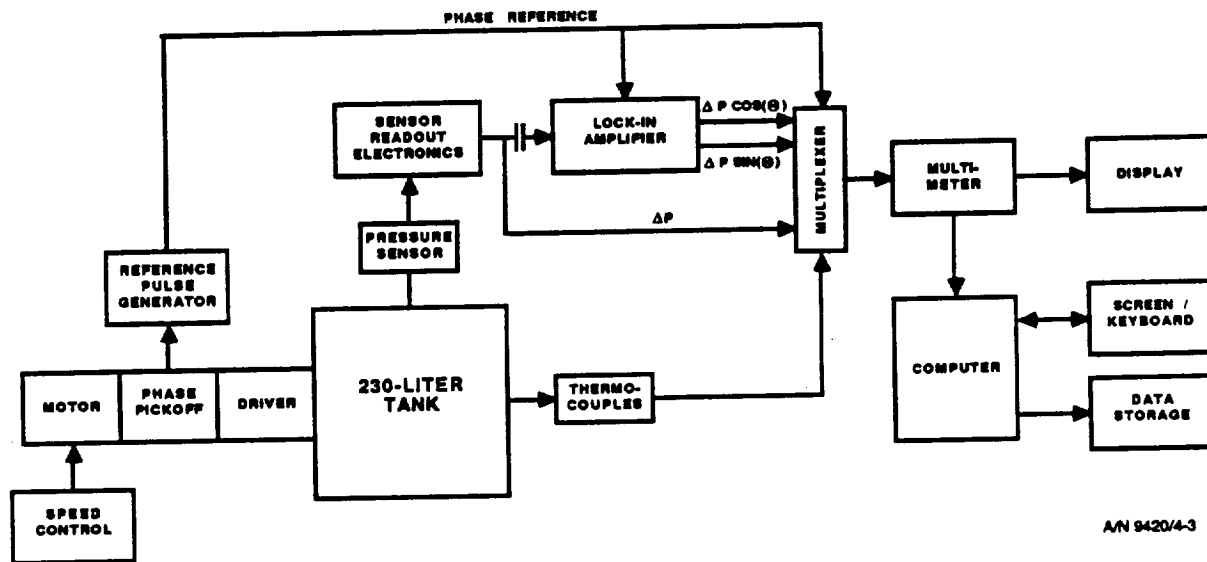
Figure 4-3 Test system block diagram

component of the pressure sensor signal to a high-level dc signal. All analog signals are measured and digitized by a Wavetek model 52 programmable multimeter. The data is read from the multimeter screen, and two Δp signals are sent to the computer for recording.

This particular lock-in amplifier is a versatile laboratory instrument with two signal channels. DC signals proportional to $\Delta p \cos(\theta)$ and $\Delta p \sin(\theta)$, where θ is the compressor shaft rotation angle, are produced. Recording these two signals enables us to measure both the magnitude of Δp and its time shift relative to top dead center of the compressor. This phase measurement turned out to be a very sensitive diagnostic tool for validating the boundary layer model and for diagnosing experimental effects such as tank leakage.

The lock-in amplifier uses the reference signal from the compression driver to isolate the ac Δp signal from noise at all other frequencies. As shown in Figure 4-4, the reference signal drives a switch that rectifies any signal component that is synchronous with it. The low-pass output filter smooths this to a dc signal proportional to Δp, but signal components originating at
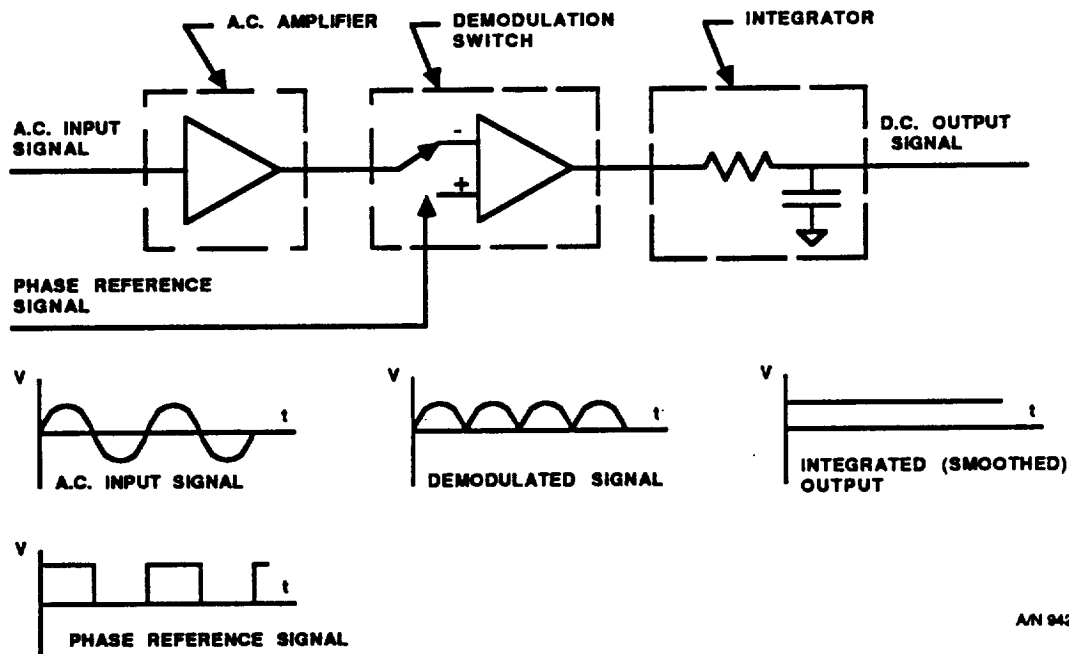
Figure 4-4 Lock-in amplifier concept

any other frequency will tend to be integrated to zero. This circuit concept
is routinely used to achieve maximum sensitivity for periodic signals, and is
easily incorporated in flight hardware.

The programmable multimeter serves as the hub of the data acquisition system.
It measures the dc voltages corresponding to p and Δp, measures the compres-
sion driver frequency, and converts the thermocouple voltages into tempera-
ture readings. All data is displayed on a screen for manual recording, and
the Δp cos(θ) and Δp sin(θ) signals are digitized to 12 bits and transmitted,
together with the current time, via an RS-232 port to the computer.

Labtech Notebook (R) software is used in the PC-XT compatible computer to
receive the data from the multimeter. This software displays the Δp signals
on the screen to aid in monitoring the experiment behavior in real time. The
data is recorded on floppy disks in a format compatible with the data analy-
sis spreadsheet.

Signal spectrum analyzers and other general laboratory electronic equipment are used as necessary to clarify our understanding of the system behavior and to diagnose problems.

Auxiliary Hardware

For most tests the tank is supported either vertically on a three-point support ring, or horizontally in the stiff wooden cradle shown in Figure 4-2. A commercial drum handler is used to maneuver the tank within the lab; it includes a hydraulic lift and a hand-crank tilt mechanism. We originally intended to use this handler to test the system in many orientations but structural resonances made this impractical, as discussed in Section 4.3.4.

Test Procedure

All of the test data presented here was taken according to formal test procedures developed in response to the analysis and exploratory testing that had gone before. The test procedures specified the test configuration and all equipment settings. Detailed laboratory notebooks were kept and photographs were taken as appropriate to document the details of special setups.

Before each test series, a leak check was done by pressurizing the tank to about 20 torr over atmosphere and measuring the leak-down rate. Before-and-after readings were taken to check for drifts in driver frequency. The data were monitored in real time to detect problems such as occasional digital data transmission errors or changes in driver frequency. Redundant data headers and time stamps were used to prevent mix-ups during the data analysis process. All measurements were taken with the same electronic equipment settings (gains, phase offsets, etc.) for internal consistency, and periodic calibration checks were made to insure that everything is operating properly.

The lock-in amplifier uses a 2-pole (12 dB/octave) output filter with a 12.5 s time constant to limit the effective noise bandwidth of the Δp signals to 0.01 Hz. The data was sampled every 10 s, and 5 min of data (30 samples) were taken in each run.

4.3.1.2 Data Analysis

Routine data reduction was done using a Symphony (R) spreadsheet incorporating the most significant elements of the analytical model presented in Section 4.2. Specialized analysis to examine specific aspects of the model is discussed in the various appendices.

For most testing, the data was analyzed two ways:

- To compute the water mass, using the analytical model

- To check the analytical model by examining the measured gas compressibility and signal phase as a function of the test parameters

Figure 4-5 shows the logic used, the data inputs, and the computed output quantities.

Each data run produced 30 values of $p \cos(\theta)$ and $p \sin(\theta)$. A mean amplitude, standard deviation, and phase angle was then computed for each run. The behavior of the amplitude and phase vs frequency and the noise were examined to check for symptoms of experimental problems.

Density and Calculated Gamma

The average reading of the eight thermocouples was entered, and a second-order equation fitted to tabulated density data was used to compute the water density. The water vapor pressure was looked up manually and entered, where it was used to calculate the effective γ of the air/water vapor (or helium/water vapor) mixture according to equation (4-10).

Boundary Layer Coefficient

For the conditions of these tests, and probably for all practical flight applications, only the first term of the boundary layer correction in equation (4-9) is needed, and D and E may be ignored. This means that we need

Figure 4-5 Data analysis logic
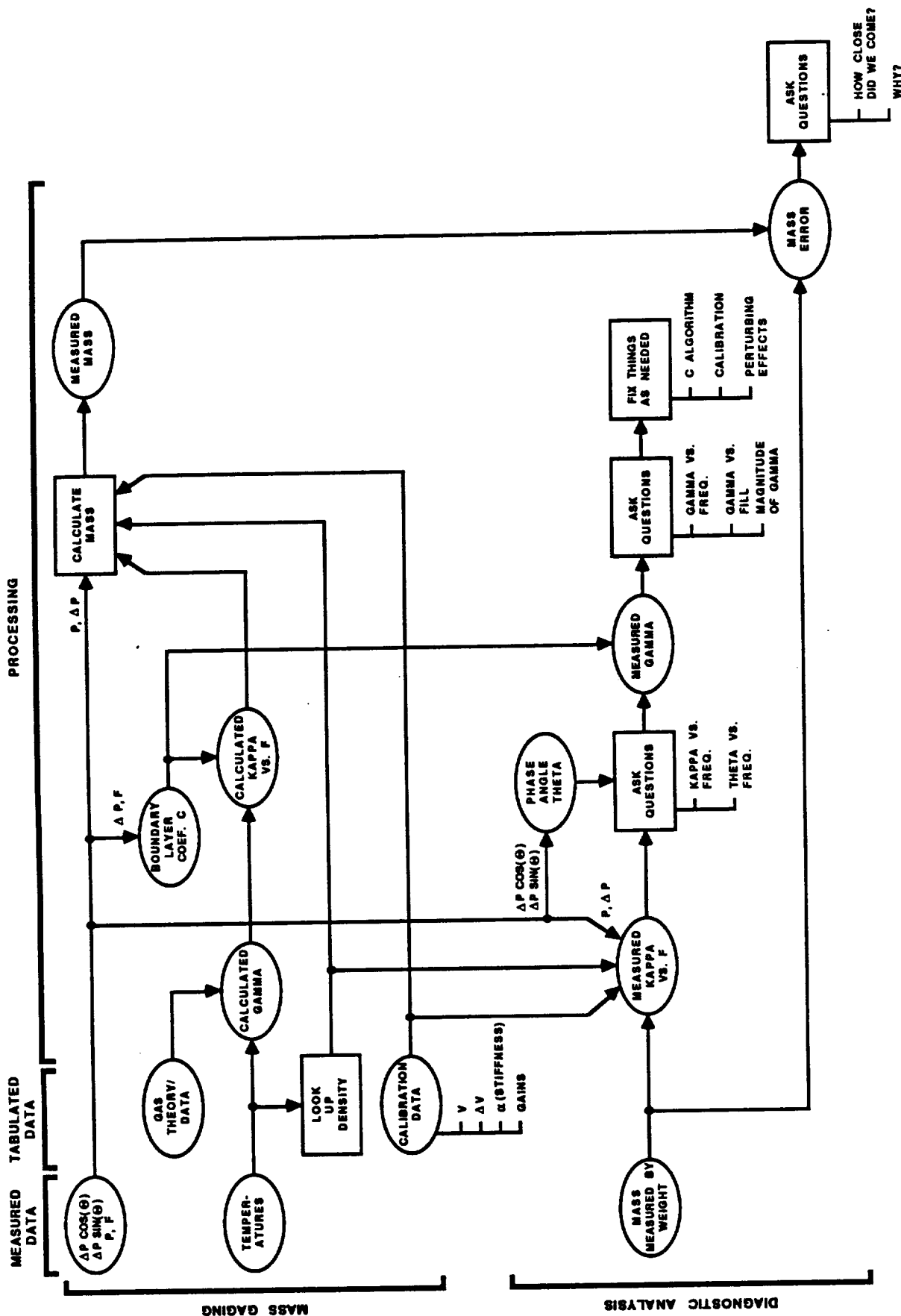
measurements at two frequencies to have two equations in two unknowns, the coefficient C and the water mass M. Since a typical data set consisted of measurements at several frequencies, we picked two to compute C according to:

$$C = (f_1 f_2)^{1/2} \left[\frac{\Delta p_2 [\Delta V + \alpha p_1] - \Delta p_1 [\Delta V + \alpha p_2]}{\Delta p_1 \sqrt{f_2} [\Delta V + \alpha p_2] - \Delta p_2 \sqrt{f_1} [\Delta V + \alpha p_1]} \right] \qquad (4\text{-}36)$$

Values of C computed using different pairs of frequencies were examined for consistency.

Calculated Kappa

According to equation (4-8), the effective compressibility of the ullage is then given by:

$$\kappa = \gamma / (1 + C / \sqrt{f}) \qquad (4\text{-}37)$$

Mass Calculation

The water mass M is then given by:

$$M = \rho \{ V + \kappa p [(\Delta V / \Delta p) + \alpha] \} \qquad (4\text{-}38)$$

where α is the tank expansion coefficient (volume increase per torr increase in pressure). Possible confusion regarding the sign in (4-38) can be avoided by remembering that $\Delta V / \Delta p$ is always negative and that α is about 0.3 percent of $\Delta V / \Delta p$.

M is computed for each frequency measured, using the single value of C computed using two selected measurements. The M values computed for these two frequencies will be identical because equations (4-36) and (4-38) are equivalent to the flight algorithm given in equations (2-5) and (2-6).

Measured Kappa

For diagnostic purposes, the effective κ is computed using the actual mass determined by weight, according to:

$$\kappa = -\frac{\Delta p \ (V - M/\rho)}{p \ (\Delta V + \alpha \Delta p)} \qquad (4\text{-}39)$$

The behavior of κ with frequency, plus the signal phase angle, were used in verifying the boundary layer aspect of the model.

Measured Gamma

The measured value of γ is given by:

$$\gamma = \kappa \ (1 + C/\sqrt{f}) \qquad (4\text{-}40)$$

This should turn out to be equal to the effective γ predicted from (4-10) and will be independent of fill level and frequency. Deviations from the predicted value and dependence on frequency were used to diagnose problems in the calibration. Independence of frequency is a sensitive test of the boundary layer correction.

4.3.1.3   Calibration

The gage calibration was done much more conservatively for these tests than will be required for the flight system; each contributor to the calibration is measured independently. This permits accurate comparison of the absolute value of each measured quantity with the analytical model, but results in more error accumulation than would occur with the end-to-end calibration that will be used for flight.

A digital platform scale was used to weigh the tank for calibration and for each run; it has a 1000 lb capacity and ± 0.1 lb accuracy. The scale is compatible with the tank handler; the wheels of the handler fit around the outside of the scale so the tank can be set on it easily.

The tank volume V_T was measured to be 232.4 ± 0.1 Kg by weighing. The compression driver displacement ΔV was measured to be 18.00 ± 0.05 cc using a high-resolution graduated cylinder. The tank stiffness $\beta = \alpha/V_T$ was measured to be $(4.74 \pm 0.10) \times 10^{-6}$/torr by measuring the pressure rise when the compression driver was rotated with the tank full, and correcting for approximately

50 cc of residual bubbles. (This value is consistent with measurements made using two different methods.) The accuracy of the MKS pressure sensor is specified to be ±0.08 percent, and cross-checks with other precision sensors were consistent with this. The gain and phase response of the lock-in amplifier were measured in the BECD Metrology Laboratory from 0.6 to 6.0 Hz with a precision of about $3x10^{-5}$ and 0.1 deg, respectively.

4.3.2   Mass Gaging Accuracy

The basic test consisted of running the gage over a range of frequencies at each of five standard fill levels. Using the data analysis scheme discussed in Section 4.3.1.2, we examined the data three ways:

- Amplitude and phase behavior vs frequency at each fill level to check for the presence of resonances, leaks, or other perturbing effects

- Absolute value, frequency dependence, and fill-level dependence of γ and C to verify agreement with the analytical model

- Computed water mass vs known mass to determine accuracy

This section focuses on the mass gaging accuracy results; the sections following address the various perturbing effects and the detailed validation of the analytical model.

The accuracy of the mass measurements evolved substantially during the program. Initially there were mysteriously "good" and "bad" runs, and altering the test conditions had unexpected impacts on the data. As our understanding grew, we refined the analytical model and the experimental procedure; as we did so the unexplained variability in the data diminished.

Once it became obvious that the mass gaging accuracy under nominal conditions far exceeded our design goal of 1 percent, we concentrated our efforts on understanding the various perturbations. We therefore made no attempt to

improve the accuracy further, or to do a detailed analysis of the noise contributors. The basic performance is good enough that this is best left to the flight hardware development effort.

For purposes of assessing the basic gaging accuracy, the standard test conditions were as follows:

- Tank vertical, with pressure sensor dry and on top

- Water and air near room temperature

- Compression driver mounted on the side, near the top

- Five standard fill levels: 0, 25, 50, 75, and 90 percent

- Five standard frequencies: 0.6, 1, 2, 3, and 4 Hz

The frequency was restricted to 2 Hz and below at 90 percent full because the driver was submerged at the highest fill level, and we were concerned about fatigue stresses at high speeds because the commercial bellows assembly was not designed for liquid service.

A total of 435 test runs were made with formal documentation and control, and a comparable number of informal exploratory test runs were made. We present here a typical data set taken on December 21-22, 1987, using both the MKS capacitance manometer and the Validyne variable reluctance pressure sensor.

Table 4-1 shows the mass measured with the MKS pressure sensor. Corrections for water density and for effective γ due to water vapor have been applied. The value of C for the boundary layer correction was computed using the 1 and 4 Hz data, except at the 90 percent fill level. The pairs of numbers underlined therefore correspond directly to the mass gaging algorithm given in Section 2, and are identical as would be expected.

The RMS gaging error at all frequencies is 0.27 percent of tank capacity (232.4 Kg). The underlined numbers that use the algorithm of Section 2 show an RMS error of 0.19 percent. There is no apparent trend with fill level.

Table 4-1

MASS GAGING ACCURACY WITH MKS SENSOR

NOMINAL FILL LEVEL (%)	0	25	50	75	90
KNOWN WATER MASS (Kg)	0.0	58.0	115.9	174.0	208.7

FREQUENCY (Hz)	MEASURED WATER MASS (Kg)				
0.6	1.0	58.7	117.4	174.5	209.2
1.0	0.6	57.9	116.6	174.2	209.0
2.0	0.3	57.9	116.7	174.1	209.0
3.0	1.0	58.5	116.8	174.2	--
4.0	0.6	57.9	116.6	174.2	--

RMS error with 2-frequency algorithm = 0.44 Kg (0.19%)

Table 4-2

MASS GAGING ACCURACY WITH VALIDYNE SENSOR

NOMINAL FILL LEVEL (%)	0	25	50	75	90
KNOWN WATER MASS (Kg)	0.0	58.0	115.9	174.0	208.7

FREQUENCY (Hz)	MEASURED WATER MASS (Kg)				
0.6 Hz	1.2	62.3	120.7	174.7	209.2
1.0 Hz	2.9	61.5	117.6	174.5	209.0
2.0 Hz	1.6	62.0	117.8	174.2	209.0
3.0 Hz	3.8	58.3	118.3	174.4	--
4.0 Hz	2.9	61.5	117.6	174.5	--

RMS error with 2-frequency algorithm = 2.19 Kg (0.94%)

Table 4-2 shows that the equivalent data measured with the Validyne sensor displays an overall RMS error of 1.04 percent, plus a strong trend toward larger gaging errors at low fill levels. This is what would be expected from the larger electrical noise of this sensor.

Both tables show a systematic measurement bias, reporting a water mass higher than truth. Twenty of the 23 MKS measurements err on the high side, as do all 23 of the Validyne measurements. This is almost certainly due to the calibration method used.

The flight system will be calibrated by comparing several known fluid masses with the signals actually obtained with the flight tank on the ground. This procedure not only is simple and direct, but it also allows several potential calibration error sources to cancel out. For this testing program we instead measured the tank volume V_T, stiffness α, displacement ΔV, and electronic gains independently. This allowed us to make detailed comparisons of the measured C, γ, etc., with the analytical model, but has degraded the mass measurement accuracies reported here because of calibration error buildup.

The data here shows that we have demonstrated mass gaging accuracy of ±0.27 percent RMS, including the calibration bias. The conclusion to be drawn is that compression gaging is fundamentally capable of meeting the ±1.0 percent accuracy goal, with room in the overall system error budget for perturbing effects and design tradeoffs.

4.3.3   Verification of Analytical Model

The following sections discuss the tests done specifically for the purpose of verifying the accuracy of the analytical model.

4.3.3.1   Boundary Layers

The compressibility of the gas in the boundary layers at gas-solid and gas-liquid interfaces differs from that in the bulk of the gas. The theory of the boundary layer correction is outlined in Section 4.2.1.1. The experimental methods used to prove the correctness of the theory are presented in

this Section. A detailed account of the experimental results may be found in Appendix C.

The theory has been verified in three ways. All parameters in equation (4-17) can be measured except γ. If the value of γ calculated from the experimental data is independent of frequency and fill level and also agrees with the handbook value within the experimental uncertainty, the theory has passed a critical test. The data show that these requirements on γ are fulfilled.

Figures 4-6, 4-7, and 4-8 compare the measured compressibility κ with the value of γ calculated using the boundary layer correction. The lines are the uncorrected κ data and the points are the values of γ calculated from (4-17). All of the raw κ data depend on frequency and fill level. The correction is smallest when the fill level is low because the ratio of surface area to volume of the gas is smallest. Figures 4-6 and 4-7 show the data for air and water at fill levels of 0 percent and 90 percent. The corrected γ values do not have a trend with frequency and fill level, and agree with the handbook value of 1.396 within the measurement uncertainty. Figure 4-8 shows the results for helium gas and water at a fill level of 50 percent. The boundary layer length for helium is larger than that of water by a factor of about 2.5, so this is a more stringent test of the theory because the correction is correspondingly larger. Again, the frequency dependence of γ is removed and the data agree with the handbook value of 1.65 within measurement uncertainty.

Another way to check the theory is to compare the measured phase angle between the compressor and the pressure transducer with the value predicted by the theory; again, data show good agreement. This test is independent of the previous results for γ. Theoretical and measured values of the phase shift are shown in Figures 4-9 and 4-10.

If the value of the boundary layer parameter C is stated correctly by equation (4-17), then the boundary layer lengths $(\gamma/\kappa_b - 1)d$ should be constant as the fill level changes and should agree with the handbook value. Or stated another way, the value of C should change with fill level as A/V,
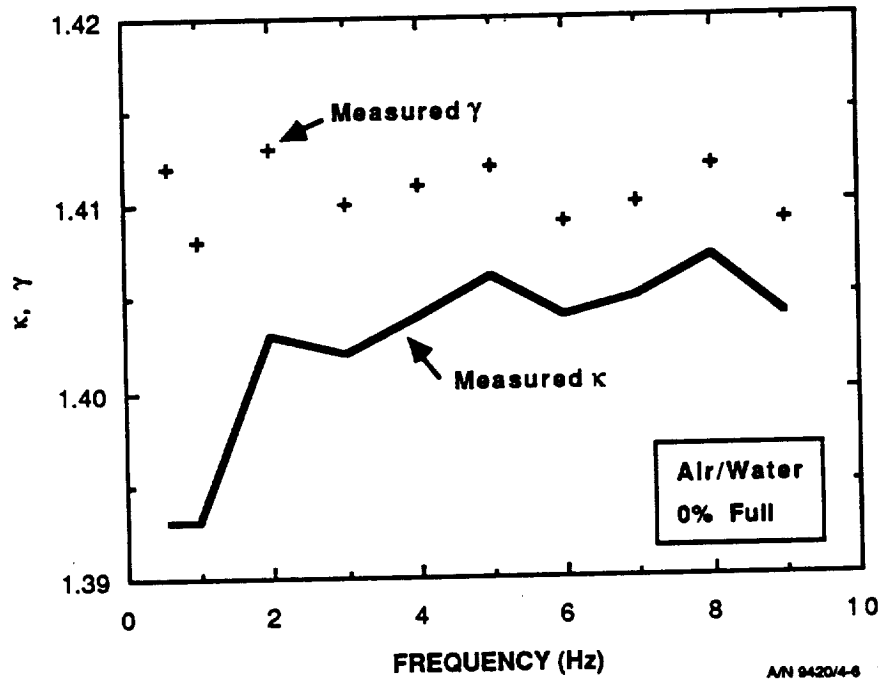
Figure 4-6   Amplitude response with air, 0 percent full
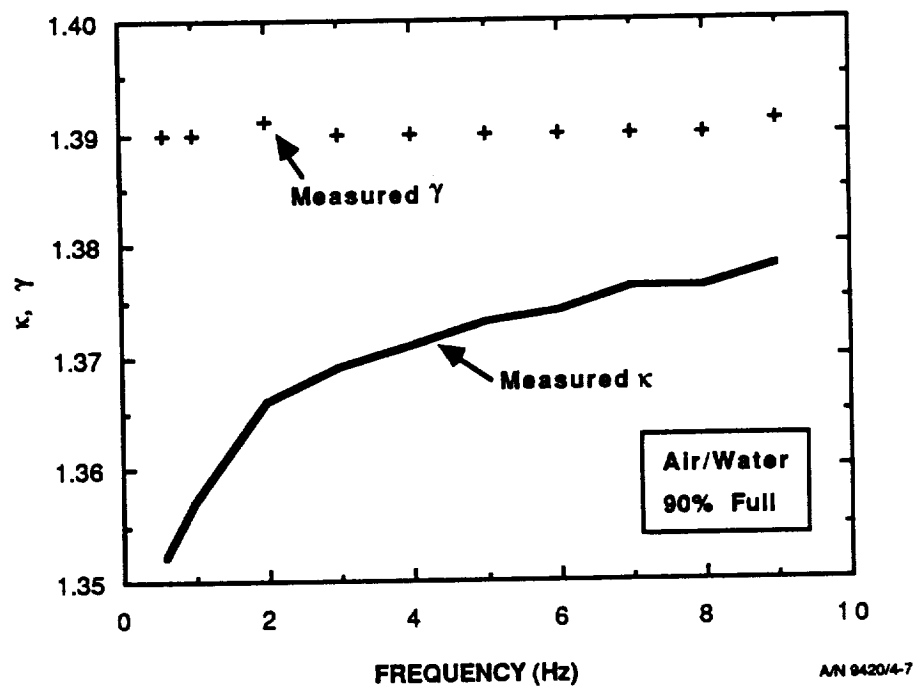
Figure 4-7   Amplitude response with air, 90 percent full
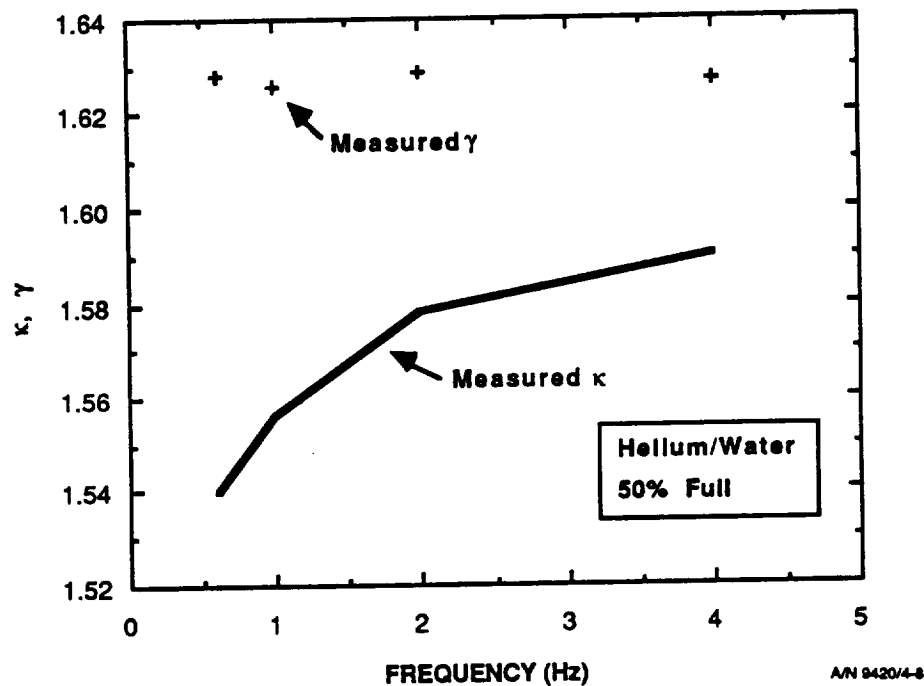
Figure 4-8 Amplitude response with helium, 50 percent full

where A is the area of the interface and V is the gas volume. The ex-
perimental results show that the measured dependence of C on fill level is
that which is predicted. The data for an empty tank using air is the best
comparison between theory and experiment because a handbook value of the
boundary layer at a gas-solid interface is tabulated. In our case the hand-
book value is 0.25 cm and the measured value is 0.255 cm. The air-water
boundary layer length is not known to sufficient accuracy to serve as a test.
Our measured value shows this length to be close to three times that of the
air-solid value. When these boundary layer lengths are used in equation
(4-16), the experimental dependence of C on fill level agrees with the cal-
culated value.

The boundary layer theory has survived three independent tests and according-
ly, may be accepted with confidence.

Figure 4-9 Phase response with air, 90 percent full

Figure 4-10 Phase response with helium, 50 percent full

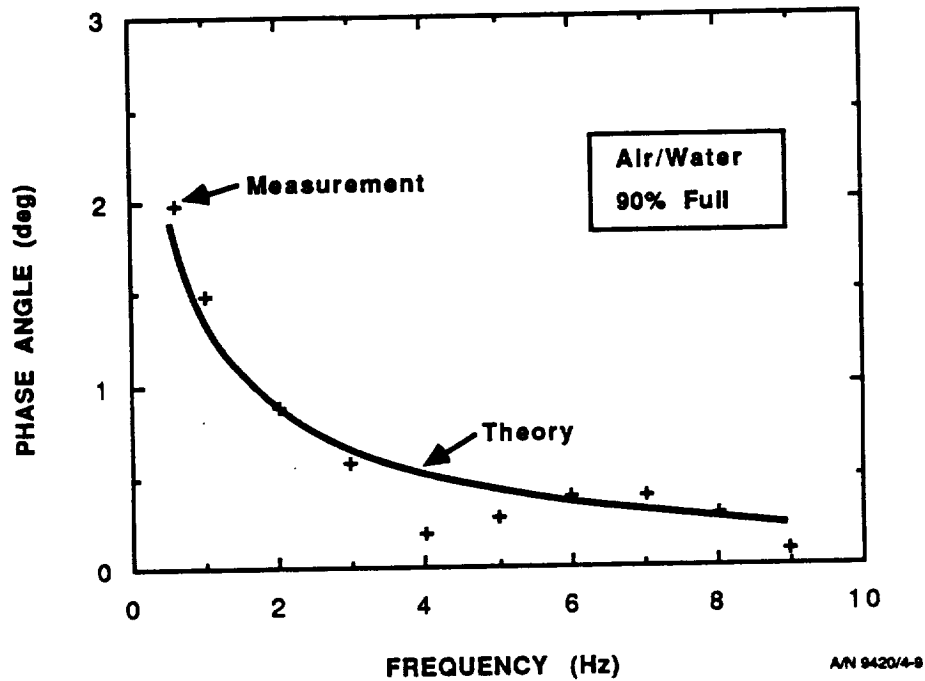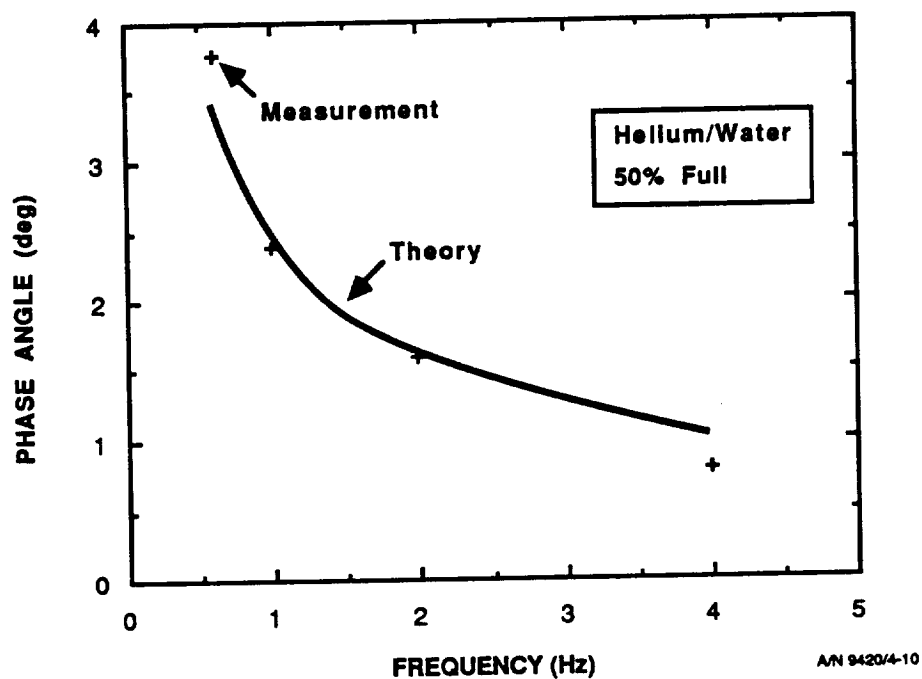## 4.3.3.2   Thermal Stratification

Testing with thermal stratification is important to evaluate the performance of the compression gaging system in a space environment. Space vehicles are subject to nonuniform solar radiation resulting in significant temperature gradients, or stratification, within fluid tanks. This test demonstrated that one percent accuracy can be obtained provided that the temperature is monitored and appropriate corrections are applied.

Temperature gradients were set up using electrical heater tapes wrapped around the tank. The tank was filled to 55 percent and a 23.0 °C gradient in the gas was produced with a heater at the top. Another run was made with the heater at the water/air interface, so that the water had a 21.2 °C gradient but the air was at a nearly uniform temperature. These runs were interspersed with runs at uniform temperature for comparison.

Table 4-3 shows that the mass errors lie well within the ±1 percent goal, despite the thermal stratification. The RMS average of these errors is 0.22 percent. The eight thermocouple readings were simply averaged for each run, and the same temperature correction was applied to the water density and to the effective γ of the air/water vapor mixture. This corresponds to the procedure that would be used in flight, since there would be no way of knowing which temperature sensors are in liquid and which are in gas. For comparison, we used our knowledge of the thermocouple location to apply separate density and γ corrections, but found no improvement.

The conclusion is that the compression gaging system responds to temperature exactly as would be expected from the simple physics involved. The question of what sort of thermal environment is anticipated for a given application and whether special temperature monitoring measures should be taken is discussed in Section 5.3.3.

Table 4-3

COMPENSATION FOR THERMAL STRATIFICATION

| | MASS ERROR (PERCENT OF CAPACITY) | |
FREQUENCY (HZ)	WATER STRATIFIED	AIR STRATIFIED
0.6	0.35	0.24
1.0	0.16	-0.23
2.0	0.06	-0.10
4.0	-0.10	-0.34

4.3.3.3   Wet Pressure Transducer Response

Comparative tests with the pressure transducer in contact with air and with water were found to lead to different values of γ; this identified a potential problem with the transducer. Figure 4-11 shows the Δp signal after correction for the boundary layer effect. When the sensor is filled with air the response is nearly flat, but the signal amplitude and phase (not shown) vary strongly with frequency when it is filled with water. This behavior strongly suggests a mechanical resonance at a frequency somewhere above our maximum of 9 Hz.

When the transducer is dry the mechanical resonance of the diaphragm is on the order of 1 KHz. When water fills the diaphragm chamber and the lead-in tube, the mass that moves with the diaphragm is increased several orders of magnitude and the resonant frequency drops accordingly. In the case of the Breadboard Apparatus, the moving mass is dominated by the water in the lead-in tube (approximately 5x200 mm).

Equation (4-27) in Section 4.2.2.3 gives the expected wet resonant frequency in terms of the transducer characteristics, and the full theory is developed in Appendix H. Detailed information from MKS, the transducer manufacturer, led to a predicted wet resonance of 40 Hz. When a resonance factor of the
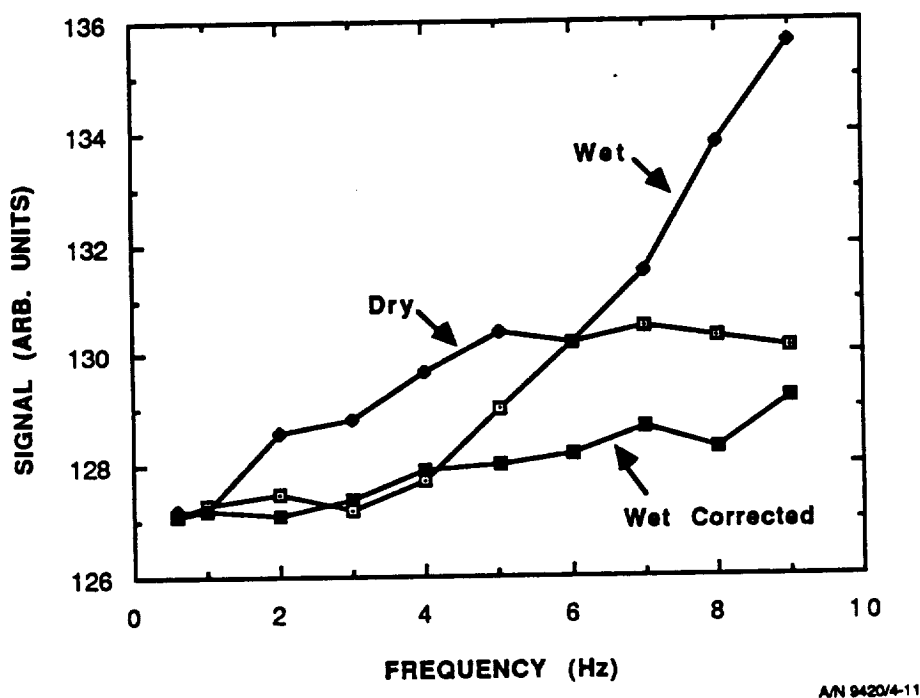
Figure 4-11 Wet vs. dry pressure transducer response

form shown in equation (4-19) is applied, the "wet corrected" curve in Figure 4-11 results. The fact that this curve is flat to ±0.2 percent over the 0.8 to 9 Hz frequency range indicates that the predicted resonance is very close to the actual value, and that this aspect of the analytical model is correct.

Appendix H shows that by shortening the lead-in tube and increasing its diameter (or eliminating it altogether) the resonance when wet can be raised far enough above the driver frequency to eliminate this effect as an error source for gaging.

4.3.3.4 Multiple Bubble Effects

The principal limitation of laboratory testing of this gaging technique for usability in space is the inability to reproduce in 1 g the variety of liquid/gas distributions likely to occur on orbit. We used plastic cups to produce several large bubbles in the tank, expecting to see no effect on the

gage response other than a small shift due to the different pressures in bubbles at different depths. To our surprise, we observed the cooperative bubble resonance discussed in Section 4.2.2.1. To our knowledge, this phenomenon has not been previously reported. The fact that the data presented here matches the detailed theory developed in Appendices F and G gives us confidence that we now understand it, that the analytical model describes it correctly, and that it can be avoided in flight.

In zero gravity, the most common bubble shape will be spherical. The buoyancy forces in 1 g are so large that attempting to simulate spherical bubbles larger than about 1 L with elastic balloons is impractical, and their behavior would be dominated by the enormous "surface tension" of the rubber (see Appendix J). The test scheme we adopted used 12 7.9-L plastic cups attached to a structure built around the three staybolts that stiffen the tank, as shown in Figure 4-12. The cups were mounted in the tank with their open ends down, as shown in Figure 4-13, forming 12 identical bubbles when the tank was filled with water. The pressure transducer communicated with the 13th bubble at the top of the tank.

The lowest cooperative resonance mode consists of the 12 identical bubbles oscillating in phase, with the 13th bubble at the top 180° out of phase. In that case, equation (4-25) for the pressure amplitude in the 13th bubble becomes:

$$X_1 = \frac{L_2 \, \Delta V}{V_1 L_2 + n V_2 L_1} \tag{4-41}$$

where n is the number of cups filled with air, V_1 and V_2 are the volumes of the bubble at the top and of each cup, and L_1 and L_2 are the functions defined in equation (4-22). The numerator goes through a minimum at the single-bubble resonance of each cup, and the denominator goes through a minimum at the cooperative resonance.

All of the relevant dimensions were measured, and Figure 4-14 shows that the predicted amplitude response matches the measured data very closely. Figure 4-15 shows that the measured phase response also closely matches that predicted in Appendix F.
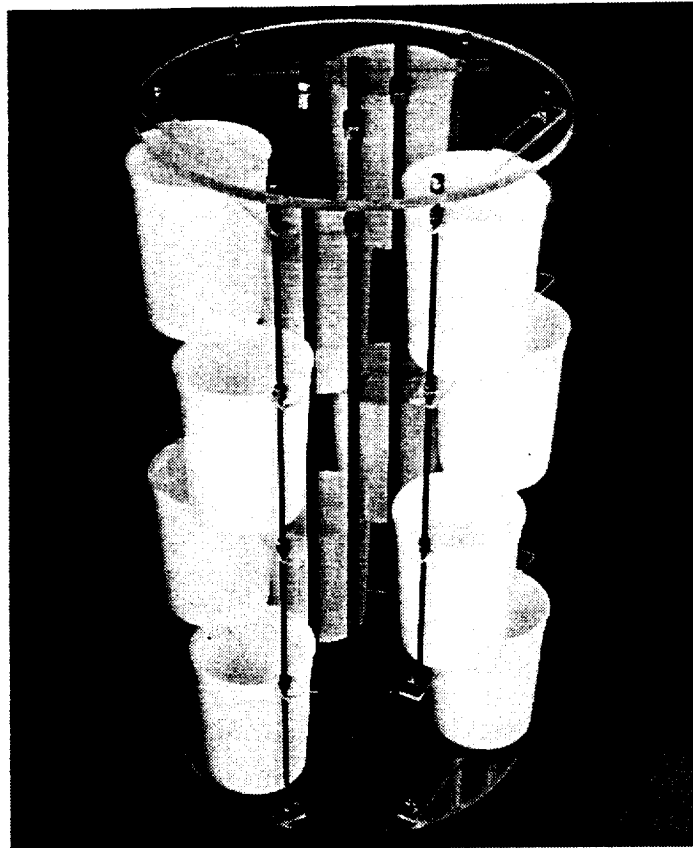
A/N 9420/4-12

Figure 4-12 Multiple-bubble apparatus
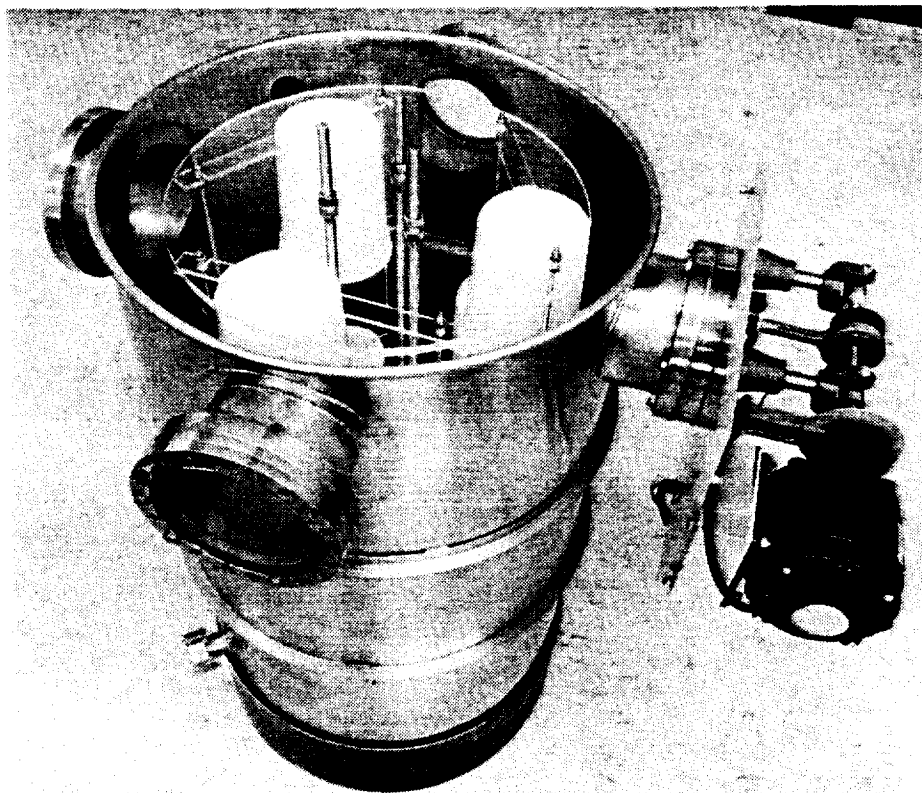
A/N 9420/4-13

Figure 4-13 Multiple-bubble test setup

ORIGINAL PAGE
BLACK AND WHITE PHOTOGRAPH
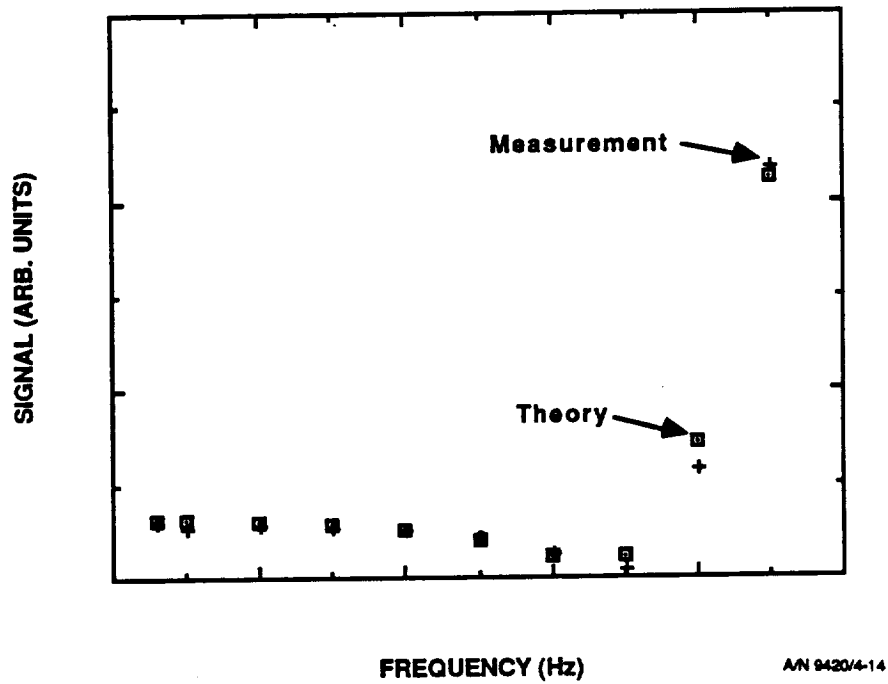
Figure 4-14 Amplitude response with 12 cups
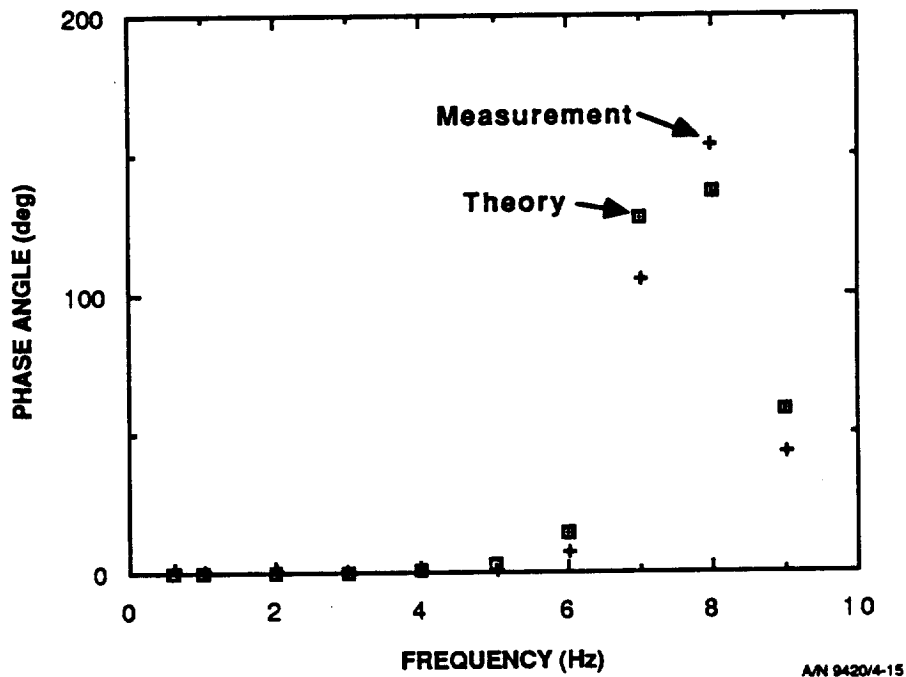
Figure 4-15 Phase response with 12 cups

A few measurements were also made using non-elastic mylar balloons held in weighted mesh bags. The non-elastic material avoided any exaggerated surface tension effects, but the balloon geometry was difficult to determine and wrinkling of the flaccid material on the bottom introduced an unknown amount of damping. Even so, Appendix F shows that the measured response agreed qualitatively with the predictions.

The agreement of the experimental data with the predictions shows that the analytical model provides a useful description of this effect. The lowest possible frequency for the cooperative resonance sets the upper limit on the acceptable operating frequency.

4.3.4 Miscellaneous Experimental Effects

In the course of the experimental work many surprises were encountered. All discrepancies between the measured data and the predictions of the analytical model were investigated. In some cases these led to improvements in the model, and in others they turned out to be due to problems with the laboratory apparatus or procedures. The fact that at the end of the testing there were no unexplained mysteries in the data gives us confidence in the correctness of the analytical model of compression gaging.

In this section we will comment briefly on the major experimental effects encountered and the measures taken to deal with them. Hopefully this will allow future experimenters to proceed efficiently and to bypass much of the exploration we went through.

4.3.4.1 Gravity Head Effects

Gravity in the laboratory (or during ground calibration of a flight system) introduces two simple effects that are not present in flight. Whenever the pressure transducer is submerged it will register the gas pressure in the ullage plus an additional $\rho g h$ due to the gravity head from being h cm below the gas-liquid interface. Since the gaging algorithm depends on the gas pressure, a simple correction must be applied.

A less obvious effect is due to gravity waves on the surface of the liquid. When the compression driver port is below the liquid surface, it will excite waves whose amplitude can depend strongly on the driver frequency because of standing wave resonances. The waves produce an oscillating component in the liquid pressure whose amplitude decays away from the surface. When the pressure sensor is also below the surface, the Δp signal recorded will be distorted.

Because surface waves excited by the compression driver are at the same frequency at the Δp signal, they are not rejected by the lock-in amplifier. The amplitude of these waves depends critically on the resonances of the gas-liquid interface at the moment. Wild gyrations in signal phase angle vs frequency and vs tank orientation were our most sensitive diagnostic indicator that the Δp signal contained a component that depended on such resonances.

This surface wave effect was a significant confusing factor in the initial experiments. Once we had isolated the problem, we dealt with it by not taking data with the driver and the sensor submerged simultaneously. For ground operations with a flight system, we would recommend placing the gage head near the top so that it is above the interface.

4.3.4.2 Structural Resonances

Initially we planned to use the commercial drum handler to support the test tank in many orientations during testing. When supporting the tank, this unit turned out to have structural resonances in the frequency range of our testing. These resonances were excited by the compression driver, and the resulting acceleration of the tank produced spurious signals whenever the pressure sensor was under water, as discussed in Section 4.2.2.2. Because it varied with water mass, orientation of the driver relative to the compliant axes of the drum handler, and with the drum handler adjustments, this effect acted like an almost-random perturbation to the data.

axes of the drum handler, and with the drum handler adjustments, this effect acted like an almost-random perturbation to the data.

Once these resonances were identified we eliminated them by using rigid structures to support the tank. This effect was a nuisance for the development testing because we needed to sweep the operating frequency over a wide range to verify the analytical model. In a flight system attention will have to be paid to structural resonance, but it is not likely to be a significant problem because:

- Launch compatibility will require that the lowest resonance of any local structure is well above the gage driver frequency.

- Momentum imbalance in the compression driver will be controlled to a level low enough to avoid exciting larger Space Station structures.

4.3.4.3 Amplifier Calibration Errors

The amplitude and phase response of the lock-in amplifier departed slightly from nominal and therefore introduced small departures from the predicted signal behavior. On one occasion a component failure led to a large calibration shift. These problems were uncovered as we tightened our standards for agreement between the analytical model and the test data.

For maximum consistency, all data was taken with the same equipment settings. Precision measurements of the true amplifier phase nonlinearity and gain were made in the BECD Metrology Laboratory, and corrections were applied in the data analysis. Periodic checks were made with calibration signals to verify the health and stability of the system.

The electronic calibration requirements are less stringent for the flight system than they were for these development tests. We needed to know precisely the gain and phase response of the electronics because we were using the signal phase and the absolute value of γ computed from data taken over a

wide frequency range to guide us in refining the analytical model. By cali-
brating the gaging system on the flight tank, not only the tank volume and
compressibility, but also the gain coefficients for the p and Δp signals are
determined imperically. Because the flight system will be operated at only a
few fixed frequencies, ideal phase behavior is not required. The flight
circuits must be designed for maximum stability, and it may be useful to
incorporate an internal signal generator to periodically check and correct
for long-term drifts.

4.3.4.4   Bubbles in Pressure Transducer Tubulation

Initial testing with the pressure sensor below water gave unpredictable re-
sults until it was realized that the long, narrow tube (approximately
200x5 mm) between the tank and the diaphragm chamber was trapping a variable
number of air bubbles. Appendix H discusses the shift in mechanical resonant
frequency expected from liquid contacting the diaphragm, and addresses the
situation with a single bubble in the lead-in tube. The complex and varying
resonances due to several bubbles made this data impossible to deal with.

This source of variability was eliminated by operating the pressure sensor
either completely dry or completely filled with water. Before testing with
the sensor under water, it was filled with water and partially evacuated
several times to eliminate trapped bubbles. Before tests with it above the
water level, it was dried with solvents and then by evacuation for about one
hour.

This effect will be avoided in the flight system by using a sensor with a
more open inlet design, as discussed in Section 5.1.3. Shortening and in-
creasing the diameter of the lead-in tube (or eliminating it) to meet the
requirements given in Appendix H will make trapping large bubbles impossible.
Completely open-faced packaging would eliminate the possibility of trapping
small bubbles around the edges of the diaphragm, but the results of Appen-
dix H imply that small bubbles may not be significant.

4.3.4.5 Tank Leakage

Occasional leakage in the tank was initially a major contributor to non-repeatability from run to run. We did the analysis in Appendix I and found that the observed distortions in phase angle were exactly what would be expected from leakage. We eliminated the problem by performing a simple leak-down test before each test series. This will not be a problem in flight gaging systems because the leak rates that can affect gaging are much larger than the performance standards for flight tankage.

Section 5

FLIGHT SYSTEM

Section 5

FLIGHT SYSTEM

During this program we learned enough about the compression gaging technique to gain insight into the development of the flight system hardware. In this section we suggest an overall architecture and discuss what is presently known about each of its elements. Many details will change as design trade-offs are performed, but the information here will be useful in planning the operational hardware development.

5.1   SYSTEM ARCHITECTURE

The gaging system concept shown in Figure 5-1 permits an orderly and cost-effective approach to developing practical mass gaging systems for the many different Space Station fluid subsystems. The gage head attached to the tank must be selected from a series of standard units, but a single head design can work for many different fluid systems. The electronics module can be designed to be compatible with all gaging applications with little modification.
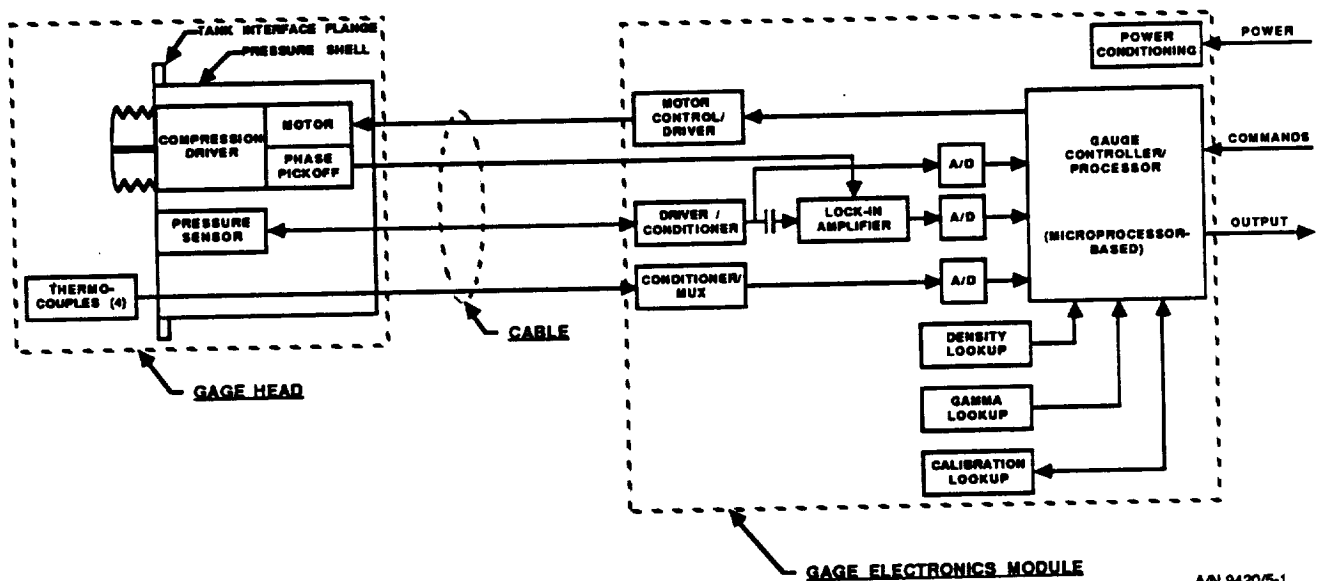
Figure 5-1 Flight system concept

From an overall Space Station development point of view, this permits the compression gaging system to be developed as a standard subsystem. By surveying the likely gaging system users, it will be possible to specify a limited number of gage heads with different displacements from which a suitable match can be made to any fluid system. The commonality of design and the clean interface to the tank permits the fluid system designers to treat the mass gage as a component, with minimum design or programmatic impact on the larger fluid system programs.

The gage head must have a compression driver with a displacement ΔV appropriate to the tank volume V, but the same head can be used with any fluid. As discussed below, it may cost-effective to develop cryogen-compatible gage heads and to use them with little or no modification on room-temperature tanks as well.

Extensions of this simple architecture should also be considered. Section 5.4 discusses the use of multiple gage heads on a single tank for redundancy, and the sharing of a single electronics module among several tanks for mass efficiency. Redundant arrangements involving cross-strapping between multiple heads and modules for maximum reliability are also possible.

5.1.1   Gage Head

From the point of view of the fluid system using it, the most important feature of the gaging system is the gage head and its interfaces to the tank. The simplest interface concept is that shown in Figure 5-1; the driver, pressure sensor, and temperature sensors are housed together in one unit that attaches to a single flange on the tank. In this concept, a number of thermometers are mounted on a lightweight support that extends into the tank from the gage head. Depending on the thermal environment expected and the gaging accuracy required, it may be desirable to locate some of the temperature sensors elsewhere on the tank. This tradeoff between gaging accuracy and interface complexity is discussed below in Section 5.3.3.

The two key design parameters for the gage head are the compression driver displacement ΔV, and whether the head is to be used at room temperature or at

cryogenic temperatures. We are currently assuming that $\Delta V = 10^{-4} V_{tank}$, but slightly smaller values may be adequate.

The gage head incorporates a pressure shell that surrounds all components which communicate with the tank interior, and acts as an extension of the tank wall. This housing must be designed to meet whatever safety and containment redundancy requirements are applied to the tank. All of the components in our baseline are metallic and appear to present no materials compatibility problems for any of the fluids of interest, with the possible exception of hydrogen embrittlement.

5.1.2   Compression Driver

The key component of the compression driver is the means of sealing the piston or other displacer. The system error budget requires that ΔV be repeatable to 0.2 percent, and of course it must not leak. As discussed in Section 3.5.6, we have baselined a bellows-sealed piston driven by a crankshaft because of its simplicity and because the repeatability of ΔV is controlled simply by bearing clearances. The metallic bellows are also usable with cryogens.

A linear motor replacing the crankshaft might permit a smaller and lighter package, but the control system required to give the requisite repeatability would be complex, and might degrade the system reliability. A flexible diaphragm might or might not be able to maintain the ΔV repeatability under varying conditions of tank pressure or liquid position. A detailed tradeoff of possible configurations for this mechanism is needed in the flight development phase.

For purposes of our testing, we adapted a bellows-sealed piston assembly manufactured by Metal Bellows Corporation of Sharon Massachusets for a commercial gas compressor. This unit is not cryogen-compatible, but equivalent bellows are routinely made from 300-series stainless steels that are suitable for cryogenic use.

The bellows in this unit were designed for service with gas, and we were concerned that incompressible liquid trapped near the welds between the leaves might lead to premature fatigue failure. We therefore ran a life test of over 1.0×10^6 cycles at 1 Hz with the bellows full of water, and found that it still passed a helium mass spectrometer leak test. (This is equivalent to 15 years of service with one measurement per day, at 3 minutes per measurement at 1 Hz.) A flight unit would use a bellows profile designed with clearances for liquid, and would presumably have an even longer fatigue life.

We briefly explored the packaging of a large driver ($\Delta V = 1$ liter) suitable for a 10,000 liter (350 ft^3) tank. Figure 5-2 shows a concept that addresses the issues of compactness and minimizing the pressure differential across the bellows. The piston extends into the tank, thereby reducing the size of the housing required to accommodate a connecting rod long enough to keep the rocking angle small. The piston travels in a guide (open to the tank) that controls bellows squirm. An angle resolver on the crankshaft provides the phase reference signal and any feedback required for the motor controller,
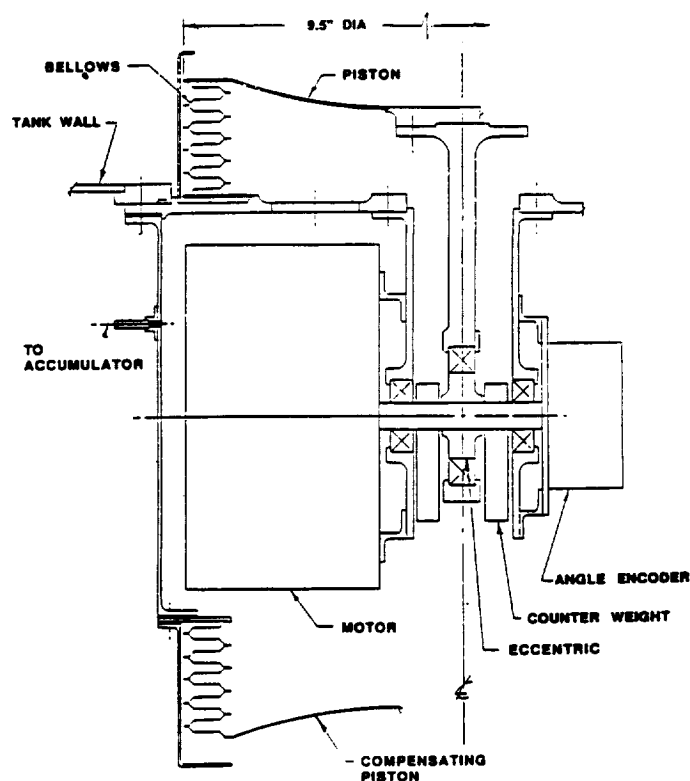
AN 94205-2

Figure 5-2 Compression driver concept

and a counterweight is used to minimize the momentum imbalance in the direction that would contribute a spurious Δp signal to the pressure sensor.

With large drivers such as this, the tank pressure can impose large torques on the crankshaft unless the pressure in the housing is approximately equal to than in the tank. The concept shown here uses a direct-drive motor with a pressure equalization scheme. The housing is filled with an inert gas that is kept near the tank pressure but is separated from the tank contents by a bellows accumulator (not shown). The accumulator is connected to the driver housing by a small orifice sized so that gas does not flow to and from the accumulator fast enough to reduce the effective displacement of the driver. In this sketch, a compensating bellows is provided to minimize the load due to compressing the gas in the housing, although a detailed tradeoff is needed to see if this is necessary. Likewise, a tradeoff is needed to compare this equal-pressure configuration with one in which gear reduction is used to provide the torque necessary to overcome any pressure differential.

An accurate estimate of the power consumed by the compression driver can not be made until the mechanical design questions have been explored further. During the concept selection process, the unit shown in Figure 5-2 was estimated to consume 79W at 1 Hz, using an off-the-shelf motor. This led to the estimate of approximately 100W for the entire gaging system. Since this is dominated by the driver and the driver size scales with the tank size, gages for smaller tanks will consume less.

The compression driver is the only hardware element that must be adapted to the fluid system with which it will be used. The two principal design parameters are displacement and whether the driver is to operate at room temperature or at cryogenic temperatures. The welded metal bellows technology is available in sizes than can accommodate the full range of tank sizes considered, and is compatible with cryogenic use. Our experience at BECD with cryogenic mechanisms and with dry lubrication has shown that there are no fundamental barriers involved. It is likely that designs developed for cryogenic service can be used directly for room-temperature service as well.

The one area in which cryogenic use can differ fundamentally from room-temperature use is in the location of the driver motor. For room temperature applications the motor should be tightly integrated with the driver to minimize mass. The power dissipated by the motor goes directly into the tank and its contents; with a cryogen tank, this energy warms the liquid, and effectively leads to liquid mass loss due to boiloff. A cryogenic driver whose motor is mounted on the warm vacuum shell of the tank would not experience the concentrated heat input during the gage operation, but would experience a continuous small heat leak along the insulating drive shaft connecting the motor to the tank. The tradeoff between these two packaging configurations will consider the following:

- Motor power dissipation when operating

- Duration of measurement needed to produce required accuracy

- How often liquid mass measurements are needed

- Required lifetime of cryogen tank (i.e. allowable heat leak)

- Other heat inputs to the tank

- Mass penalty of remote motor configuration

- Benefit of easy access to the motor for repair

- Development cost/schedule impact of developing two different cryogenic gage head configurations

This tradeoff also interacts strongly with the philosophy adopted regarding developing a "universal" family of gage heads versus developing systems optimized for individual applications.

5.1.3   Pressure Sensor

The ease with which commercial equipment met our accuracy goal in the bread-
board system gives confidence that developing flight hardware for room-tem-
perature applications is feasible. Further investigation of the internal
details of the pressure sensor has led us to believe that it will be mod-
erately straightforward to develop a single pressure sensor that can meet our
needs at cryogenic temperatures as well. This sensor could then be common to
all gage head designs.

We used two types of commercial pressure sensors in our breadboard system
that were expected to be candidates for flight use. Most of our measurements
were made using a 1000-torr Model 390 absolute sensor from MKS Instruments
Inc. of Andover, Massachusets. This is a capacitance manometer in which the
deflection of a metal diaphragm changes the capacitance between the diaphragm
and two internal electrodes, and capacitance bridge electronics measure the
deflection. These are laboratory-quality sensors that have been flown in
space, but which are not intended for cryogenic use.

We also made some measurements with a Model DP-10 1000-torr sensor from
Validyne Engineering Corp. of Northridge, California. This all-welded unit
is intended for room-temperature industrial use, and is rugged and compact,
but has also been used successfully at extremely low temperatures in cryo-
genic laboratories. The Validyne sensor family uses a variable reluctance
principle, in which motion changes the inductance of a pair of coils located
on either side of the diaphragm. We found the noise in the Δp measurement to
be about a factor of five worse than with the MKS sensor, but this may have
been due to the much simpler readout electronics provided by Validyne. (Note
that we were asking both of these sensors to do something they were never
designed to do, namely to accurately resolve a tiny ac pressure signal riding
on top of a large constant pressure.) We also verified the operation and
vacuum integrity of this sensor at liquid nitrogen temperature.

There are three issues involved in developing a pressure sensor suitable for
use in a family of compression gaging systems:

- Controlling the geometry to control the effect of liquid contacting the gage

- Adapting the sensor to cryogenic use

- Satisfying safety and flight qualification requirements

At this point it is clear that the accuracy and resolution of the MKS sensor is more than adequate, and that of the Validyne sensor might be made adequate with some optimization of the electronics for our use. Both units use materials and construction techniques that appear to be rugged and have flown on scientific payloads on Spacelab 2. The driving issues therefore are cryogenic compatibility and controlling the effect of liquid contacting the sensor.

Section 4 and Appendix H show that the pressure sensor reading of Δp can be distorted by dynamic effects if liquid contacts the diaphragm or enters the tubulation attaching the sensor to the tank. The effect of the liquid is to lower the resonant frequency of the sensor by adding to the mass that is accelerated by the springy diaphragm. The cure is to adjust the geometry of the entrance of the gage to keep the effective mass contributed by the liquid low enough. The ideal situation would be a pressure sensor whose diaphragm is flush with the tank wall.

The MKS sensor appears to be readily adaptable to this requirement. Because all of the electrodes and connections are on one side of the diaphragm, it is possible to eliminate the usual connection tubulation and expose the diaphragm to the tank through a fairly large hole. (MKS already lists such a model as available on special order.) The Validyne sensor requires a magnetic sensing coil close to the diaphragm on the tank side, so the effective inertia of the liquid trapped between the coil and the diaphragm would have to be evaluated to decide whether it is worthwhile to explore constructing a magnetic sensor with a special open geometry.

The ability of the Validyne sensor to operate at low temperatures is well-established, although there are some questions about its stability and reli-

ability when cold. The MKS sensor has never been used at cryogenic tempera-
tures, but the better noise characteristics and open geometry compatibility
of the MKS sensor make it attractive to adapt it. Information we have re-
ceived about the internal construction of the MKS sensor head make it appear
to be surprisingly close to a cryogen-compatible design as is. The on-board
electronics used in the commercial unit to keep the noise low could not be
used cold, but our experience at BECD in bringing small signals out of cryo-
genic environments with or without cold buffer electronics makes the electri-
cal problems seem tractable.

5.1.4   Electronics Module

A block diagram of the electrical system to support the FQG is shown in
Figure 5-1. Preliminary analysis of the electronics requirements indicates
that a single electronics module design will work with all fluids and all
tanks. Only the temperature sensor interface, the power rating of the motor
driver, and the data loaded into memory will need to be adapted to each class
of users.

The major functions performed by the electrical system are:

- Interface commands, data and power with the spacecraft
- Temperature and pressure signal conditioning
- Compressor driver control and phase pickoff
- Storage of temperature, density and calibration data
- Computation of fluid mass

None of the subsystems in Figure 5-1 have any critical requirement that would
require special design effort except possibly for the pressure sensor condi-
tioning electronics. All other components are available as commercial mono-
lithic devices.

Because of the low level output from the pressure transducer, a low noise
lock-in amplifier will be required. Such an amplifier has been designed by
BECD for use on a Shuttle experiment; this amplifier is quite straightforward
and and is constructed using flight qualified components.

The entire electrical system required to support most FQG systems can be contained in a box approximately 5x7x3 inches, and consuming less than 20 W from the spacecraft power system. Larger tanks will require more power for the compressor driver, probably up to 100 W for tanks of 10,000 liters. In order to protect the low-level temperature and pressure signals, it may be necessary to locate some buffer electronics at the gage head. The head can be separated from the main electronics module by up to 10 m with no performance impact.

Each of the major subsystems are described in more detail in the sections below.

Microprocessor

The microprocessor performs three basic tasks:

- Perform all calculations necessary to compute the fluid quantity from the temperature, pressure and calibration inputs

- Manage the data and command interfaces with the spacecraft

- Control the sequencing and operation of the gage system

From a computational or data rate point of view, this is a benign requirement for a microprocessor. We estimate that a PROM capacity of about 4 K and a RAM capacity of less than 0.5 K will required to perform all of the designated microprocessor tasks. This combined with the very low data rates and limited computational requirements indicates that the entire task can be performed with a single-chip microprocessor, where both RAM and ROM are contained within the monolithic processor chip and no external memory is required.

Existing single-chip microprocessors that are well suited to this task are the 8052, 8048 and the 6801. Because of the straightforward nature of this application, virtually any of the 20 or so existing devices on the market today could be used. Of more importance than the hardware selection is the

existence of software development systems and the flight qualification of the selected chip. BECD has direct experience with the 8032 family for space applications.

Analog Signal Conditioning

Analog signal conditioning is necessary to amplify the low level signals from the temperature and pressure sensors up to usable levels before analog-to-digital (A-D) conversion. Signal conditioning electronics for the temperature sensors is straightforward, and is available as a monolithic circuit for thermocouple, diode or RTD sensor types. In practice, it may be advisable to use different sensor types for different cryogens because of their differing saturation temperatures. To meet the fluid quantity computational requirements, readout resolution of the order of 1.0 Kelvin is adequate.

The low level nature of the signal at the output of the pressure sensor, combined with the very low data frequencies (0.05 to 5.0 Hz), require the use of lock-in amplifiers to extract the pressure signals with reasonable signal-to-noise ratio. A lock-in amplifier is functionally no different from a conventional amplifier in that it it simply amplifies very low level ac signals with a minimum of noise and drift effects. It converts only the ac signal within a very narrow frequency band centered at the modulation frequency into a dc output.

To extract both the average and differential pressures, two lock-in amplifiers will be connected in tandem. The first, which is modulated at about 1 KHz, amplifies the low level signal directly at the output of the pressure sensor. The second, which is ac coupled to discard the dc component (the average pressure), operates from the output of the first lock-in stage. This high level lock-in is operated at the compression frequency and is synchronized by the phase pickoff. Because of the high level inputs, this lock-in is straightforward and is used primarily because of the simplicity with which it can extract the synchronous differential pressure signal.

For the pressure sensor that we have been using on the FQG test program, the electrical sensing element is a capacitive bridge which is excited with a 1 KHz sine wave. The first lock-in amplifier is slaved to this excitation frequency; the low frequency analog pressure signal is thereby shifted up to 1 KHz where the all of amplification takes place, thus avoiding the low frequency electronic noise present in conventional amplifiers. After amplification, the 1 KHz carrier is removed, restoring the original dc and low frequency signal.

Two pressure ranges are required for the FQG application: the average pressure ranging to about 1000 torr and measured to 0.2 percent resolution, and the differential pressure up to about 1 torr and measured to 0.5 percent resolution. These readout resolutions require digitizing resolutions of nine and eight bits respectively. Accordingly, we can obtain margin by setting the the A-D converter resolution at ten bits. Such a converter exists in monolithic form from a number of vendors, with direct compatibility to the microprocessor.

Power System and Compressor Driver

The gaging system will require regulated supply voltages of ±15 and + 5 VDC. These voltages are generated with conventional dc to dc converters, directly from the Space Station power bus. Since high precision speed control is not required for the compressor, the constant velocity control system will be straightforward, and may be driven open-loop from the microprocessor. The compression driver design must be completed before the detailed requirements on the motor driver can be established. We estimate the maximum power needed for a 10,000 liter system to be about 100 W. Since many vendors supply monolithic drivers for motors ranging from a few watts to beyond 1 kW, device availability is not in question.

5.2   SOFTWARE AND CALIBRATION

The software needed for the flight gaging system is extremely modest. The mass computation algorithm in equations (2-5) and (2-6) is a simple algebraic

expression, with two square roots being the most complex computation required. (For a fixed-frequency system, these can be precomputed and stored in RAM.) In the simplest possible program, the microprocessor would always perform the two-frequency measurement at preset frequencies and report the result. It would be only slightly more complex to perform a first measurement at a high frequency (suitable for a tank more than half full) and use equation (2-2) to either report the result or to trigger a program to perform the two-frequency measurement appropriate for a nearly empty tank. The complexity of the program required may be less than that in a computerized automobile ignition system. A single electronics module could easily be designed to have enough processing power to be able to serve several tanks having more than one type of fluid, as discussed in Section 5.3.4 below.

Calibration of the gaging system consists of two steps: assembling and loading the data characteristic of the fluid and the temperature sensors used, and making a modest number (4 or more if the electronic gains are not well-known) measurements with known quantities of liquid in the flight tank. The liquid density would be loaded into the processor ROM as a function of temperature sensor voltage, and if necessary a table of γ vs. thermometer voltage would be loaded as well. The N calibration measurements would be fitted to determine the values of tank volume V, expansion coefficient α, and the gains of the p and Δp electronics.

It may be significant that the calibration of the flight tank need not be done with the flight fluid. None of the four unknown quantities depend on the fluid, although V and α depend weakly on temperature. It may be desirable, for instance, to calibrate individual specimens of a cryogen tank with water and then apply calculated corrections to the values of V and α. Or a calibration may be done with a less hazardous fluid (e.g. water instead of hydrazine) at the same temperature. The potential cost savings in preparing the overall fluid system for flight should be explored.

5.3   ADAPTING TO SPECIFIC APPLICATIONS

This section examines the design questions and tradeoffs involved in adapting the compression gaging system components to particular fluid system applications. It is important to note that these tradeoffs amount to selecting which standard components to use in a particular application, and need not detract from the hardware commonality benefits of this system architecture.

5.3.1   Impact on/Sensitivity to Tank Design

It is our goal to develop a gaging system that can be viewed by fluid system designers as a component that is simply attached to the final tank, with little impact on the tank design, performance, or development. This is to be contrasted with gaging techniques like large-volume capacitance gaging around which the tank must be designed. Likewise, it is a goal to have a gaging system that is insensitive to small changes in the tank design, so that modifications or variations in construction do not affect the operation of the gage or require extensive recalibration. This is to be contrasted to techniques like RF mode analysis in which changes in internal baffles or the liquid acquisition system could significantly alter the mode structure of the tank cavity.

The compression gaging system can interface with the fluid tank at a single flange. The liquid motion and pressure changes introduced by the compression driver are tiny, and will not affect the behavior of the tank and its contents. The gage head can be located wherever convenience dictates, independently of any internal structure. The only tank parameters that the gaging system is sensitive to are the volume V and stiffness a. The optimum operating frequencies depend weakly enough on the volume that small variations in V will not invalidate the frequencies programmed into the electronics module, so small changes in V or a will be compensated in the calibration.

5.3.2   Driver Displacement

The displacement ΔV of the compression driver is an important parameter because, with larger tanks at least, it drives the gaging system mass and bulk. For present purposes we are conservatively assuming $\Delta V = 1 \times 10^{-4} \, V_{TANK}$, although the displacement of our breadboard unit is less than that. The final displacement-to-volume ratio will be determined by two things: the noise level of the pressure sensor and its electronics, and the gaging accuracy required. Once the detailed development work has established what the sensor noise is, the user can perform the displacement (i.e. weight) vs. accuracy tradeoff.

From an overall Space Station development point of view, it will probably be most practical to survey the potential gage system users, and then develop a limited number of compression drivers in different sizes. The wider the gaps between available displacements, the smaller the development effort required but the less tradeoff flexibility available to the user.

5.3.3   Temperature Monitoring

Because convection does not operate in zero gravity, non-uniform thermal environments can produce large temperature inhomogeneities ("thermal stratification") in tanks in space. If the tank temperature were measured at only one location, significant errors in computed mass could result from the variation of liquid density with temperature.

When analyzing the seriousness of this effect, it is important to recognize that some of our previous flight experience could be misleading. Sizeable temperature gradients have been experienced in supercritical fluid tanks, and significant pressure transients have resulted when the fluid was stirred. The reason this experience may be misleading is that the very small density differences within the supercritical fluid means that the constant small accelerations of the vehicle have very little stirring effect. As we gain experience with two-phase fluid systems operating for long periods in orbit on manned vehicles, it will be important to see to what extent the normal small motions stir the liquid and limit the thermal stratification.

In principle, an accurate value of liquid mass can be computed if many temperature sensors are located throughout the tank and a suitable average is taken. In practice, the interface complexities of the wiring, and especially the number of electrical penetrations of the tank that are required, will cause the fluid system designers to want to minimize the number of thermometers used and probably constrain where they can be mounted.

The baseline concept shows four sensors mounted on a support structure that is part of the gage head. The practicalities of this support structure will probably keep all of the sensors close to the gage head, except on very small tanks. On large tanks, a tradeoff will need to be performed regarding the mass gaging errors caused by the expected level of thermal stratification if the temperature is monitored at a few points close to the gage head, as opposed to monitoring it a larger number of points more evenly distributed around the tank. This tradeoff may reveal, for instance, that the reliability and manufacturing complexity penalties make mounting the thermometers inside the tank unattractive, and a suitable number of external ones will suffice.

5.3.4   Redundancy and Commonality

So far we have discussed only gaging systems consisting of a single gage head connected to a single electronics module. There are two other possibilities that should also be considered:

- Multiple gage heads on a single tank to give redundancy

- One electronics module serving more than one tank

The reliability improvement from using multiple gage heads on a single tank is obvious. The compression drivers would be synchronized so that the effective ΔV is the sum of the displacements of the drivers. The signal could be read from any one of the sensors, or an average could be taken for improved accuracy. Failure of one sensor could be detected (by on-board voting or by examination of the data on the ground) and the failed one ignored.

Failure of one of the drivers would reduce the effective ΔV, but measurements could still be made with slightly degraded accuracy.

Since a single electronics module can serve gage heads attached to any tank (provided that different motor power levels and possibly different temperature sensor types are taken into account), and since the microprocessor is likely to have excess computing capacity, it is tempting to use one electronics module to serve gaging systems on several tanks. The mass savings would come at the expense of more complex interfaces, and possibly logistics, within the overall system. Serving a group of tanks, each having say three gage heads, with two or three electronics modules could produce a highly robust fluid gaging system. Fail-safe electronics or semi-manual switching could be used to cross-strap around failed or degraded units. Very high long-term reliability could be achieved, again at the cost of complexity and reduced independence of individual fluid subsystems.

RECOMMENDATIONS
for
FLIGHT DEVELOPMENT

Section 6
RECOMMENDATIONS FOR FLIGHT DEVELOPMENT

We recommend proceeding toward developing a multi-user compression gaging system for flight. The results of this project have demonstrated that accuracy at the 1 percent level is achievable, and that the physics and technology involved are well enough understood to permit planning an orderly and low-risk hardware development effort.

The first priority must be demonstrating the operation of this gaging system in zero gravity. Because compression gaging is sensitive to large-scale fluid motion, this testing cannot be done reliably with a zero-gravity aircraft flight. The duration of near-zero gravity is too short (about 30 sec) for the effects of the violent maneuver immediately preceding it to die out before the measurement is made. The usable test beds therefore are:

- Space Shuttle, using a non-hazardous fluid such as water or possibly liquid nitrogen

- Free-flying satellite launched on an ELV, such as COLDSAT, using liquid hydrogen or oxygen

- Sounding rocket(s), using any fluid in a small tank for a short duration

Using a non-cryogenic fluid for the first zero-gravity testing would allow off-the-shelf components to be used. But because of the high flight testing costs it may be more cost-effective to tackle the cryogenic packaging issues at the beginning and use the flight demonstration hardware as prototypes for the final flight system components.

The decision between a cryogenic or non-cryogenic initial flight demonstration should be guided by small laboratory cryogenic tests. A simple test setup based on the existing breadboard apparatus could be tested quickly with liquid nitrogen, and then with liquid hydrogen in a suitable hazardous test

facility. Such tests could be performed at the BECD Cryogenic Research Center in Mead, Colorado. This testing would confirm that the behavior of compression gaging with condensible vapor is as expected. The most important benefit of this initial cryogenic testing, however, will be to assess the technical difficulty of developing a cryogen-compatible compression driver and pressure sensor.

In conjunction with the first flight demonstration, we recommend that a system design study be performed to:

- Survey potential user systems for tank sizes, fluids and storage conditions, operating constraints, and any special requirements

- Lay out the system architecture with emphasis on modularity, flexibility, and suitability for phased implementation

- Define the displacements and types (i.e. cryogenic or non-cryogenic) of gage heads needed and their relative priority for development

- Analyze costs and benefits of different development strategies (e.g. one or two gage head designs for cryogenic and non-cryogenic use)

This study will result in a recommended configuration for the flight system and a recommended development strategy. This information, together with the results of the flight demonstration test, will be used for the final go/no-go decision for operational hardware development.

Once the decision to commit to operational hardware is made, the development strategy should allow phased implementation. The gage head size with the highest near-term priority would be developed first, along with the pressure sensor, the electronics module, and the baseline version of the flight software. When the complete gaging system has been successfully tested, the gage head size with the second-highest priority would be developed, and so forth. The same pressure sensor and electronic module would be used for all sizes of

the system. Evolutionary enhancements or customizing of the electronics or
the software may or may not be necessary, but could be accommodated easily if
suitable allowances are made in the initial system design.

Appendix A

BIBLIOGRAPHY

Appendix A
BIBLIOGRAPHY

This Appendix presents the bibliography developed during the FQG program for use during concept selection. The citations are catagorized by the principal topic addressed. Certain useful background information is included in addition to articles devoted explicitly to the topic of fluid gaging.

FLUID QUANTITY GAUGING BIBLIOGRAPHY

SUBJECT: GAUGING SURVEY

AUTHORS	INSTITUTIONS	YEAR	TITLE/DESCRIPTION	CITATION
TRW, NASA	TRW, NASA	1971	Propellant Quantity Gauging System Under Zero G (shuttle), (Final Report)	N71-36104
Beech Aircraft Corp.	BEECH	1985	FQG for Cryogenic Fluids, Literature Search and Preliminary Review of Potential Concepts	BEECH AIRCRAFT CO.
Crane, R.A.	U. of S. FLORIDA	1982	Mass Gauging in Low Gravity (Report)	UNIV. OF S. FLORIDA
Monti, R., Golia, C.	NAPOLI UNIVERSITY NAPLES, ITALY	1985	Liquid Gauging Technologies For Space Station's Utilization	36th ASTRO CONGRESS STOCKHOLM,86A-15626
Trinks, H.	TECHNISCHE UNIV. HAMBURG	1985	Assesment Study of Liquid Content Measurement Methods Applicable to Space Missions	N85-28135
Hansman, R.J., Meserole, J.S.	MIT BOEING	1988	Fundamental Limitations on Low Gravity Fluid Gauging Technologies Imposed by Orbital Mission Requirements	A88-3402, 24TH JT PROPULSION CONF.

SUBJECT: RF GAUGING

AUTHORS	INSTITUTIONS	YEAR	TITLE/DESCRIPTION	CITATION
Collier, Ellerbruch, Cruz, Stokes, Luft, Peterson, Heister	NBS	1973	Mass Quantity Gauging by RF Mode Analysis, (Interim Report)	N-27390 NBS, 1973
Lockhart, James D.	NASA	1966	RF Liquid-Level Sensing Technique, (Report)	N66-23798, LOCKHEED
Bahr, A.J.	SRI	1975	Study of Zero-G Propellant Gauging Based on Tank Electromagnetic Resonances, (Report)	N77-78308 STANFORD RSCH INST.
Bendix Aerospace	BENDIX	1972	Summary, RF Quantity Gauging System, (Report)	N72-24320
Trent, Dan S.	NBS	1977	Report, NBS RF Quantity Gauging System Test	JSC-11817
Beech Aircraft Corp.	BEECH	1985	Survey, Development System Survey	BEECH AIRCRAFT CO.

SUBJECT: ULTRASONICS

AUTHORS	INSTITUTIONS	YEAR	TITLE/DESCRIPTION	CITATION
Gelly, J., Maerfeld, C., Maguer, P.	-	1982	Abnormal Backscattering Off Low Roughtness Surface of Metallic Objects Immersed in Water	ACOUSTICAL IMAGING, VOL 12, P.733.
Chapelon, J., Shankar, P., Newhouse, V.	Drexel Univ.	1985	Applications of the Double Frequency Technique in Bubble Sizing and Pressure Measurements in Fluids	ACOUSTICAL IMAGING, VOL 14, P. 753.
Herment, A., Reynaud, R., Arcile, C. et al	-	1985	Range Resolution With a New Signal Processor Implementing a Fast Kalman Estimator	ACOUSTICAL IMAGING, VOL 14, P. 657.
Doshi, N., Smith, R., Johnson, R.L.	TRW	1973	TRW Acousto-Optical Nonimmersion Flaw-Imaging System	TRW SYSTEMS GROUP REDONDO BEACH, CA.
Doshi, N., Smith, R., Johnson, R.L.	TRW	1973	Nonimmersion Pulse-Echo Acousto-Optical Nondestructive Imaging System (Final Report)	AD-760554 MARCH, 1973
		1972	IEEE Sonics and Ultrasonics Symposiums	
		1967	International Symposium on Acoustical Holography and...	

SUBJECT: PVT GAUGING

AUTHORS	INSTITUTIONS	YEAR	TITLE/DESCRIPTION	CITATION
Garner, Douglas H., Howell, William E.	NASA Langley	1984	Volumetric Fuel Quantity Gauge (Patent Application)	N84-32787
Duhon, D.D.	McDonnell Douglas NASA	1975	Error Analysis of the Shuttle Orbital Maneuvering System PVT Propellant Gauging Module (Report)	N7710143 MD TECH SERVICES CO
Duhon, D.D.	McDonnell Douglas NASA	1975	Error Analysis of the Shuttle Reaction Control System Propellant Gauging Module (Report)	N76-32240 MD TECH SERVICES CO
Doshi, N.H.	Doshi and Assoc.	1986	Mass/Volume Gauging System	DOSHI & ASSOC. INGLEWOOD, CA.
Duhon, D.D.	McDONNELL, NASA	1975	The Shuttle Orbital Maneuvering System PVT Propellant Quantity Gaugin Accuracy and Leak Detection Allowance for Four Instruments	N76-32241

SUBJECT: CAPACITANCE GAUGING

AUTHORS	INSTITUTIONS	YEAR	TITLE/DESCRIPTION	CITATION
Cohn, Irving H.	SIMMONDS	1966	Capacitance Gauging of Liquids Likely to Be Used in Space, Too (Article)	SPACE/AERONAUTICS APRIL 1966, P. 122
Dammig, A., Sherburne, A., Brooks, R.	NASA	1972	Capacitive Tank Gauging apparatus Being Independent of Liquid Distribution, (Patent)	PATENT # 3,639,835
	TRANS-SONICS NASA	1967	Capacitance Propellant Gauging Study for Orbiting Spacecraft	

SUBJECT: NUCLEONIC GAUGING

AUTHORS	INSTITUTIONS	YEAR	TITLE/DESCRIPTION	CITATION
Bupp, F.E.	TRW, AFRPL	1972	Development of Zero-G Gauging System (gamma ray), (Final Report)	AD-749967 TRW
Bupp, F.E.	TRW, AFRPL	1972	Phase 1B and 2, Development of Zero-G Gauing System (gamma ray), (Report)	AD-745566
Bupp, F.E.	TRW, NASA	1976	Summary, Zero-G Flight Test of A Gauging System (Report)	N76-23349, VOL 1 CONTRACT NAS9-14349
	GENERAL NUCLEONICS	-	Nucleonic Fluid Measurement Systems	GENERAL NUCLEONICS 115 S. SPRING ST CLAREMONT, CA 91711

SUBJECT: RIGS GAUGING

AUTHORS	INSTITUTIONS	YEAR	TITLE/DESCRIPTION	CITATION
Paine, T., Siegel, B., Lieberman, S.	NASA	1971	Resonant Infrasonic Gaugin Apparatus, (Patent)	PATENT # 3,596,510
Kaminskas, R.A., McGuire, D.	TRW, NASA	1974	Phase II, Augmented RIGS	NT4-23042 TRW SYSTEMS GROUP

SUBJECT: OTHER GAUGING METHODS

AUTHORS	INSTITUTIONS	YEAR	TITLE/DESCRIPTION	CITATION
Smith, Harvey A.	NASA, ?	1967	Spherical Tank Gauge, (Patent), (Bladder Gauging)	N75-23565
Long, John W.	USAF-WRIGHT PATT	1974	The State of the art in Oil Quantity Gaging on U.S. Military and Commercial Aircraft, (Oil Gauging)	AERONAUTICAL SYSTEM WRIGHT-PATT, 1974
Orazietti, A.J., Orton, G. Schreib, R.	McDONNELL DOUGLAS, INTELSAT	1986	Propellant Gauging for Geostationary Satellites (ultrasonic, nucleonic, ultrasonic torsional waveguide, ultrasonic fluid......), (AIAA Report)	22ND JT PROPULSION CONF, HUNTSVILLE AIAA 86-1716
Rimer, M. Stephson, D.G.	GRUMMAN, NASA		The Effect of Liquid Oscillations on the LM Propellant Quantity Gauge System, (Apollo Program)	N72-16858
Tate, S., Hromadka R.	MARQUARDT CO. NASA	1970	Evaluation and Demonstration of Propellant Quantity Gauging System for Auxiliary Propulsion Systems	N70-32145 MARQUARDT CO.
Orton, George	McDONNELL DOUGLAS	1987	Shuttle Get Away Special Experiments	N87-21141, P. 14
Dominick, Sam M.	MARTIN MARIETTA	1986?	Fluid Management on the Space Station	A-861565
Eberhardt, R.N.	MARTIN MARIETTA	1985	Managing Fluids in Space	A86-32904
Hansman, R. John	MIT	1987	The Coupled dynamics of Fluids and Spacecraft in Low Gravity and Low Gravity Fluid Measurement	N87-21141 p. 23

SUBJECT: FLOW METERS

AUTHORS	INSTITUTIONS	YEAR	TITLE/DESCRIPTION	CITATION
	MICRO MOTION	1985	Micro Motion Model D Mass Flow Meters (Instruction Manual)	DECEMBER, 85
	OMEGA ENG.	1985	Flow Measurement and Control Handbook and Encyclopedia	
Seriale-Grush, J. M.	NASA JSC	1985	1 1/2-inch Controltron Flowmeter Performance Evaluation	JSC-20412
Korane, K.J.		1986	Sorting Out Flow Sensors (Article)	MACHINE DESIGN MARCH 20, 86, P. 67

SUBJECT: CRYOGENIC FLUID TRANSFER

AUTHORS	INSTITUTIONS	YEAR	TITLE/DESCRIPTION	CITATION
Aydelott, J.C., Gille, J.P., Eberhardt, R.	NASA-LEWIS MARTIN MARIETTA	1984	JPC, On-Orbit Cryogenic Fluid Transfer (Article)	AIAA 84-1343 20TH JT PROPULSION CONF., CINCINANTI
Tegart, J., Kirkland, Z.	MARTIN MARIETTA	1985	JPC, On-Orbit Propellant Resupply Demonstration - Flight Results, (Article)	AIAA 85-1233 21ST JT PROPULSION CONF.
Gorin, Barney F.	FAIRCHILD	1986	Mission Requirements and Design Definition for an Orbital Spacecraft consumables Resupply System (OSCRS), (Article)	AIAA-86-1602 FAIRCHILD SPACE CO
Szara, R.J.	U of CHICAGO	1966	Rapid, Low-Loss Liquid Helium Transfer, (Article)	ADVANCES IN CRYO ENGINEERNG, VOL. 13 PLENUM PRESS, P 232

SUBJECT: LOW G FLUID BEHAVIOR

AUTHORS	INSTITUTIONS	YEAR	TITLE/DESCRIPTION	CITATION
Satterlee, H.M., Hollister, M.P.	NASA, LOCKHEED	1967	Engineers Handbook: Low-g Propellant Behavior	N68-22463
Stark, J., Bradshaw R., Blatt, M.	GENERAL DYNAMICS NASA	1974	Low-G Fluid Behavior Technology Summaries (extensive Bibliography)	N75-14060
Concus, P., Crane, G.E. Satterlee, H.M.	NASA, LOCKHEED	1969	Small Amplitude Lateral Sloshing in Spheroidal Container Under Low Gravitational Conditions (Report)	N69-21507
Hastings, G., Hill, D., Satterlee, H.M.	LOCKHEED, NASA	1966	The Literature of Low-G Propellant Behavior	N66-38975
Blackmon, J.R.	McDONNELL DOUGLAS	1969	Proceedings of Low-G Seminar	N71-13101 TO 13119
Young, N., Goldstein, J., Block, M.	Baird Atomic	1959	The Motion of Bubbles in a Vertical Temperature Gradient	J. FLUID MECH., VOL 6, P. 350

SUBJECT: FLUID PROPERTIES

AUTHORS	INSTITUTIONS	YEAR	TITLE/DESCRIPTION	CITATION
Beighly, C., Fish, W. Anderson, R.	AEROJET-GENERAL	1969	Advanced Fuels and Oxidizers	A69-31747, 2ND INTL CONF ON SPACE ENG.
Sengers, J., Levelt, H. Straub, J., Watanabe, K.	VARIOUS	1985	Assessment of Critical Parameter Values for H2O and D2O	J. PHYSICAL CHEM. REF DATA, VOL 14, #1, 1985, PAGE 193
Chang, E.T., Gocken, N.A., Poston, T.M.	AEROSPACE CORP.	1969	Solubilities of Gases in Simple and Complex Propellants	JRNL OF SPACECRAFT 6, 1177 (1969)
Chang, E.T., Gocken, N.A., Poston, T.M.	AEROSPACE CORP.	1968	Thermodynamic Properties of Gases in Propellants. II Solubilities of He, N2, & Ar gas in Hydrazine, MMH, UDMH	J. PHYSICAL CHEM. 72, 639, (1968)
Chang, E.T., Gocken, N.A.	AEROSPACE CORP.	1968	Thermodynamic Properties of Gases in Propellants. III	J. PHYSICAL CHEM. 72, 2556, (1968)
Kestin, J., Sengers, J.V. Kamgar-Parsi, B.	VARIOUS	1984	Thermophysical Properties of Fluid H2O	J. PHYSICAL CHEM. VOL. 13, #1, P.175
Straty, G., Diller, D.,	NBS	1980	(P,V,T) of Saturated and Compressed Fluid Nitrogen	J CHEM THERMODYNAMIC VOL 12, P. 927
Hiza, M.J., Kidnay, A.J., Miller, R.C.	NBS	1975	Equilibrium Properties of Fluid Mixtures: A Bibliography of Data on Fluids of Cryogenic Interest (Book)	NY:IFI/PLENUM, 75
Hiza, M.J., Kidnay, A.J., Miller, R.C.	NBS	1981	Equilibrium Properties of Fluid Mixtures: A Bibliography of Experimental Data on Selected Fluids (Handbook)	NY:IFI/PLENUM, 82
Wright, Alfred C.	MARTIN, AFRPL	1977	USAF Propellant Handbooks, Vol II, Nitric Acid/ Nitrogen Tetroxide Oxidizers	AD-A036741 MARTIN MARIETTA, 77
	ROCKETDYNE, AFRPL	1967	Engineering Property Data on Rocket Propellants (Annual Summary Report)	AD-382340
Nesterenko, V.B., Bazhin, M.A., Bubnoy, V.P.	USSR, ACADEMY OF SCIENCES	1969	Calculation of the Thermodynamic Properties of Nitrogen Textroxide Tanking Nonideality Into Account	AD-702969
Chu, I.C., Girling, P.M.	INTERNATIONAL COAL REFINING CO.	1984	Conversion of Thermophysical Property Data	
Perkins, H.	NASA-MARSHALL	1965	Effects of various Additives on Physical Properties and Performance of MMH	N66-16155, NASA
Mitchel, R.C., Melvold, R., Quaglino, J.	ROCKETDYNE AFRPL	1973	Engineering Properties of Rocket Propellants	AD771580 ROCKWELL INTL
Liley, P.E.	PURDUE UNIVERSITY	1973	Transport Properties of Selected Elements and Compounds in the Gaseous State (part 2)	AD-782024, THERMO- PHYSICAL PROPERTIES RSCH CTR, PURDUE
McPeak, A.W.	AFRPL	1969	Heterogeneous Fuel Handbook	AD-345696, AFRPL

Ottosen, P., Mannov, G.	RISO NAT'L LAB	1980	Thermal and Mechanical Properties of Nitrogen	N81-22147/5 RISO NATL LAB
Gosman, A., McCarty, R., Hust, J.	NBS, NSRDS	1969	Thermodynamic Properties of argon From the Triple Point to 300K at Pressures to 1000 Atmospheres	NSRDS NBS 27
Chang, E.T., Gocken, N.A., Poston, T.M.	AEROSPACE CORP. AIRFORCE	1967	Thermodynamic Properties of Gases in Propellants: Solubilities of He, N2, and Ar in Hydrazine, Methyl-hydrazine and Unsymmetrical Dimethylhydrazine	J. PHYSICAL CHEM. 72, P. 639 1968
Chang, E.T., Gocken, N.A.	AEROSPACE CORP.	1964	Thermodynamic Properties of Hyrdrazine, Unsymmetrical Dimethylhydrazine, and Their Mixtures	AD-458288 AEROSPACE CORP. 64
	JOHN HOPKINS UNIV	1961	"Liquid Propellant Manual, Chemical Propellant Information Agency"	LIQUID PROPELLANT INFO AGENCY,JH UNIV
Sherman, A., Gerhman, R., Osugi, J.	NASA-MARSHALL McDONNELL DOUGLAS	1971	Technical Support Package, Brief No. 71-10078, Updated, Expanded. Fluid Properties Handbook"	N71-10078 NASA - MARSHALL SFC
Johnson, V.	U.S. AIRFORCE	1960	"Compendium of the Properties of Materials at Low Temp."	WRIGHT AIR DEVELOP-MENT DIV,US AIRFORC
DUPONT	DUPONT	1969	"Freon Product Information"	du Pont, de Nemours &Co, Wilmington, DE
Touloukian, Y.S.	PURDUE UNIV	1970	Thermophysical Properties of Matter", Thermophysical Properties Research Center	PURDUE UNIVERSITY
Kit, B., Evered, D.			Rocket Propellant Handbook	MacMILLAN CO., N.Y.
Scott, Russell B.,	D. VAN-NOSTRAND & CO.		Cryogenic Engineering	D. VAN-NOSTRAND AND CO, PRINCETON, N.J.
Chang, E.T., Gokcen, N.A., Poston, T.M.	BELL AEROSPACE		Thermodynamic Properties of Gases in Propellants	CHEM THERMODYNAMICS LABORATORIES, BELL
Schmidt, Eckart W.	ROCKET RESEARCH	1984	Hydrazine and Its Derivatives, Preparation, Properties, Applications.	JOHN WILEY & SONS,
VARIOUS	VARIOUS	1963	Perry's Chemical Engineer's Handbook	McGRAW-HILL BOOK CO

SUBJECT: GENERAL INFORMATION USED ON PROGRAM

AUTHORS	INSTITUTIONS	YEAR	TITLE/DESCRIPTION	CITATION
Taipale, H.J.	UNIVAC	1968	Reliability Report for a Fixed Mica Capacitor, DTIC	AD-878867
Stark, J., Leonhard, F., Bennet, F.O. Jr.	GENERAL DYNAMICS, NASA	1974	Cryogenic Thermal Control Technology Summaries	N75-14061 GD/CONVAIR
Lawrence, R.J.	JSC	1981	JSC Reduced Gravity Aircraft User's Guide (KC-135) Flight Operations Directorate Aircraft Operations Div.	JSC-17385 MAY, 1981
Midgley, P.	UNIV. OF BRISTOL	1969	Structural Materials for Use at Cryogenic Temperatures	A69-42159 AIAA
Pinson, Larry D.	NASA LANGLEY	1964	Longitudinal Spring Constants for Liquid-Propellant With Ellipsoidal Ends	N65-10632 NASA-LANGLEY
Nuccio, P.P.	CHEMTRIC, INC., NASA	1975	Vapor Compression Distillation Module (Space Station)	N75-31747 CHEMTRIC, INC.

DEFINITIONS

N - National Technical Information Service, U.S. Dept. of Commerce (NTIS)
AD - Defence Technical Information Center, Defense Logistics Agency (DTIC)
A - American Institute of Aeronautics and Astronautics (AIAA)
   (Open Literature Accessioned by AIAA and announced in IAA)
JSC - Johnson Space Center

Appendix B

RESONANCE GAGING
CONCEPT

Appendix B
RESONANCE GAGING CONCEPT

Basic Concept

The basic idea behind the resonance approach to compression gauging described here is to measure frequency instead of signal amplitude. Because this is frequently easier, it appeared to offer the possibility of achieving adequate accuracy with a smaller change in the bubble volume, and therefore smaller displacement mechanisms for large storage tanks.

The fundamental difference between our approach and the RIGS approach developed by TRW is that we use a control system and multiple measurements to separate the bubble compressibility (and hence volume) out from the diaphragm inertia. This is critical because the effective inertia of the diaphragm is higher when liquid is in contact with it than when it is not. This is a potentially fatal source of variability in zero g. TRW's approach to eliminating this "wet vs dry" variability was to use a flexible bag to keep the liquid away from the diaphragm. This presented a serious materials problem when trying to apply the system to cryogens.

Our system is shown schematically in Figure B-1. A flexible diaphragm is connected to an actuator which applies a known force and measures the position of the diaphragm. The control system operates in such a way that the "spring constant" of the system and its effective inertia are measured separately. (The damping of the system may or may not be measured.) Since the bubble volume computation depends only on the spring constant, it is independent of the variable inertia.

In concept, this could be done by driving the diaphragm with a known force at three or more different frequencies near resonance, and mapping out the "tuning curve" of its amplitude response. This would give us three equations in three unknowns (mass, spring constant, and damping), and we could solve them. The alternative used here applies a variable amount of electrical feedback to alter the effective spring constant, thereby shifting the resonance.
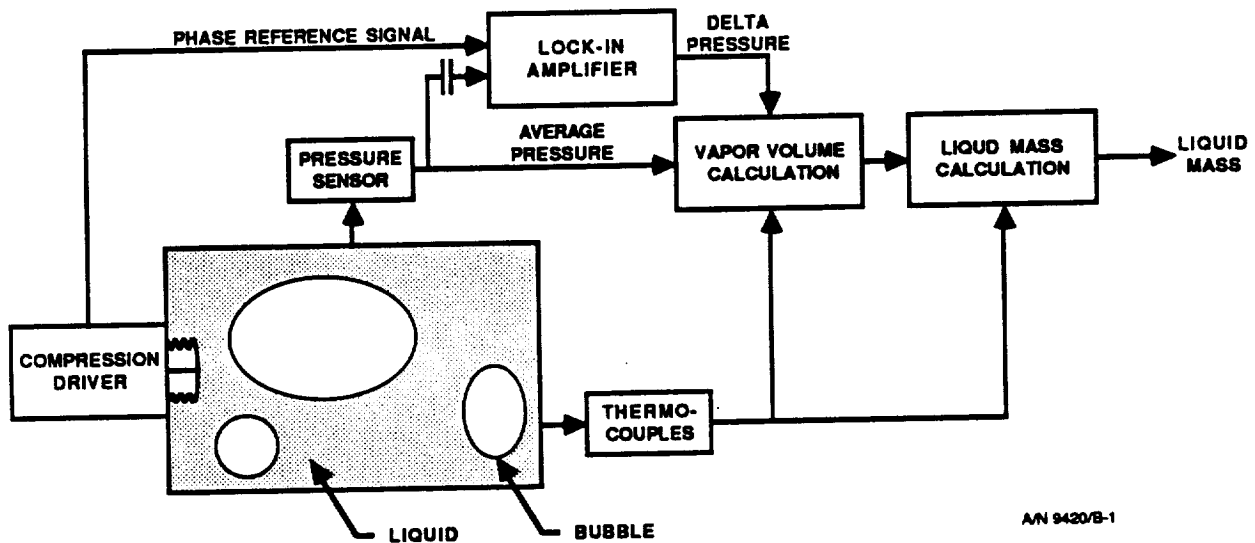
Figure B-1 Resonant gaging concept

In the control system concept shown below, the "resonance" measured is not the frequency at which we get maximum amplitude response, but rather the frequency at which the driving force and the diaphragm position are 90° out of phase. Two attractive features of this choice are:

- The resonant frequency is of the form $\sqrt{k/m}$, and is independent of the damping of the system, and

- We will get better resolution on the frequency than by mapping out the peak of the tuning curve with signal amplitude measurements.

Underlying Assumptions

The following assumptions underly the resonance concept:

- The resonance frequencies are high enough that the departure from ideal adiabatic behavior does not impair accuracy.

*   Other resonance phenomena (bubble or structure) do not interfere, either because they lie at other frequencies or because they are not excited.

*   The liquid/vapor distribution near the diaphragm does not change during the measurement enough to degrade the accuracy.

*   The characteristics (gains, spring constants, etc.) of the control system and diaphragm are either stable after pre-launch calibration or are calibratable in flight.

Control System Concept

The system shown in Figure B-2 consists of the mechanical resonant system plus an amplifier with gain K feeding a signal from the position transducer back to the voice coil driver. The fact that K can be varied allows us to make the measurement of the bubble compressibility independent of the amount of liquid moving with the diaphragm.
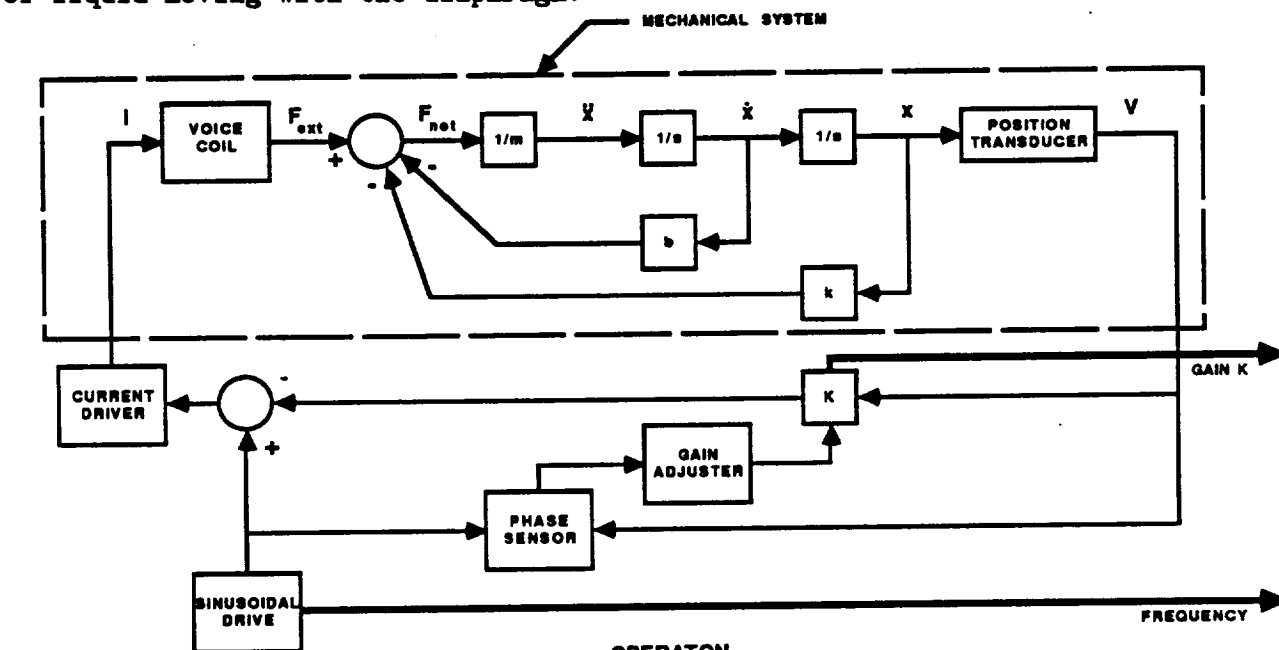
GOVERNING EQUATION

$$F_{net} = F_{ext} - (k+K)\dot{x} - b\ddot{x} = m\ddot{x}$$

$$k = k_D + k_s$$

$$m = m_D + m_L$$

OPERATON

1) SET DRIVE TO OMEGA > 10 HZ.
2) ADJUST K TILL PHASE = 90 DEG.
3) RECORD K.
4) REPEAT FOR ANOTHER OMEGA.

A/N 9420/B-2

Figure B-2 Resonance gage control system

When K = 0, the spring constant of the system is $k = k_D + k_B$, where k_D is the spring constant of the diaphragm, and k_B is the "spring constant" of the bubble compressibility. The resonant frequency Ω_o (in the sense of $90°$ phase shift between the driving force and the position) is then

$$\Omega_o = [\, (k_D+k_B) \, / \, (m_D+m_L) \,]^{1/2} \, , \qquad\qquad \text{(B-1)}$$

where m_D is the mass of the diaphragm, and m_L is the effective mass of the liquid moving with it. m_D and k_D are known from preflight calibration. Because m_L varies depending on whether liquid or a bubble are next to the diaphragm, measuring Ω_o alone is not sufficient to determine k_B.

The feedback is now switched on, and the new resonant frequency is measured. Because of the additional electronic "spring," the new frequency Ω_K is given by

$$\Omega_K = [\, (k_D+k_B+K) \, / \, (m_D+m_L) \,]^{1/2} \, . \qquad\qquad \text{(B-2)}$$

We now have two equations in the two unknowns k_B and m_L, so we can solve for k_B independently of m_L.

The diagram shows the phase sensor adjusting K to resonate at a predetermined frequency Ω, while these words describe a system with the phase sensor adjusting the frequency to resonate at a given K. It could be done either way. With a high Q, the system would respond slowly to changes in the driving frequency.

In this discussion we have spoken of the "spring constant of the bubble." When working out the governing equations in detail to arrive at the design requirements, we express this in terms of the diaphragm (taken to be a rigid piston) dimensions:

$$k_B = \gamma p A^2 / V \, , \qquad\qquad \text{(B-3)}$$

where γ is C_p/C_V, p is the pressure, A is the piston area, and V is the bubble volume.

Appendix C

ACOUSTIC BOUNDARY LAYER

Appendix C
ACOUSTIC BOUNDARY LAYERS

INTRODUCTION

In the compression gaging method the volume of the ullage is inferred from the formula:

$$V_b = \kappa p \, \frac{\Delta V}{\Delta p} \qquad\qquad (C\text{-}1)$$

where:

V_b	=	volume of the ullage
p	=	mean pressure
$1/\kappa p$	=	compressibility of the gas
ΔV	=	compressor displacement
Δp	=	measured pressure amplitude

The value of κ is not constant throughout a bubble. When the bubble touches the solid walls of the container there is a solid-gas boundary layer in which the thermodynamic variables vary with position. A gas-liquid boundary layer occurs at a liquid interface. In each of these boundary layers $1/\kappa$ varies exponentially from a value of $1/\kappa_b$ at the interface to $1/\gamma$ at the outer edge. Here, γ is the ratio of specific heats of the gas and κ_b refers to the value of κ at the boundary. The correct value of κ to use in equation (C-1) is the volume average over the ullage.

THE PLANE BOUNDARY LAYER

We begin by examining the boundary layer at a planar interface. This treatment will accurately describe the situation when the boundary layer thickness is small compared to the bubble dimensions.

Complex Compressibility

An exponential boundary layer occurs because the compressor is driven sinusoidally and all the governing equations for the thermodynamic variables at the interface are of the constant coefficient diffusion type. They have the form:

$$\frac{\partial \psi(y,t)}{\partial t} = D \frac{\partial^2 \psi}{\partial y^2} \tag{C-2}$$

where ψ is any thermodynamic variable, D is the diffusivity constant and y the distance from the interface. Since:

$$\psi(y,t) = \psi(y) \exp(-i\omega t) \tag{C-3}$$

equation (C-2) reduces to:

$$\frac{d^2\psi}{dy^2} + \frac{i\omega}{D} \psi(y) = 0 \tag{C-4}$$

A solution of (C-4) is:

$$\psi(y) = A + \psi_o \exp[(-i\omega/D)^{1/2}y] = A + \psi_o \exp[(i-1)y/d]; \tag{C-5}$$

$$d = \sqrt{2D/\omega}$$

where A is a constant and d is the boundary layer length. All the thermodynamic variables have this form near the interface. Since the compressibility is the ratio of the local volume variation to the pressure variation, it has the form:

$$\frac{1}{\kappa} = \frac{1}{\gamma} + (\frac{1}{\kappa_b} - \frac{1}{\gamma}) \exp (i-1)\frac{y}{d} \tag{C-6}$$

The complex value of $1/\kappa$ implies that ΔV and Δp are out of phase.

If two or more diffusive processes occur, so that we are dealing with coupled simultaneous diffusion equations, the structure is similar to (C-6) :

$$\frac{1}{\kappa} = \frac{1}{\gamma} + (\frac{1}{\kappa_{b1}} - \frac{1}{\gamma}) \exp (i-1)\frac{y}{d_1} + (\frac{1}{\kappa_{b2}} - \frac{1}{\gamma}) \exp (i-1)\frac{y}{d_2} \tag{C-7}$$

where each process has a different κ_{bj} and d_j.

At a solid-gas interface the acoustic boundary layer is entirely thermal and has a thickness d of:

$$d = \sqrt{\frac{2k}{\rho c_p \omega}} \equiv \frac{d_o}{\sqrt{f}} \qquad\qquad (C-8)$$

where:

k	=	thermal conductivity of the gas
ρ	=	density of the gas
c_p	=	specific heat of the gas
ω	=	angular frequency of the compressor
f	=	frequency of the compressor

For air $d = 0.25/(f)^{1/2}$ cm at STP so $d_o = 0.25$ cm at 1 Hz.

At a solid boundary equation (C-6) applies, and if the solid has good thermal conductivity $\kappa_b = 1$ (i.e. the compression is isothermal). At the outer edge of the layer $\kappa = \gamma$.

At a liquid-gas interface there are thermal and diffusive layers and equation (C-7) applies. These layers are quite complicated because the interface moves and evaporation/condensation occurs. It is necessary to solve a coupled system of dynamic and energy conservation equations to find the value of κ_b and the boundary layer thickness d.

The volume average of $1/\kappa$ required in equation (C-1) can be found by multiplying the fractional volume outside the boundary layer by $1/\gamma$ and the fractional volume inside the boundary layer by the average value of $1/\kappa$ inside the boundary layer. A volume average inside the layer is an average over y. For the boundary layer like (C-6), the average value of $1/\kappa$ to a distance $y = L$ is:

$$\frac{1}{\kappa_{L}} = \frac{1}{\gamma} + (\frac{1}{\kappa_b} - \frac{1}{\gamma}) \frac{d}{2L} (1+i)\left[1-\exp(i-1)\frac{L}{d}\right] \qquad (C-9)$$

When L>>d (C-9) reduces to:

$$\frac{1}{\kappa_{Ls}} = \frac{1}{\gamma} + (\frac{1}{\kappa_b} - \frac{1}{\gamma}) + (\frac{1}{\kappa_b} - \frac{1}{\gamma}) \frac{d}{2L}(1+i) \qquad (C-10)$$

We can evaluate the average in this way whenever the boundary layers from opposite sides of the bubble do not overlap.

For a boundary layer like (C-7) an equation similar to (C-10) is found:

$$\frac{1}{\kappa_{L1}} = \frac{1}{\gamma} + (\frac{1}{\kappa_{b1}} - \frac{1}{\gamma}) \frac{d_1}{2L} (1+i) + (\frac{1}{\kappa_{b2}} - \frac{1}{\gamma}) \frac{d_2}{2L} (1+i) \qquad (C-11)$$

If we define V_o as the total ullage volume, V_{sb} as the volume in the solid-gas layers, and V_{1b} as the volume in the liquid-gas layers, then the average of $1/\kappa$ over the ullage is:

$$\frac{1}{\kappa_{av}} = \frac{1}{\gamma} \frac{(V_o - V_{sb} - V_{1b})}{V_o} + \frac{1}{\kappa_{Ls}} \frac{V_{sb}}{V_o} + \frac{1}{\kappa_{L1}} \frac{V_{1b}}{V_o} \qquad (C-12)$$

The volume in a boundary can be written as the area times the distance used in averaging L. Thus,

$$V_{sb} = A_s L \; ; \quad V_{1b} = A_1 L \qquad (C-13)$$

and the volume average of κ required in equation (C-1) is:

$$\frac{1}{\kappa_{av}} = \frac{1}{\gamma} + \frac{(1+i)}{2V_o} \left[(\frac{1}{\kappa_b} - \frac{1}{\gamma}) A_s d + (\frac{1}{\kappa_{b1}} - \frac{1}{\gamma}) A_1 d \right] \qquad (C-14)$$

Note that L does not appear in (C-14).

If we multiply (C-14) by γ and invert, then κ_{av} can be written:

$$\kappa_{av} = \frac{\gamma}{1 + \frac{(1+i)}{2V_o} \left[(\frac{\gamma}{\kappa_b} - 1) A_2 d + (\frac{\gamma}{\kappa_{b1}} - 1) A_1 d \right]} \qquad (C-15)$$

Recall that each boundary length can be written $d = d_o/(f)^{1/2}$, and define C as:

$$C = \frac{1}{V_o} \left[(\frac{\gamma}{\kappa_b} - 1) A_s d_o + (\frac{\gamma}{\kappa_{b1}} - 1) A_s d_{1o} + (\frac{\gamma}{\kappa_{b2}} - 1) A_1 d_{2o} \right] \qquad (C-16)$$

then:

$$\kappa_{av} = \frac{\gamma}{1 + \frac{(1+i)}{2} \frac{C}{\sqrt{f}}} \qquad (C-17)$$

The areas of the interfaces, the boundary layer thicknesses and the value of κ at the boundary are usually difficult to measure or calculate. However, we do not need to know these factors to operate the gage.

It is possible to find C from the measured data by making measurements at two different frequencies. To determine how to extract C from the data we will begin with equation (C-1). Equation (C-1) is modified when the compressibility of the tank and the acoustic boundary layer are considered. Let β be the compressibility of the tank, V_t the volume of the tank and $\alpha = \beta V_t$. Then equation (C-1) can be written:

$$V_b = \frac{\gamma p (\frac{\Delta V}{\Delta p})(1 - \alpha \frac{\Delta p}{\Delta V})}{1 + \frac{(1+i)C}{2\sqrt{f}}} \qquad (C-18)$$

Of these quantities all except α, C and γ are measured, and γ is known from the composition of the gas. If we make measurements at the same fill level, V_b will be constant.

To find α keep ΔV and f fixed and measure Δp at two different tank pressures p. Then, equating the two sets of data in (C-18):

$$p_1 \frac{\Delta V}{\Delta p_1} - \alpha p_1 = p_2 \frac{\Delta V}{\Delta p_2} - \alpha p_2 \qquad (C-19)$$

Solving for a

$$a = \Delta V \frac{\left[\dfrac{P_1}{\Delta P_1} - \dfrac{P_2}{\Delta P_2}\right]}{P_1 - P_2} \tag{C-20}$$

To find C keep ΔV and p fixed and measure Δp at two different frequencies. Then equating the two sets of data in (C-18):

$$\frac{(1+i)C}{2} = \frac{\sqrt{f_1 f_2}\left[(\Delta p_1 P_2 - \Delta p_2 P_1)\right]}{\sqrt{f_1}\,\Delta p_2 P_1 - \sqrt{f_2}\,\Delta p_1 P_2} \tag{C-21}$$

Here, we have omitted a term in aC since they are both small quantities.

When a and C are determined, all the quantities needed to find V_b are known.

Phase Differences

Some of the quantities in equations (C-18) and (C-21) are complex. The data generated by the experimental equipment consists of separate measurements of the amplitudes and phases of these complex quantities. It is necessary to rewrite (C-18) and (C-21) in terms of the magnitude and angle of the measured data.

The pressure variation Δp is out of phase with the compressor displacement ΔV. Then, $\Delta V / \Delta p$ must have the same complex phase as the denominator of (C-18) since V_b is real. The angle of the denominator (in radians) is:

$$\phi = \arctan \frac{\dfrac{C}{2\sqrt{f}}}{1 + \dfrac{C}{2\sqrt{f}}} \simeq \arctan \frac{C}{2\sqrt{f}} \simeq \frac{C}{2\sqrt{f}} \tag{C-22}$$

Δp leads ΔV by this angle.

Since both $\Delta V / \Delta p$ and the denominator of (C-18) are complex, V_b must be found from the magnitude of equation (C-18). The amplitude of $\Delta V / \Delta p$ is the amplitude of ΔV divided by the amplitude of Δp. The magnitude of the denominator is:

$$\left[(1 + \frac{C}{2\sqrt{f}})^2 + (\frac{C}{2\sqrt{f}})^2\right]^{1/2} \doteq 1 + \frac{C}{2\sqrt{f}} \qquad \text{(C-23)}$$

since $C \ll 1$. In that case (C-18) becomes:

$$V_b = \gamma p \frac{\left[\frac{|\Delta V|}{|\Delta p|} - a\right]}{1 + \frac{C}{2\sqrt{f}}} \qquad \text{(C-24)}$$

In order to find C equate the real part of each side of (C-21):

$$\frac{C}{2} = \frac{\sqrt{f_1 f_2} \left[\Delta p_1 p_2 \cos\theta_1 - \Delta p_2 p_1 \cos\theta_2\right]}{\sqrt{f_1} \, \Delta p_2 p_1 \cos\theta_2 - \sqrt{f_1} \, \Delta p_1 p_2 \cos\theta_1} \qquad \text{(C-25)}$$

where θ_1 and θ_2 are the phase angles between ΔV and Δp_1 and Δp_2 respectively. Since C is a small correction to V_b and θ_1 is usually less than $20°$, it is possible to set $\cos\theta_1 = 1$ in formula (C-25).

CORNER BOUNDARY LAYERS

So far we have assumed that the interfaces are plane. If there is a corner, the boundary layers from each plane overlap at the corner. The volume of the corner is counted twice in formulas (C-14) and (C-16) for an inside corner, and is omitted for and outside corner. The volume of the corner, V_c, equals the square of the boundary layer thickness times the length of the perimeter of the corner, l_c.

$$V_c = d_o^2 \frac{l_c}{f} \qquad \text{for a solid-liquid interface}$$
$$\qquad \qquad \qquad \qquad \qquad \qquad \qquad \text{(C-26)}$$
$$= d_i^2 \frac{l_c}{f} \qquad \text{for a gas-liquid interface}$$

In either case an analysis similar to that leading to equation (C-11) results in:

$$\kappa_{av} = \frac{\gamma}{1 + \frac{C}{2\sqrt{f}} - \frac{D}{f}} \qquad \text{(C-27)}$$

It is possible, using data points at three different frequencies, to find C and D with formulas similar to (C-12). If the phase angles between ΔV and Δp are small enough so that $\cos\phi \sim 1$, the equations for finding C and D are:

$$\frac{C}{2}\left[\frac{\Delta p_i p_j}{\sqrt{f_i}} - \frac{\Delta p_j p_i}{\sqrt{f_j}}\right] - D\left[\frac{\Delta p_i p_j}{f_i} - \frac{\Delta p_j p_i}{f_j}\right] = [\Delta p_j p_i - \Delta p_i p_j] \qquad (C-28)$$

Three or more equations of this form must be solved simultaneously for three or more values of f_i. For maximum accuracy in determining C and D it is best to use more than three equations of the form (C-28). The data reduction procedure for the overdetermined case is described in Appendix D. When $D = 0$, equation (C-28) reduces to (C-25).

CURVED INTERFACES

Overlap of the boundary layer also occurs when the interface is curved. We can gain insight into the general case of an arbitrary shape by analyzing a spherical bubble. The reasoning and procedure are parallel to that for a plane interface. The equation that is analogous to (C-4) is:

$$\frac{d^2\psi(r)}{dr^2} + \frac{2}{r}\frac{d\psi(r)}{dr} + \frac{i\omega}{D}\psi(r) = 0 \qquad (C-29)$$

The boundary layer approximation applies when the layer length, d, is $d \sim R/3$, where R is the radius of the bubble. In that case we can replace $2/r$ in the second term of (C-29) by $2/R$. Then it becomes a constant coefficient equation and has solutions in terms of exponentials. The eigenvalue equation corresponding to (C-29) is:

$$s = -(1/R) \pm \sqrt{(1/R)^2 - 2i(1/d)^2} \quad ; \quad d = \sqrt{2D/\omega} \qquad (C-30)$$

Since $d \ll R$, we can expand (C-30) in a power series in d/R as:

$$s = -\frac{1}{R} \pm \left[\frac{(1-i)}{d}\right]\left[1 + \frac{i}{4}\left(\frac{d}{R}\right)^2 + \frac{1}{16}\left(\frac{d}{R}\right)^4 + \ldots\right] \qquad (C-31)$$

or

$$s = \frac{(1-i)}{d} - \frac{1}{d} \left(\frac{d}{R} \right) + \frac{(1-i)}{4} \frac{i}{d} \left(\frac{d}{R} \right)^2 + 0 \left(\frac{d}{R} \right)^4 \tag{C-32}$$

The solution of (C-29) for a spherical bubble with $r = R - x$ and the correct choice of sign in equation (C-31) is:

$$\psi(x) = A + \psi_o \exp(-sx/d) \tag{C-33}$$

where A is again a constant. The compressibility in the boundary layer, corresponding to equation (C-6) is:

$$\frac{1}{\kappa} = \frac{1}{\gamma} + \left[\frac{1}{\kappa_i} - \frac{1}{\gamma} \right] \exp(-sR+sr)$$
$$= \frac{1}{\gamma} + \left[\frac{1}{\kappa_i} - \frac{1}{\gamma} \right] \exp(-sx) \tag{C-34}$$

The average compressibility in the boundary layer results from averaging (C-34) over a volume element $4\pi r^2 dr$ from $x = 0$ to L. When the procedure represented by equations (C-9) through (C-16) are carried out we find:

$$C_R = \left[\frac{3}{sR} - \frac{6}{s^2R^2} + \frac{2}{s^3R^3} + 0\frac{1}{s^4R^4} \right] \left[\frac{\gamma}{\kappa_b} - 1 \right] \tag{C-35}$$

for each boundary at the bubble interface. Comparing C_R with the corresponding quantity in equations (C-15) and (C-16), it is seen that as $R \to \infty$, $A_s d_o/V_o$ for a sphere is $4\pi R^2 d_o/(4/3)\pi R^3 = 3d_o/R$, and $1/s = d_o(1+i)/2$, the values for a plane surface. Thus, (C-35) and (C-16) give the same value of κ_{av} as the interface becomes flat. The importance of (C-35) is that it shows the form of the overlap terms for a curved surface. Substituting (C-32) into (C-35) and carrying out the power series expansion we find terms in d/R, $(d/R)^2$ and $(d/R)^3$ that have a frequency dependence like:

$$K_{av} = \frac{\gamma}{1 + \frac{(1+i)}{2} \frac{C}{f^{1/2}} - \frac{D}{f} + \frac{E}{f^{3/2}}} \tag{C-36}$$

The method of (C-28) can be used to find C, D and E. However, E is so small in all practical applications that it can be neglected.

Since a square corner and a spherical curvature have a dependence for the overlap term of -D/f, it is safe to assume that any corner or curved surface can be treated in this way, and equations (C-27) and (C-28) can be used for any interface.

SMALL BUBBLES

The formulas listed above assume that the boundary layers from two sides of an enclosure do not overlap midway between the interface. If Λ is half the distance between the surfaces, then, the largest value of L that can be used in equation (C-4) is $L \sim \Lambda/3$. When overlap of this type occurs, formula (C-15) becomes:

$$\kappa_{av} = \frac{\gamma}{1 + \left[\frac{\gamma}{\kappa_b} - 1\right]\frac{A_s d_o}{V_o\sqrt{f}}\left[1 - \exp\left(-R\frac{\sqrt{f}}{d_o}\right)\right]} \qquad (C-37)$$

and the correction in the denominator of equation (C-12) is no longer proportional to $1/(f)^{1/2}$. In this case it is very difficult to correct for the boundary layer. The compression gaging method has an accuracy of better than 1% only when less than 1% of the ullage volume is in bubbles with radius $R < 3d$.

EXPERIMENTAL RESULTS

This analytical model has been verified experimentally in several ways. For normal operation the volume of the bubble is measured using equation (C-24), which may be modified by (C-27) for greater accuracy. All the quantities on the right hand side of (C-24) are measured except γ. A handbook value of γ is used to complete the calculation. To verify the theory, V_b is also measured and γ is calculated. If γ derived from the measured data is independent of the frequency and the fill level, and also agrees with the handbook value within error, the model is considered adequate. This is the first check of the theory.

The theory also predicts the phase angle between the compressor and the pressure transducer via equation (C-22). As a second and independent check on the correctness of the theory, the phase angle calculated from the measured value of C is compared with the measured phase angle.

A third independent check can be made using equation (C-16) which defines C. Most of the parameters in (C-16) can be measured, and predict the dependence of C on fill level. The measured values of C for various fill levels can be combined with the measured dimensions of the apparatus to find the boundary layer lengths. If these are independent of fill level and frequency, and agree with the handbook values within the estimated error, the theory is proven again. All three methods of verifying the data have been used and the agreement is good in each case.
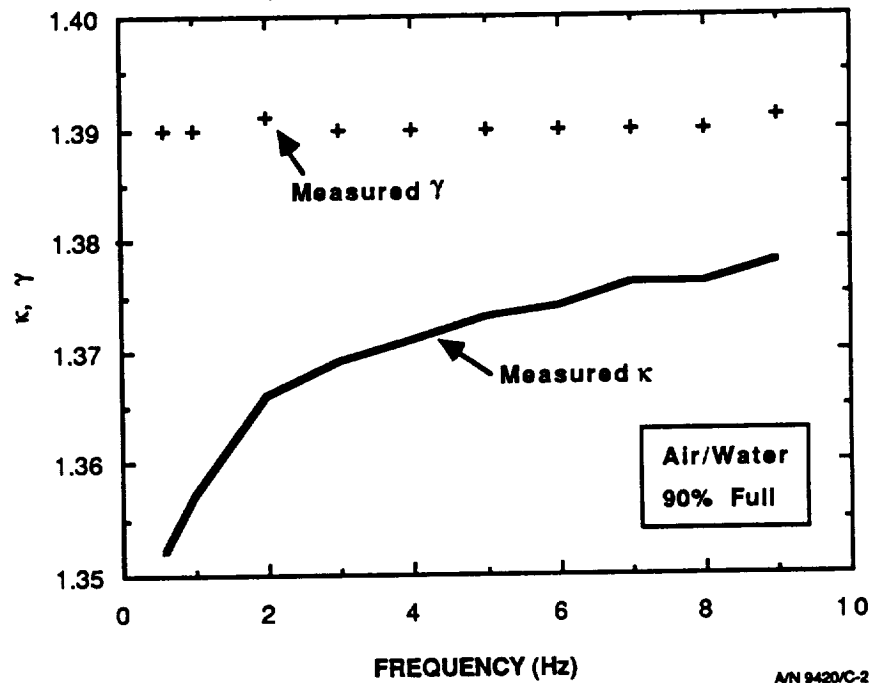
Measurements of γ

The correction for the boundary layer is rather small. For the breadboard test apparatus using air and water, the correction is roughly 1% of the volume when the tank is empty and 5% when 90% full. Thus, C/2 ranges from 0.01 to about 0.05.

The calculation of C using equation (C-25) involves taking the difference of two nearly equal quantities, both in the numerator and the denominator. This leads to a large error accumulation. Since C is a small correction, it is not necessary for normal operation to know C very accurately. However, to verify the theory, it is desirable to find C to the best attainable accuracy. Data were taken at ten frequencies. This leads to 45 different pairs of frequencies and 45 equations like (C-25). Statistical methods were used to find the least squares values of both C and D (see equation C-27). The details of the statistical method are described in Appendix D. With C and D in hand, the value of κ is calculated from (C-1), and then (C-27) is solved with known C and D to find γ. Figures C-1 and C-2 show the result when the tank is empty and 90 percent full, respectively. The line is the measured κ, and the points are the values of γ calculated using the measured values of C and D. For Figure C-1, C/2 = 0.010 and D ~ 0.001, while for Figure C-2, C/2 = 0.03 and D ~ 0.006. For both sets of data the inferred value of γ does not have a trend with frequency and equals the handbook value of 1.398 within the
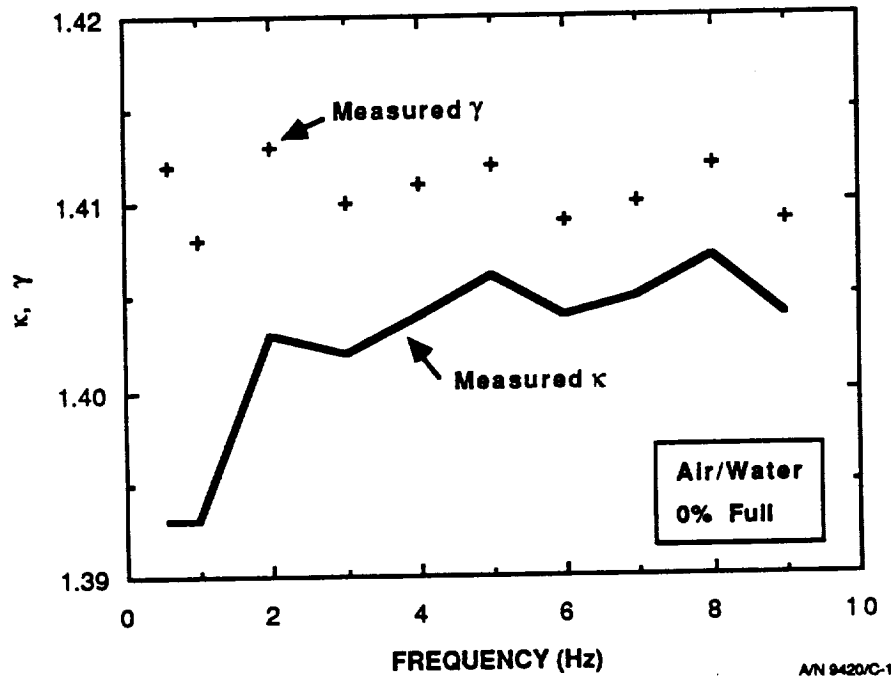
Figure C-1 Amplitude response with air, 0 percent full

Figure C-2 Amplitude response with air, 90 percent full

estimated measurement accuracy of the apparatus. Data at intermediate fill levels resulted in similar results.

The boundary layer lengths for helium gas are much larger than that for air, and equation (C-16) shows that C is proportional to the boundary layer lengths. Thus, a larger value of C can be expected for He. Adequate accuracy is achieved with four frequency points. Figure C-3 shows the data at 50% full for He and water. Here $C/2 = 0.52$ and $D \sim 0.004$. At 90% full the correction to the volume for He gas will be about 15%. Again, the inferred value of γ is independent of frequency. This first test of the theory, as proposed above, shows agreement.

Phase Angles

A comparison of the observed phase angle and the value calculated using the measured value of C in equation (C-22) was made for all the data. This angle is very small, ranging from about $0.5°$ when empty to $2.5°$ when 90 percent full, for our apparatus using air and water. Figure C-4 shows the calculated values as a curve and the measured angles as points, measured with air at a fill level of 90 percent. All the data show agreement similar to that of Figure C-4.

The small discrepancies between the theory and measurements in Figure C-4 are believed to be due mostly in errors in the calibration of the electronics because the same pattern of high and low points occurs in all data sets at the same frequencies. The calibration curve of phase vs. frequency of the electronics has a discontinuity at 4 Hz and another at 7 Hz. If the calibration curve were smooth, the two sets of points would have negligible spread.

For He gas the value of C is much larger and the angle can get as large as $10°$. The data for He gas at 50% full is shown in Figure C-5. This second test of the theory, as proposed, therefore shows agreement.
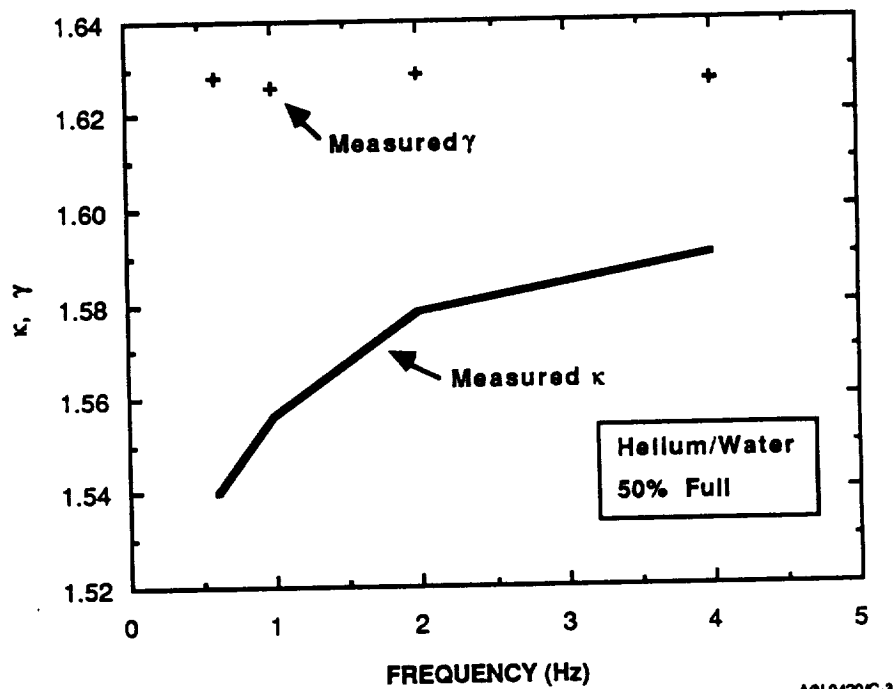
Figure C-3   Amplitude response with helium, 50 percent full
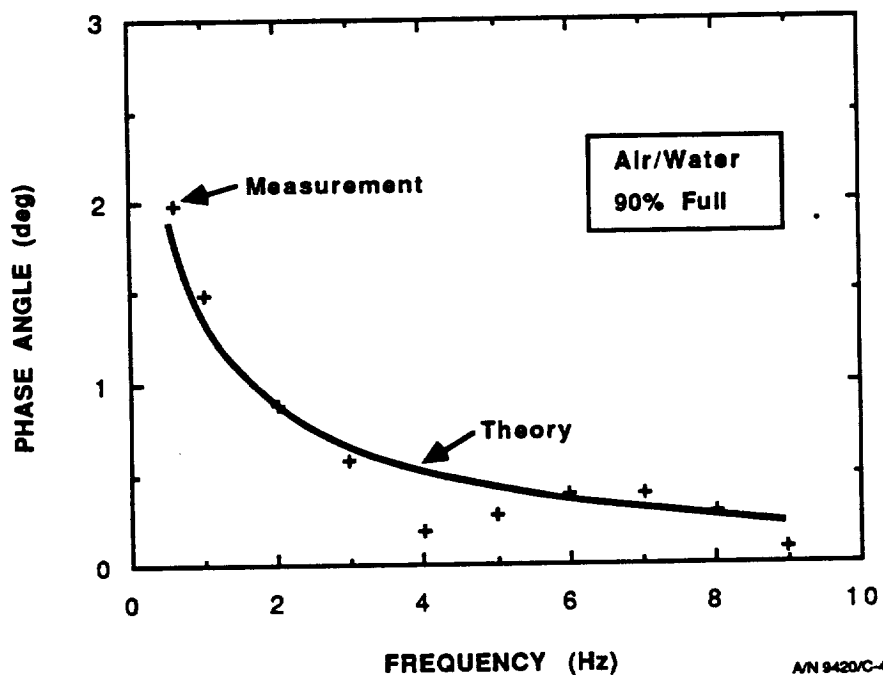
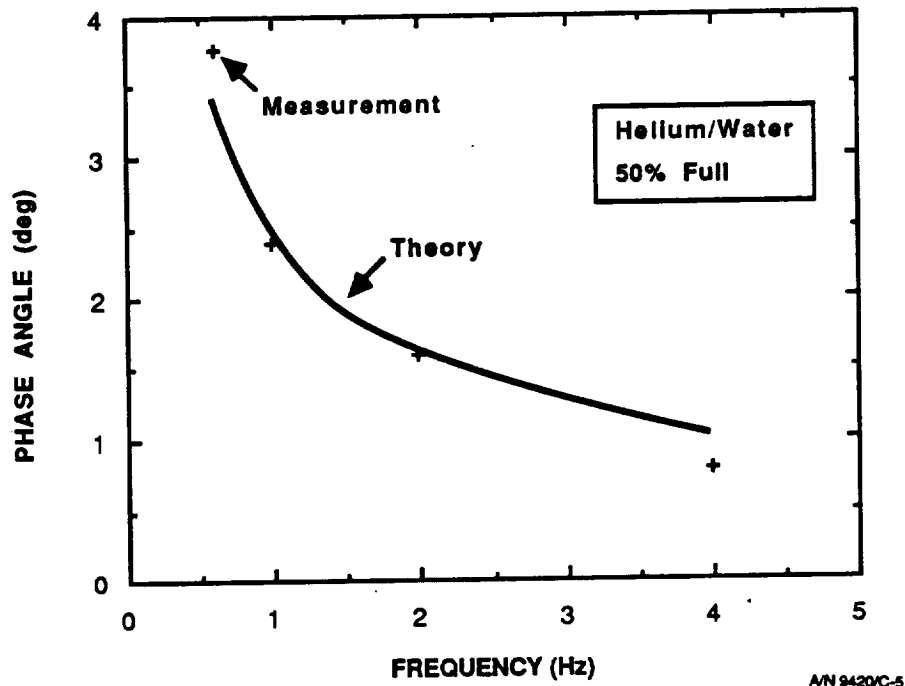Figure C-4   Phase response with air, 90 percent full

Figure C-5 Phase response with helium, 50 percent full

Boundary Layer Lengths

The values of C derived from the experimental data by making a least squares fit to equation (C-25) are used via (C-16) to find $(\gamma/\kappa_b - 1)d$ for each of the boundary layers. The values of the areas of the interfaces of the gas at the solid walls A_s and at the liquid, A_l are estimated as a function of fill level. Neither A_s nor A_l are known very accurately because of numerous flanges and internal hardware. However, the purpose here is to demonstrate the internal consistency of the theory. Accordingly, an estimate of the d values to ±100% is adequate.

For an empty tank all the boundaries are solid and there is only one term in (C-16). In that case we find $(\gamma/\kappa_b - 1)d_o = 0.102$ cm for the data shown in Figure C-1. It can be assumed that for a stainless steel wall at f ~ 1 Hz, κ_b ~ 1. This leads to $d_o = 0.255$ cm for air for which $\gamma = 1.40$. The handbook value is $d_o = 0.25$ cm. This excellent agreement is fortuitous because the accumulated accuracy of A, κ_b and C is about 50 percent. The run-to-run variation in measured d_o is roughly 50 percent.

For other levels of fill, part of the boundary consists of an interface with the liquid. In that case there are two boundary layers, d_{1o} and d_{2o}, which are superposed. Since A_s and A_l vary with fill level, it is possible to use statistical methods to find a least squares fit to $(\gamma/\kappa_b - 1)d_o$ and to $(\gamma/\kappa_{b1} - 1)d_{1o} + (\gamma/\kappa_{b2} - 1)d_{2o}$ if C is measured vs. fill level. It is not known what value to use for κ_{b1} and κ_{b2}; they vary between 1 and γ. The best guess is that $\kappa_{b1} \sim \kappa_{b2} \sim 1$. In that case the data for air results in $d_{1o} + d_{2o} \sim 3d_o$, which is reasonable. Although the results on the boundary layer lengths are not as convincing as the other two tests of the theory, the experimental values are consistent with the predictions.

Appendix D

COMPUTER PROGRAM
for the
ACOUSTIC BOUNDARY
LAYER

Appendix D
COMPUTER PROGRAM FOR THE ACOUSTIC BOUNDARY LAYER

When maximum accuracy is desired for compression gaging, the basic measuring formula must be corrected for the acoustic boundary layer. The theory of the correction is explained in Appendix C. There are two parameters, CC and D, which are used in the correction. They are deduced from the measured data. The purpose of this report is to describe how the data are processed to find CC and D.

The correction is of the form:

$$V = \frac{p\gamma\Delta V}{\Delta p}\left[\frac{1}{1 + \frac{CC}{\sqrt{f}} - \frac{D}{f}}\right] \qquad (D\text{-}1)$$

where f is the frequency of the compressor, p is the mean storage pressure and Δp is the pressure variation due to the compressor. (Note that for simplicity in the algebra we are computing CC=C/2, instead of the parameter C defined in Section 4.2 and Appendix C.) Measurements of p and Δp are made at several frequencies. The readings are made sufficiently fast so that V, the ullage volume, and the ullage configuration have not changed. Since the compressor displacement ΔV and the ratio of specific heats γ are constant, $V/\Delta V\gamma$ can be equated at different frequencies to get the constants CC and D. A little algebra shows that:

$$CC\left[\frac{\Delta p_a p_b}{\sqrt{f_a}} - \frac{\Delta p_b p_a}{\sqrt{f_b}}\right] + D\left[\frac{\Delta p_b p_a}{f_b} - \frac{\Delta p_a p_b}{f_a}\right] = \Delta p_b p_a - \Delta p_a p_b \qquad (D\text{-}2)$$

or   a CC + b D = R

This is a linear algebraic equation in the unknowns CC and D. Two equations of this sort have to be solved simultaneously to get the two unknowns. In matrix form (D-2) can be written as

$$S\begin{pmatrix} CC \\ D \end{pmatrix} = R \qquad (D\text{-}3)$$

Then,

$$\left(\begin{smallmatrix} CC \\ D \end{smallmatrix} \right) = S^{-1}R \qquad\qquad (D-4)$$

Since the coefficients in (D-2) are the difference of quantities of nearly the same value, the error estimates of CC and D may be large.

If more than two sets of Δp are measured, the error can be reduced considerably. The system of equations (D-2) can be overdetermined and a least square fit of the parameters can be derived by statistical methods. Equation (D-3) has the same form but the matrix $S_{i,j}$ is not square. It has a length equal to the number of pairs of Δp and a width of two. R also has a length equal to the number of pairs of Δp.

When a system is overdetermined the least-square value of the unknowns is:

$$\left(\begin{smallmatrix} CC \\ D \end{smallmatrix} \right) = (S^T S)^{-1} SR \qquad\qquad (D-5)$$

Here, S^T is the transpose of S. The dimensions of the matrix is such that $S^T S$ is square and can be inverted and the resulting product is a vector of length two.

The next step is to find as many equations of the form (D-2) as possible with the given data. One equation results from every <u>pair</u> of readings. If n readings are taken, there are $(n-1)n/2$ pairs.

The program proceeds as follows. The values of the mean pressure, p_k, the variable pressure, dp_k, the frequency, f_k and the phase shift between the compressor and the variable pressure, ϕ_k are arranged in a table. The program calculates all possible pairs of subscripts and calculates the values of a, b and R in equation (D-2) for each pair of subscripts. The values corresponding to a are called $prf_{k,1}$, those associated with b, $pf_{k,1}$ and for R, $dr_{k,1}$. The matrix elements $S_{m,1}$, $S_{m,2}$ and r_m are formed by selecting the correct subscripts. Then, the operations required by (D-5) are performed and finally CC and D are printed out.

At this point all the data to solve (D-1) are available except γ. The known value of γ for the stored gas can be inserted into (D-1) to find V. In the case of testing, V is measured dirctly instead of being derived from (D-1) and γ is computed. A constant value of γ indicates that the correction for the acoustic boundary layer has been successful and that there are no other effects that have been overlooked. The program, as used to reduce the test data, computes and plots γ vs. frequency.

The theory indicates that ϕ_k should be related to CC as:

$$\phi_k = \arctan\left[\frac{CC}{\sqrt{f}}\right]\left[\frac{180}{\pi}\right] \tag{D-6}$$

The program calculates the angle from (D-6) as ph_k and plots both ph_k and ϕ_k vs. frequency. Agreement of ph_k and ϕ_k indicates a successful correction. This is a double check on the constancy of γ.

Appendix E

EFFECTS
of
RESONANCE

Appendix E
EFFECTS OF RESONANCES

INTRODUCTION

For accurate results, the analysis of compression gauging must account for resonances in the system. A resonance can occur whenever a part of the system has both inertia and a corresponding restoring force. A resonance is only excited when the driving force moves the system in the pattern of the resonant mode.

The effect of each resonance is to multiply the measuring formula by a resonance factor. If there are two resonances at natural frequencies ω_{n1} and ω_{n2} the measuring formula has the form:

$$V = \frac{\gamma p \Delta V}{\Delta p} \cdot \left[\frac{\omega_{n1}^2}{\omega_{n1}^2 - \omega^2 + 2i\varsigma_1\omega\,\omega_{n1}} \right] \cdot \left[\frac{\omega_{n2}^2}{\omega_{n1}^2 - \omega^2 + 2i\varsigma_2\omega\,\omega_{n2}} \right] \qquad (E-1)$$

Additional resonances require further products.

There are several potential sources of resonance in compression gauging: (1) the tank structure, (2) surface waves, (3) the pressure transducer, and (4) oscillation of the ullage bubbles. Each source of resonance may have a series of resonances. The series of one source may overlap that of another and the sequence of possible resonance frequencies can be quite complicated. Each resonance may be coupled to each other resonance. If the resonance envelopes overlap, i.e., the resonant frequencies are close, the coupling between the modes will shift the natural frequencies of each of the coupled pair. This further complicates the analysis.

For some of the sources of resonance, the location, line shape and coupling to other modes depend on the fill level and/or the ullage configuration. Since these are not known, it is not possible to include the resonances in the measuring formula. It appears that the only method of operation which seems feasible is to operate in a frequency range well below the lowest relevant resonance. The resonance factors in equation (E-1) produce an error of 0.5 percent for a frequency 1/15 that of the natural frequency. Thus, the

upper limit of the compressor frequency is 1/15 that of the lowest resonance that could perturb Δp significantly.

There is also a limiting lower frequency value determined by the time required to make a measurement and by the size of the ullage bubbles. The data processing necessary to achieve a 1 percent accuracy requires an integration over several periods of the signal to reduce the noise. As the frequency decreases, the integration time therefore increases. This number depends strongly on the pressure transducer noise, the background acceleration level, the electrical interference, and the data processing algorithm. The integration time must also be less than the time for the ullage to reconfigure.

If the frequency is too low, the boundary layers from opposite sides of the ullage bubbles will overlap and the measurement will depend on the average radius of the bubbles, which is not known. For air in water the boundary layer width is $d_o/(f)^{1/2}$ where $d_o = 0.25$ cm and f is the compressor frequency. At 0.1 Hz the volume of bubbles smaller than about 1.5 cm is therefore measured incorrectly. If 99 percent of the volume is in bubbles larger than 1.5 cm in radius, for this case, the overall measurement is accurate.

It is evident that it is important to have formulas for the calculation of the lowest resonance for each source of resonance. The purpose of this appendix is to present these formulas.

TANK STRUCTURE

The lowest mode of a tank, when driven by a uniform oscillating internal pressure, is a uniform expansion and contraction. The spring constant for this type of motion for any tank strong enough to contain the fluid safely is so high that the frequency of resonance is never the lowest of the system. In section 4 we will show that the tank can be modeled as an additional bubble of very low compressibility.

SURFACE WAVES

There are two restraining forces for surface waves: gravity and capillarity. For ground testing both are operative. For space applications only capillarity occurs.

A uniform driving pressure in the liquid or gas will excite only the lowest mode on a flat surface and none of the modes of a spherical bubble in space. This follows because all modes except the lowest mode on a flat surface conserve volume. A uniform driving pressure cannot conserve volume - it cannot move the fluid in the pattern of the oscillation. The only way surface waves can be generated in the compression driving system - other than the exceptional case - is for the surface wave to couple strongly with some other resonance. In that case the other resonance must produce a nonuniform pressure which in turn excites the surface wave. An example is the cooperative resonance to be discussed below. The strong coupling only exists when the resonance envelopes of the two resonances overlap.

Motion of the storage tank produces nonuniform pressure and will excite surface waves. Since the restraining force is very small, large amplitude waves can be generated by fairly small motions of the tank. However, these oscillations do not interfere directly with the measuring process because they are not synchronous with the compressor motion. All nonsynchronous signals are removed by integration by the data processing algorithm. However, the waves excited by the tank motion will increase the noise level and the integration time required to reach a desired accuracy.

Surface waves present a problem only when they are coupled to the cooperative bubble oscillations. Thus the bubble resonance, not the surface waves, limits the frequency range of the compressor.

PRESSURE TRANSDUCER

The pressure transducer consists of an elastic diaphragm which is connected to the storage tank by a tube. The diaphragm acts as a spring and the fluid in the tube and diaphragm chamber as a mass to form a resonant system. When

the transducer is immersed in the stored liquid, the resonant frequency can be low. This resonant frequency is calculated in Appendix H. Bubbles in the lead-in tube also lower the resonant frequency. It is possible to design the transducer plumbing so that a low resonance can be avoided.

When bubbles are not present in the lead-in tube the resonant frequency is:

$$\omega_n^2 = 2\pi \, R^2/K_d \, \rho L \, V_d \tag{E-2}$$

where R is the radius of the inlet tube, ρ is the density of the fluid in the transducer, L is the length of the lead-in tube, V_d is the volume of the diaphragm chamber, and K_d is the compressibility of the diaphragm chamber. When the diaphragm is mounted in the side of the tank without a lead-in tube the resonant frequency is:

$$\omega_n^2 \text{ wet} = \left[1 + \frac{16 \, a\rho_1}{6\pi \, hp_d}\right]^{-1} \omega_n^2 \text{ dry} \tag{E-3}$$

VOLUME OSCILLATIONS OF ULLAGE BUBBLES

A bubble in an unconfined liquid has a radial resonance at:

$$\omega_n^2 = 3 \, \gamma p/\rho_1 \, R^2 \tag{E-4}$$

where p is the pressure in the bubble, γ is the ratio of specific heats, ρ_1 is the density of the liquid and R is the radius of the bubble. For an air bubble of 1 meter diameter in water the resonant frequency is 6.5 Hz. If there is a single bubble in a tank, this mode cannot occur since the bubble must follow the compressor due to the incompressibility of the liquid. There are higher modes which conserve volume, but they are not excited by a uniform pressure.

When there are two or more bubbles in the tank, a cooperative resonance occurs. The bubbles can oscillate out of phase with the compressor and with each other. Then, the volume amplitude of individual bubbles can be much larger than that of the displacement of the compressor, as is required by resonance. The lowest resonance is set by the two largest bubbles in the

tank. If R_1 and R_2 are the radii of the largest and second largest bubbles respectively, then the lowest cooperative resonance is at:

$$\omega_n^2 = (3\gamma p/\rho_1 R_1^2) \left[\frac{R_1^2 + R_1 R_2 + R_2^2}{R_2^2} \right] \qquad \text{(E-5)}$$

The lowest value occurs when $R_1 = R_2$. Then, a bubble 1 m in diameter has a resonance at 11.3 Hz.

The derivation of equation (E-5) can be found in Appendix F. The case of bubbles attached to the interior structure of the tank is also treated there.

If $1/\gamma p_2$, the compressibility of the second bubble is replaced by K, the compressibility of the tank and V_2 by the tank volume, then (E-5) gives the correct resonant frequency for a single bubble in tune with the tank structure. This is always a very high frequency.

CONCLUSION

The lowest resonance that can be excited directly by the compressor is almost always the cooperative oscillation of the ullage bubbles given by formula (E-5). Surface waves only occur when they have a resonance coupled to the cooperative oscillations. Resonant frequencies of the tank structure and the pressure transducer are higher than that of the cooperative resonance if the hardware is designed properly.

Appendix F

COOPERATIVE
BUBBLE OSCILLATION

Appendix F
COOPERATIVE BUBBLE OSCILLATION

INTRODUCTION

Bubbles resonate when the pressure in the liquid is varied sinusoidally because the gas acts as a spring and the liquid in the vicinity of the interface is a mass. The moving mass of the interface is directly coupled to the spring of compressed gas in the bubble. The experimental data on compression gauging suggests that the compressor excites the resonance of bubbles. When a resonance is excited, the gauging formula must be modified by the inclusion of a resonance factor. This report describes the impact of the resonance bubbles on compression gauging.

In the past, the research on the free oscillation of bubbles has been concerned with individual bubbles. For compression gauging there may be several bubbles in the tank. The tank is a closed system during compressive gauging and the motion of each bubble is coupled directly to that of all the other bubbles. For the low frequencies used in compression gauging the liquid can be treated as incompressible. Then, the sum of the volume changes of all the bubbles must add to the volume displacement of the compressor. This constraint strongly couples the motion of the bubbles. In this case, the resonance is not that of a single bubble but a cooperative oscillation.

A theory of the cooperative resonance of bubbles was developed as part of the fluid quantity gauging project to explain the experimental data. The theory is explained in this appendix and experimental data are presented to confirm the theory. It is shown that the cooperative resonance does not limit the practical application of compressive gauging.

RESONANCE OF SINGLE BUBBLES

The three most common types of bubbles are considered. In low g the bubbles that are not attached to the internal structure of the tank are spherical. Those that are attached are segments of spheres. In 1g the main bubble is cylindrical. Inverted cylindrical containers (buckets) are sometimes used to

simulate a low-g configuration in 1g and this results in cylindrical bubbles. The three types considered here are spherical, spherical segments and cylindrical bubbles. The calculation for spherical bubbles near a wall have been investigated for this project. The formulas contain complicated combinations of geometric parameters but no new physical principles are found. The natural frequencies of the more complicated bubbles are close to that of spheres of the same volume.

The natural angular frequency of a sphere was first calculated by Rayleigh in 1917:

$$\omega_r^2 = \frac{3\,p\gamma}{\rho_1\,R_o^2} - \frac{2\sigma}{\rho_1\,R_o^3} \qquad (F\text{-}1)$$

with p equal to the mean pressure in the bubble, γ is the ratio of specific heats of the gas, ρ_1 is the density of the liquid, and R_o is the radius of the sphere. The natural frequency of a spherical segment was calculated for this project. If the radius is R_o and the altitude is h_o, then the natural angular frequency is:

$$\omega_r^2 = \frac{6p\gamma}{\rho_1 h_o(3R_o - h_o)} - \frac{2\sigma}{\rho_1 R_o^3} \qquad (F\text{-}2)$$

The natural frequency of a bubble in an inverted cylinder was calculated for this project and the derivation is found in Appendix G:

$$\omega_r^2 = \frac{p\gamma}{\rho_1 Z_o^2} \qquad (F\text{-}3)$$

where Z_o is the length of gas in the cylinder.

COOPERATIVE RESONANCE

Spherical Bubbles

The equation of motion of the radius of a spherical bubble with subscript i is given by Rayleigh as:

$$R_i\ddot{R}_i + (3/2)\dot{R}_i^2 = \frac{1}{\rho_1}\left[P_i - P_\infty - \frac{2\sigma}{R_i} - \frac{4\mu\dot{R}_i}{R_i}\right] \qquad \text{(F-4)}$$

where p_i is the pressure in the bubble, p_∞ is the pressure in the liquid far from the bubble, σ is the surface tension, and μ is the viscosity of the liquid. In the absence of gravity p_o is uniform in the tank. For small oscillations in R_i equation (F-4) can be linearized about the mean value of R:

$$R_i = R_{oi}(1 + X_i) \qquad \text{(F-5)}$$

and the pressure in the bubble is:

$$P_i = P_{oi}(R_{oi}/R_i)^{3\kappa} \simeq P_{oi}(1 - 3\kappa_i X_i) \qquad \text{(F-6)}$$

where p_{ol} is the mean pressure in the bubble and $\kappa \simeq \gamma$ is the polytropic exponent. Then (F-4) in linearized form is:

$$\rho_1\bar{R}_{oi}^2\ddot{X}_i + 4\mu\dot{X}_i + (3\kappa_i P_{oi} - 2\sigma/R_{oi})X_i = P_{oi} - 2\sigma/R_{oi} - p_\infty \qquad \text{(F-7)}$$

$$= p_{li} - p_\infty \equiv P$$

In low g, if the thermal stratification is small, the pressure, p_{li}, in the liquid at the interface is uniform in the tank, and the right hand side of (F-7), P, is a constant. Equation (F-7) applies to each bubble. If there is only one bubble in the tank, resonance cannot occur because the volume displacement of the bubble must follow the compressor.

With two or more bubbles in the tank, the volume amplitude of all the bubbles must add up to the compressor displacement:

$$4\pi \sum_i R_{oi}^3 X_i = \Delta V_c \qquad \text{(F-8)}$$

Equation (F-8) couples all the bubbles strongly. Since the driving force is sinusoidal, (F-7) can be written as:

$$L_i X_i = [-\rho_1 R_{oi}^2\omega^2 + 4i\omega\mu + (3\kappa_i P_{oi} - 2\sigma/R_{oi})]\, X_i = P \qquad \text{(F-9)}$$

A set of equations (F-9), one for each bubble, must be solved simultaneously with (F-8) to find the unknowns P and X_i. For the present problem we do not need to know P and X_i, only the resonant frequency. In that case, we can proceed as follows. Use $L_1 X_1 = P$ to eliminate P from the remaining equations in set (F-9). The resulting equations together with (F-8) are a set of n linear algebraic equations in n unknowns, where n is the number of bubbles. The resonant frequency results from setting the determinant of the set n to zero and solving the resulting equation for ω. The number of resonances equals n-1. In the general case of n bubbles the set of linear equations is:

$$L_1 X_1 - L_i X_i = 0 \qquad\qquad i = 2, 3 \ldots n \qquad\qquad\qquad \text{(F-10)}$$

$$R_{o1}{}^3 X_1 + R_{o2}{}^3 X_2 + \ldots = \Delta V_c / 4\pi$$

The determinant of set (F-10) when there are two bubbles is:

$$R_{o1}{}^3 L_2 + R_{o2}{}^3 L_1 = 0 \qquad\qquad\qquad\qquad\qquad\qquad \text{(F-11)}$$

and when there are three bubbles the determinant is:

$$R_{o1}{}^3 L_2 L_3 + R_{o2}{}^3 L_1 L_3 + R_{o3}{}^3 L_1 L_2 = 0 \qquad\qquad\qquad \text{(F-12)}$$

The generalization for n bubbles is that each term contains all subscripts up to n.

The natural frequency is found by solving the generalization of (F-12) for the frequency ω. Equation (F-9), which defines L_i, is very general. It allows the equilibrium pressure and the polytropic coefficient of each bubble to differ. It also includes a term in the surface tension which differs for each bubble. If the thermal stratification is less than about 3K/m, p_{o1} can be treated as the same in all bubbles. If the acoustic boundary layer thickness is less than about 20 percent of the radius of the smallest bubble, if $\kappa_i = \gamma$, and if the bubbles are larger than 1 cm in diameter so that the surface term is negligible, equations (F-9) and (F-12) are less complicated. These assumptions are satisfied for our application. They will be used to simplify the calculation of the natural frequency.

The results of solving equations like (F-12) show that the resonant frequency is always that of the largest bubble, given by equation (F-1), multiplied by a factor which contains the radii of all the bubbles. This factor, which will be called the cooperative factor, is always equal to or larger than 1. For two bubbles:

$$\omega_r^2 = \frac{3\gamma p}{\rho_1 R_{o1}^2} \left[\frac{R_{o1}^3 + R_{o2}^3}{R_{o2}^2 [R_{o1} + R_{o2}]} \right] \tag{F-13}$$

When $R_{o1} = R_{o2}$, the cooperative factor equals 1. When $R_{o1} = 2R_{o2}$, the factor equals 3. For three and four bubbles the formulas are rather complicated. When $R_{o1} = R_{o2} = R_{o3}$, the factor is 3 for each of the two possible modes and when $R_{o1} = 2R_{o2} = 2R_{o3}$, the lower mode has a factor of 5/2 and the higher mode has a factor of 4.

The structure of the cooperative factor is such that the two largest bubbles determine the lowest resonance. The lowest natural frequency occurs when the ullage is in two bubbles of approximately the same size. A conservative estimate of the lowest resonance is therefore to use equation (F-1) with the largest radius that can occur when the ullage consists of two bubbles of equal radius with significant mass between them.

Spherical Segments

The equation for the time dependence of the radius of a spherical segment of altitude h_o is the same as that for a sphere, equation (F-4). However, the dependence of p_i on the radius, equation (F-6), is modified to:

$$p_i = P_{oi} \left\{ 1 - \left[\frac{6\kappa R_{oi}^2}{h_{oi}(3 R_{oi} - h_{oi})} \right] X_i \right\} \tag{F-14}$$

and (F-9) becomes:

$$L_i X_i = \left[-\rho_1 R_{oi}^2 \omega^2 + 4i\omega\mu + 6\kappa P_{oi} \frac{R_{oi}^2}{h_{oi}(3R_{oi} - h_{oi})} \right] X_i \tag{F-15}$$

Also, (F-8) is modified to read:

$$2\pi \sum_i R_{oi}^2\, h_{oi}\, X_i = \Delta V_c \qquad\qquad \text{(F-16)}$$

If there is a mixture of spheres and spherical segments, L_i for the sphere is defined by (F-9) while (F-15) is used for the segments. Likewise, for a mixture, (F-16) becomes:

$$4\pi \sum_i R_{oi}^3\, X_i + 2\pi \sum_j R_{oi}^2\, h_{oj} X_j = \Delta V_c \qquad\qquad \text{(F-17)}$$

where i sums over spheres and j sums over segments. The analysis again consists of solving:

$$R_{o1}^3\, L_2 L_3 \ldots + R_{o2}^3\, L_1\, L_3 \ldots + \tfrac{1}{2}R_{o4}^2\, h_{o4}\, L_1 L_2 \ldots + \tfrac{1}{2}R_{o5}^2 L_1 L_2 \ldots$$
$$= 0 \qquad\qquad \text{(F-18)}$$

for ω. The value of h_{o1} is determined, as a function of R_{o1}, by the contact angle of the fluid. It is not an independent variable.

These results again show that the value of the resonant frequency is never below that of (F-1) or (F-2), which ever is lower, for the largest bubble and the largest segment.

Cylindrical Bubbles

For cylindrical bubbles with a single gas-liquid interface, such as occurs in 1g, the equation corresponding to (F-7) is:

$$\rho_1 Z_{oi}^2\, \ddot{X}_i + \kappa_i \rho_{oi} X_i = P \qquad\qquad \text{(F-19)}$$

and (F-8) becomes:

$$\pi \sum r_{oi}^2\, Z_{oi} X_i = \Delta V_c \qquad\qquad \text{(F-20)}$$

where r_{oi} is the radius of the cylinder. Then, (F-9) is:

$$L_i X_i = [-\rho_1 Z_{oi}^2 \omega^2 + \kappa_i P_{oi}] X_i = P \qquad \text{(F-21)}$$

and the resonance equation, (F-12) becomes:

$$r_{o1}^2 Z_{o1} L_2 L_3 + r_{o2}^2 Z_{o2} L_1 L_3 + r_{o3}^2 L_1 L_2 = 0 \qquad \text{(F-22)}$$

for three bubbles. For two cylindrical bubbles the resonant frequency is:

$$\omega_r^2 = \frac{\kappa p_o}{\rho_1 Z_{o1}^2} \frac{[r_{o1}^2 Z_{o1} + r_{o2}^2 Z_{o2}]}{[r_{o1}^2 Z_{o1}(Z_{o2}/Z_{o1})^2 + r_{o2}^2 Z_{o2}]} \qquad \text{(F-23)}$$

Again the cooperative factor is always larger than 1. From these examples it becomes clear that the cooperative factor may be written:

$$\frac{[\text{total volume of ullage}]}{(\text{volume of 1})(\text{length ratio})^2 + (\text{volume of 2})(\text{length ratio})^2 + \ldots} \qquad \text{(F-24)}$$

EXPERIMENTAL RESULTS

Cylindrical Bubbles

The theory was tested in 1g using large inverted beakers to simulate multiple bubbles in low g. The arrangement of the beakers is shown schematically in Figure F-1.

Twelve inverted beakers are distributed roughly uniformly in the test tank. Any beaker may be filled with air or water as desired. The bubbles are all cylindrical and the formulas (E-19) through (E-24) apply. There is one large bubble and 12 small bubbles. The small bubbles all have the same dimensions and the associated L's of formula (F-21) are all very nearly the same, that is:

$$L_i = L_2 \qquad \text{for } i = 2 \ldots 13 \qquad \text{(F-25)}$$
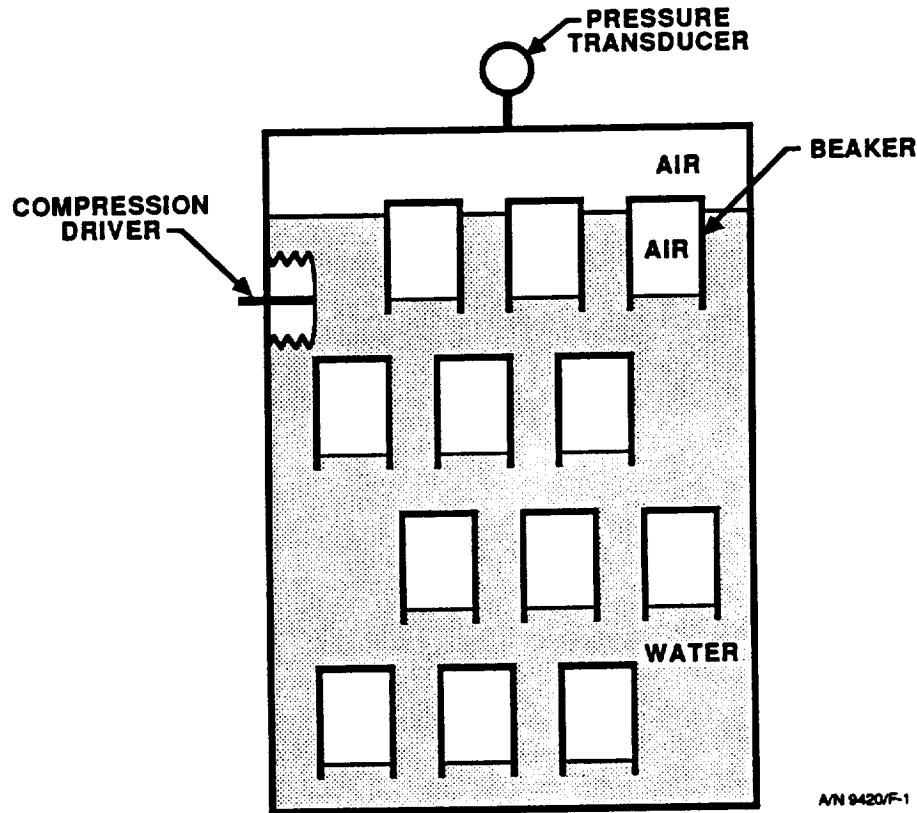
and
$$X_i = X_2$$

Figure F-1 Multiple bubble geometry

Here, we are using the subscript 1 for the large bubble at the top of the tank and 2 - 13 for the inverted beakers. The 12 small bubbles oscillate in phase and act as one bubble when the beakers are filled with air to the same volume. Then equations (F-20) and (F-21) become:

$$\pi \, r_{o1}^2 \, Z_{o1} \, X_1 \; + \; 12\pi \, r_{o2}^2 \, Z_{o2} \, X_2 \; = \; \Delta V_c \qquad\qquad \text{(F-26)}$$

$$\text{or} \qquad\qquad V_1 \, X_1 \; + \; 12 \, V_2 \, X_2 \qquad = \; \Delta V_c$$

$$\text{and} \quad L_1 \, X_1 \; = \; L_2 \, X_2$$

Solving (F-26) for X_1, the oscillating pressure amplitude measured by the pressure transducer in bubble 1:

$$X_1 \; = \; \frac{L_2 \, \Delta V_c}{V_1 \, L_2 \; + \; 12 \, V_2 \, L_1} \qquad\qquad \text{(F-27)}$$

The numerator goes through a minimum at the resonant frequency of an individual small bubble and the denominator has a minimum at the cooperative resonance. When the dimensions of the apparatus are used in equations (F-21) and (F-27), the predicted value of X_1 can be found. Figure F-2 is a comparison of theory and experiment. The line is the predicted value of X_1 vs frequency and the plus signs are the measured data. The agreement is better than would be expected from the uncertainty in the dimensions of the apparatus. When the number of beakers filled with air is three and six instead of 12, the data also show good agreement.

The phase angle between the compressor and the pressure transducer is very sensitive to resonances. A change in the resonance frequencies of either the small bubble or the cooperative resonance of about 1 percent will produce an error of $10°$ in the phase difference near resonance. The measured and predicted results are compared in Figure F-3. Considering the uncertainty in the dimensions of the apparatus, the agreement is very good. The comparison of the phase difference is an independent check on the correctness of the theory.

Mylar Balloons

Another way to simulate low-g bubbles has been tested. Mylar balloons, filled with air and held down by weighted mesh bags, are immersed in the test tank. The shape of the balloon in the tank is shown schematically in Figure F-4.

It is observed that the only part of the balloon surface which moves in response to the compressor is the flaccid bottom. It is difficult to relate this system to that of any of the three types of bubbles considered above. It is probably closest to a cylindrical bubble.

A test was conducted with three mylar balloons of sufficiently different volume so that their resonant frequencies are at least 1 Hz apart. With three balloons and an airspace at the top of the tank:
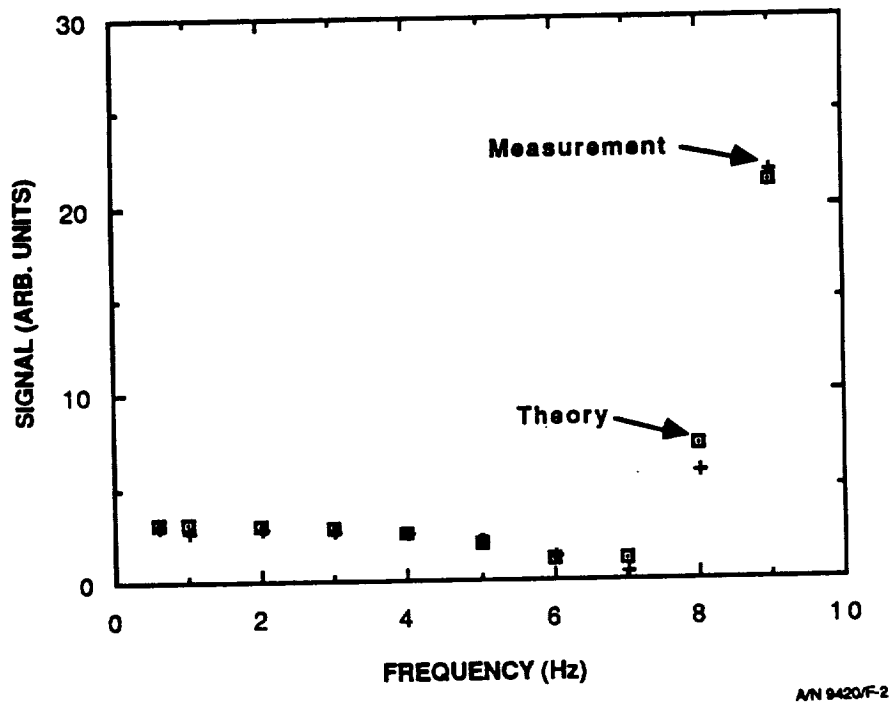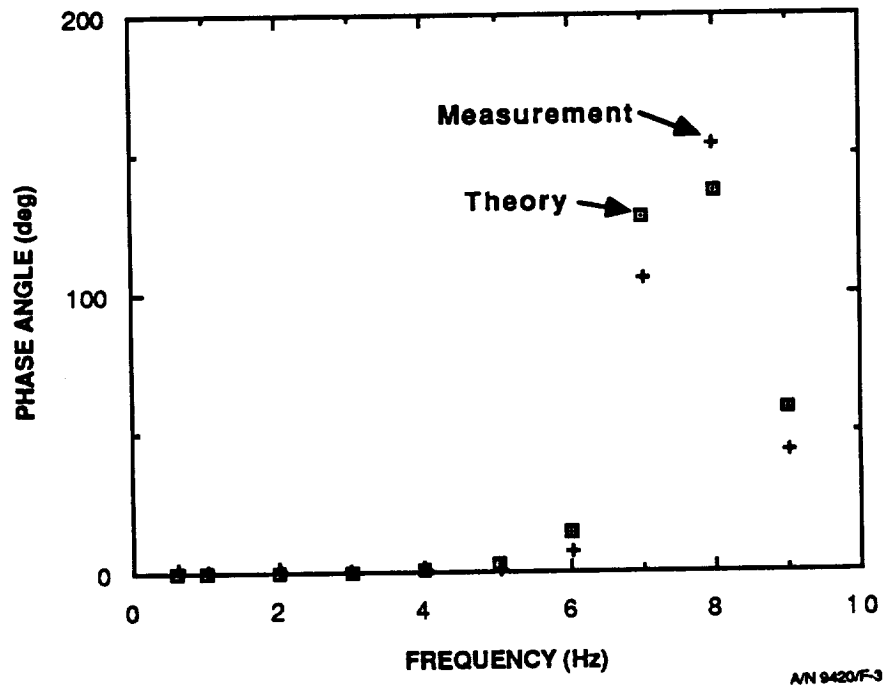
Figure F-2 Amplitude response with 12 cups

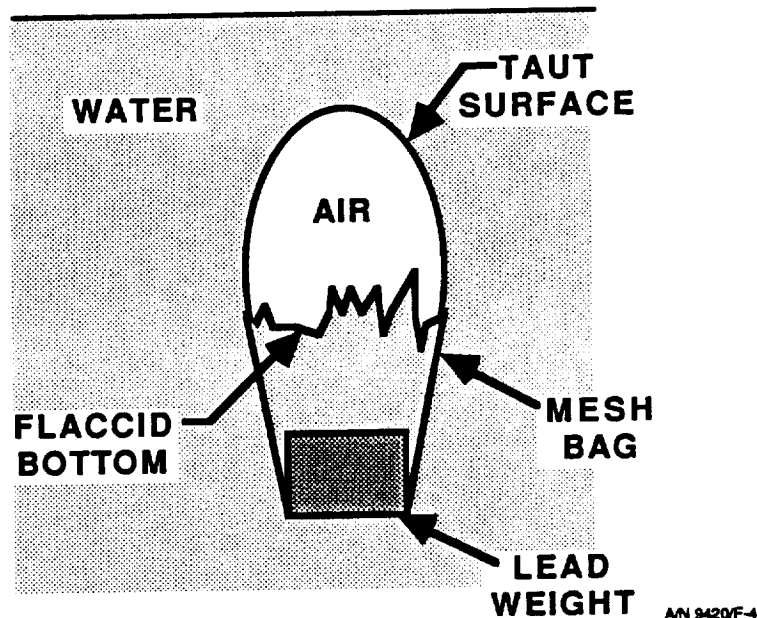Figure F-3 Phase response with 12 cups

Figure F-4 · Mylar balloon geometry

$$X_1 = \frac{L_2\ L_3\ L_4\ \Delta V_c}{V_1 L_2 L_3 L_4 + V_2 L_1 L_3 L_4 + V_3 L_1 L_2 L_4 + V_4 L_1 L_2 L_3} \qquad (F-28)$$

The resonant frequency of each balloon should appear in the data as a local minimum in the response curve and the cooperative resonance as a maximum. Figure F-5 shows the results of the response vs frequency. The various minima and the maximum are evident. The maximum and minima are roughly where they are predicted to be using formulas for a cylindrical bubble. The agreement is good considering that the shape of the balloon and the surface which is moving is very poorly defined.

CONCLUSION

Cooperative bubble resonances could cause large errors in the computed volume if the compressor frequency were close to resonance if the data are not corrected for the resonance. It appears impractical to correct for the resonance for several reasons. If there is only one resonance, i.e., two
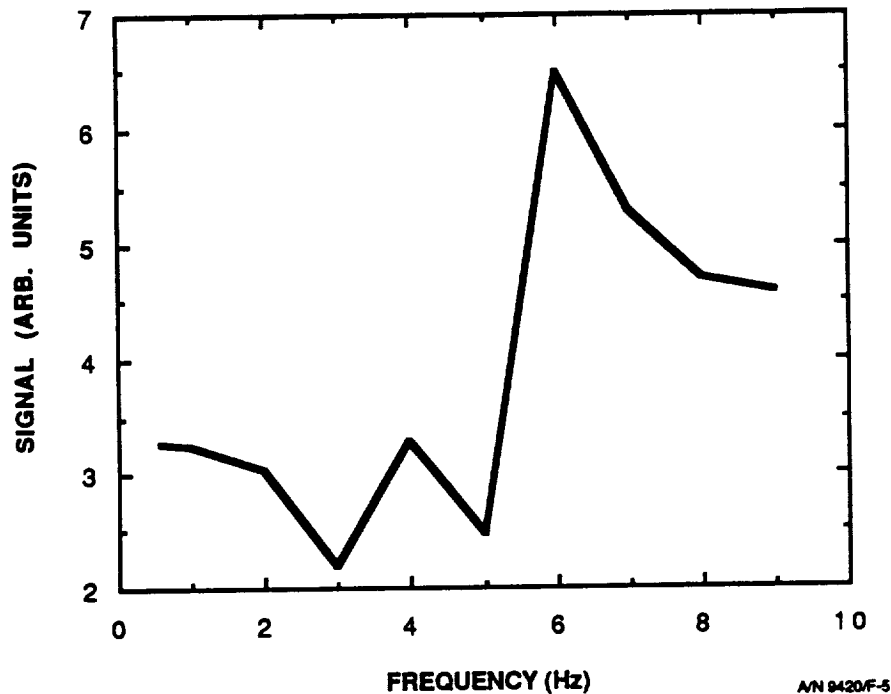
Figure F-5 Amplitude response with three balloons

large bubbles, the correction is dependent on whether the pressure transducers is connected to bubble 1 or bubble 2 or to the liquid between the bubbles. When the transducer measures bubble 1 we have:

$$X_1 = \frac{L_2 \, \Delta V_c}{V_1 L_2 + V_2 L_1} \qquad\qquad (\text{F-29})$$

When, the transducer measures bubble 2:

$$X_2 = \frac{L_1 \, \Delta V_c}{V_1 L_2 + V_2 L_1} \qquad\qquad (\text{F-30})$$

While the pressure in the liquid is:

$$P = \frac{L_1 L_2 \, \Delta V}{V_1 L_2 + V_2 L_1} \qquad\qquad (\text{F-31})$$

Another difficulty arises if there are several large bubbles of nearly the same size. Then, the response is similar to (F-28) and Figure F-5. In each case, it is necessary to measure the parameters in each L_i. Since several L_i are involved and each has two parameter, the number of measurements, each at a different frequency, becomes excessive. Also, it is not known *a priori* how many L_i are involved.

The compression gaging method will work if the compressor frequency is kept a decade below the lowest resonance. This report shows that the lowest resonance can be calculated with confidence. The resulting frequency, even for large tanks, is not unreasonably low.

RESONANCE FREQUENCY

of

CYLINDRICAL BUBBLES

Appendix G
RESONANT FREQUENCY OF CYLINDRICAL BUBBLES

It would be desirable to simulate the low-g configuration of bubbles in a storage tank in 1g. Key features of the dynamics of free bubbles can be investigated using inverted cylindrical containers. This method of simulation has been used in our research for the development of compression gauging. In order to analyze these results it is useful to have a formula for the resonant frequency of a gas bubble in an inverted cylinder. It is the purpose of this report to derive this formula.

In 1917 Rayleigh derived the natural frequency of a spherical bubble. A parallel development is used here with the spherical geometry replaced with the cylindrical symmetry. It assumes that the system is open or vented. The modification of the resonant frequency for a closed tank is derived in Appendix F.
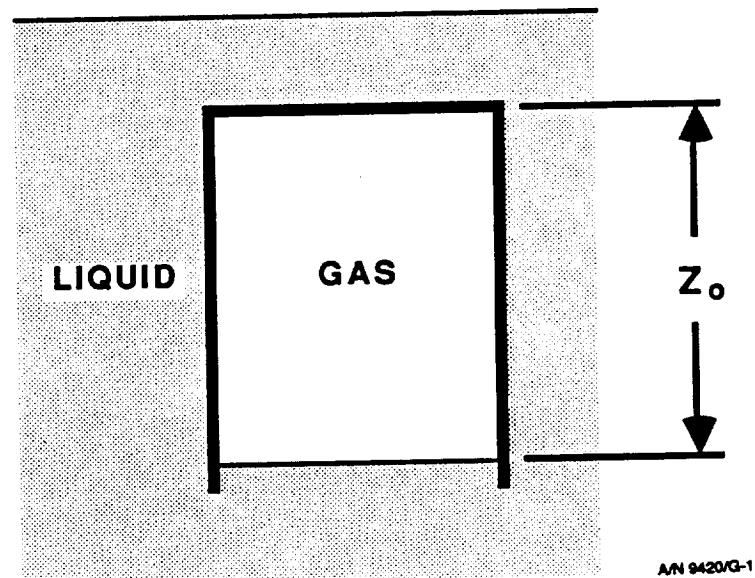
The geometry is shown in Figure G-1.

A/N 9420/G-1

Figure G-1 Cylindrical bubble geometry

It is reasonable in this case to neglect viscous loses. The velocity of the gas in the cylinder is in the z direction only. The pressure in the liquid, p_1, is uniform far from the lip of the cylinder. The pressure in the gas, p_b, is uniform and depends on the compression:

$$p_b = p_{bo} (Z_o/Z)^\gamma; \qquad p_b = p_1 \Big|_{z=0} \qquad (G-1)$$

The velocity of the liquid in the cylinder near the lip can be derived from a potential:

$$\nabla^2 \phi = 0 \qquad\qquad \dot{Z} = \nabla \phi \qquad\qquad \phi = Z\dot{Z} \qquad (G-2)$$

The equation of motion is:

$$p_1 - \rho_1 \frac{\partial \phi}{\partial t} = P_\infty (1 + \epsilon \cos \omega t) \qquad (G-3)$$

Let $z = z_o (1 + x)$. Then,

$$p_b = p_{bo} + \frac{\partial p_b}{\partial x}\bigg|_{\substack{x \\ z=0}} = p_1 \bigg|_{z=0} \qquad (G-4)$$

and

$$\frac{\partial p_b}{\partial x} = -p_{bo}\gamma$$

Then (G-3) becomes:

$$\rho_1 \frac{\partial \phi}{\partial t} + p_{bo}\,\gamma x = -P_\infty \epsilon \cos \omega t \qquad (G-5)$$

From (G-2):

$$\frac{\partial \phi}{\partial t} = \dot{Z}^2 + Z\ddot{Z} \qquad (G-6)$$

and in a linear approximation on x:

$$\frac{\partial \phi}{\partial t} = Z_o^2 \; \ddot{x} \qquad\qquad\qquad (G-7)$$

Then, (G-5) becomes:

$$\rho_1 Z_o^2 \ddot{x} + p_{bo}\gamma x = -P_\infty \epsilon \cos \omega t \qquad\qquad (G-8)$$

and finally the natural angular frequency, ω_r, is:

$$\omega_r^2 = \frac{p_{bo}\gamma}{\rho_1 Z_o^2} \qquad\qquad\qquad (G-9)$$

For a cylinder 20 cm long, the natural frequency using air and water is 9.5 Hz.

Appendix H

PRESSURE TRANSDUCER
RESONANCE

Appendix H
PRESSURE TRANSDUCER RESONANCE

The commercial pressure transducer of the breadboard gauging system is connected to the storage tank by a long, narrow lead-in tube. This design has resulted in errors of up to 5 percent in the measurement of the ullage volume when the transducer is filled with liquid. It is observed that the oscillating pressure measured by the transducer Δp_d has a stronger dependence on frequency when the transducer is immersed in liquid than when it is in air. A model is presented which shows that the transducer pressure differs from the pressure in the tank Δp due to the lead-in tube; this is a resonance effect. The transducer acts as a spring and the liquid in the tube as a mass.

The natural frequency of the diaphragm of the transducer in air is in excess of 1 kHz. The added mass of the liquid in the tube, when the transducer is immersed, lowers the natural frequency to about 40 Hz. Then, the recorded pressure amplitude differs from the tank pressure by a resonance factor.

$$\Delta p_d = \Delta p \; \frac{f_n^2}{f_n^2 - f^2 + 2i\varsigma f_n f} \qquad (H-1)$$

where f_n is the natural frequency of the transducer, f is the compressor frequency and ς is the decay constant. When $f_n \simeq 1$ kHz the correction is negligible for f in the range 1 - 10 Hz, but it results in a 5 percent correction when $f_n \simeq 40$ Hz.

The purpose of this report is to describe the model. It is desirable to operate the gauge so that the resonant frequency of the transducer is high enough so that the correction given by equation (H-1) is well below 0.5 percent. A result of the model is a design equation for f_n. With this knowledge future systems can be designed to satisfy this requirement.

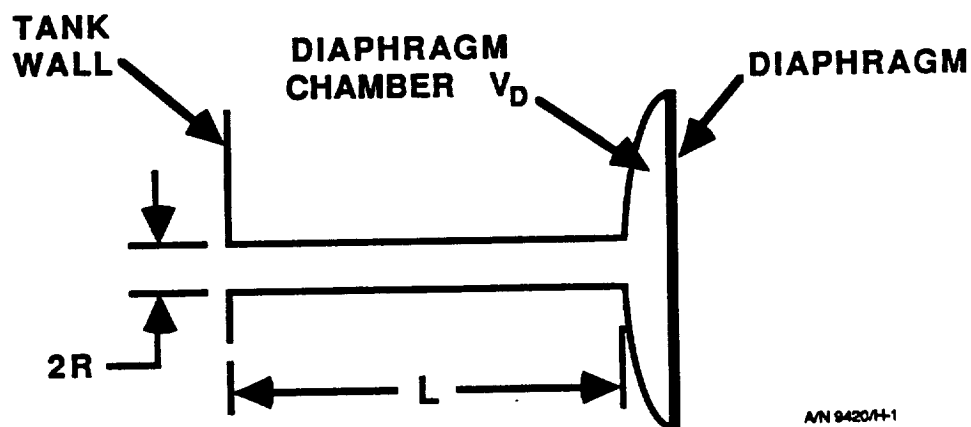The geometry of the transducer to be modeled is shown in Figure H-1.

Figure H-1 Transducer tube and diaphragm geometry

The velocity u(r,t,) of the fluid in the tube is a function of the radius r and the time t.

The diaphragm is assumed to be elastic and to have a constant compressibility. If the volume of the diaphragm chamber is V_d, and the pressure is p_d, then, the compressibility is:

$$K = \frac{1}{V_d} \; \frac{\Delta V_d}{\Delta P_d}$$

(H-2)

Then, ΔV_d is the flow into the chamber from the lead-in tube:

$$\Delta V_d = \int_o^t \int_o^r u(r,t) \; 2\pi r \; dr \; dt \;\; = \;\; \pi R^2 \int_o^t \bar{u} \; dt$$

(H-3)

The back pressure developed by the diaphragm is:

$$\Delta p_d = \frac{1}{KV_d} \Delta V_d = \pi R^2 k \int_o^t \bar{u}\, dt = \pi R^2 k\, \bar{x}(t) \tag{H-4}$$

where

$$k = \frac{1}{KV_d} = \frac{\Delta p_d}{\Delta V_d}$$

where, $\bar{x}$ is the radially averaged displacement of the fluid in the tube. The equation for the motion of the fluid in the tube is:

$$\frac{\partial u}{\partial t} = \nu\, \nabla^2 u - \frac{1}{\rho}\, \frac{dp}{dx} \tag{H-5}$$

where ν is the kinematic viscosity and ρ is the density. For pipe flow dp/dx is independent of radius and distance down the pipe; it is a constant. For incompressible flow u is also independent of the distance down the tube.

The next step is to average (H-5) radially. Now:

$$\overline{\nabla^2 u} = \int_o^R \left[\frac{1}{r}\, \frac{\partial}{\partial r}\, (r\, \frac{\partial}{\partial r})u \right] 2\pi r dr = 2\pi R\, \frac{\partial u}{\partial r}\, \Big|_R = \pi R^2 D\bar{u} \tag{H-6}$$

and this requires:

$$D = \{2\, \frac{\partial u}{\partial r}\Big|_R\}/uR \tag{H-7}$$

Also note that the pressure difference across the pipe is the difference between the impressed pressure and the back pressure of the diaphragm:

$$-dp/dx = \frac{\Delta p - \Delta p_d}{L} = \frac{\Delta p - \pi R^2 k\, \bar{x}}{L} \tag{H-8}$$

Then, (H-5) becomes:

$$\rho L \pi R^2 \, \frac{d^2 \bar{x}}{dt^2} - \nu \rho L \pi R^2 D \, \frac{d\bar{x}}{dt} + (\pi R^2)^2 \, k\bar{x} = \pi R^2 \Delta p(t) \tag{H-9}$$

or

$$\ddot{\bar{x}} - \nu D \, \dot{\bar{x}} + \frac{\pi R^2 k}{\rho L} \, \bar{x} = \frac{\Delta p}{\rho L} \tag{H-10}$$

which is of the standard form:

$$\ddot{\bar{x}} + 2\varsigma \omega_n \, \dot{\bar{x}} + \omega_n^2 \, \bar{x} = \frac{\Delta P}{\rho L}$$

where u is replaced by dx/dt. Since D is a negative parameter, equation (H-10) is a resonance equation. When Δp is sinusoidal the natural angular frequency is:

$$\omega_n = (\pi R^2 k / \rho L)^{1/2} \tag{H-11}$$

and the damping constant is:

$$\varsigma = -\nu D / 2\omega_n \tag{H-12}$$

The resonant frequency and resonance amplification are: $\omega_r = \omega_n (1 - \varsigma^2)^{1/2}$ and $G_{max} = G_o / 2\varsigma$.

The system diagram in the frequency domain is shown in **Figure H-2**.

The physical significance of (H-9) is simply a statement of Newton's first law. The first term is the total mass in the tube times the acceleration of the average displacement. The second term is the total viscous force on the fluid because $\rho L \nu D 2 \pi R \, dx/dt$ is:

$$-(\text{area of wall})(\text{shear force/area}) = -2\pi R L \eta \, \frac{\partial u}{\partial r}\Big|_R \tag{H-13}$$
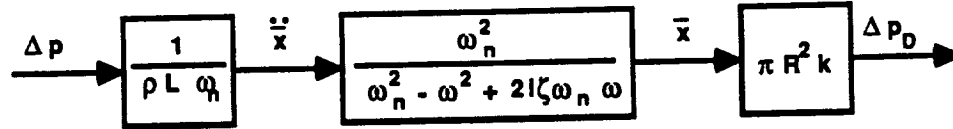
A/N 9420/H-2

Figure H-2 System diagram in the frequency domain

The next two terms are pressures multiplied by the area of the tube and this is the net external force on the mass in the tube.

To complete the problem, the value of u must be calculated to find D in equation (H-7). The steady state for a sinusoidal driving force follows from (H-5):

$$\frac{d^2 u_o}{dr^2} + \frac{1}{r}\frac{du_o}{dr} - \frac{i\omega}{\nu} u_o = -\frac{1}{L\eta}\Delta p - \frac{\pi R^2}{i\omega}\bar{u}_o \qquad (H-14)$$

with $u_o = 0$ at $r = R$. The right hand side is a constant; call it $\nabla P_o/\eta$. Also let $C^2 = -i\omega/\nu$. Then the solution of (H-14) is:

$$u(r,t) = \frac{i\nabla P_o}{\rho\omega}\left[1 - \frac{J_o(rC)}{J_o(RC)}\right]\exp(i\omega t) \qquad (H-15)$$

It follows that:

$$\frac{du}{dr}\Big|_R = \frac{i\nabla P_o}{\rho\omega}\;\frac{J_1(RC)}{J_o(RC)} \qquad (H-16)$$

and

$$\pi R^2 \bar{u}_o = \int_o^R 2\pi r u \, dr = \frac{\pi i \nabla P_o}{\rho \omega} \left[\frac{R^2}{2} - \frac{R}{C} \cdot \frac{J_1(RC)}{J_o(RC)} \right] \qquad \text{(H-17)}$$

The ratio of (H-16) and (H-17) leads to D, according to the definition in equation (H-7).

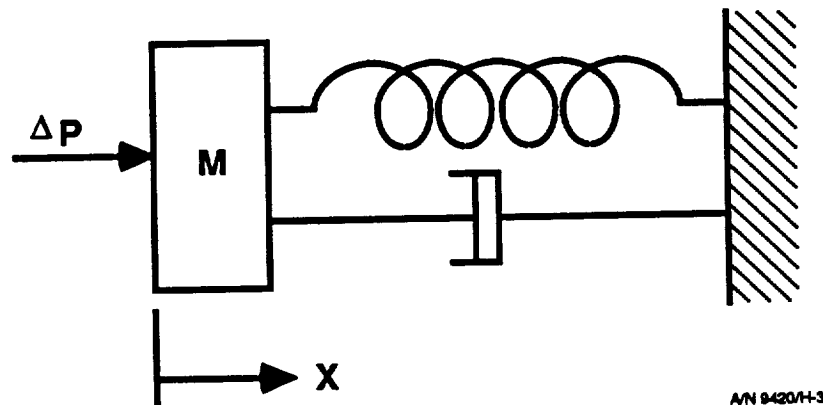Since ∇P_o contains u_o we can rewrite (H-17) as:

$$\pi R^2 \bar{u}_o = \frac{\pi i}{\rho \omega} \left[\frac{R^2}{2} - \frac{R}{C} \frac{J_1(RC)}{J_o(RC)} \right] \cdot \frac{1}{L} \left[\Delta p - \frac{\pi R^2 k}{i \omega} \bar{u}_o \right] \qquad \text{(H-18)}$$

and solving for u_o:

$$\bar{u}_o = \frac{a \frac{\Delta p}{L}}{1 + \pi R^2 ab/L} \; ; \quad a = \frac{i}{\rho \omega} \left[\frac{1}{2} - \frac{J_1(RC)}{J_o(RC)} \right] ; \quad b = \frac{\kappa}{i \omega} \qquad \text{(H-19)}$$

This system may be represented as a system of one mass and one spring; as in Figure H-3, with spring constant $\pi R^2 k$, mass ρL, dashpot constant $-\nu D \rho L$, and an external force Δp.

Figure H-3 Mass-spring equivalent model

If a bubble occurs in the tube, the system may be modeled as two masses, two springs and two dashpots as shown in Figure H-4.
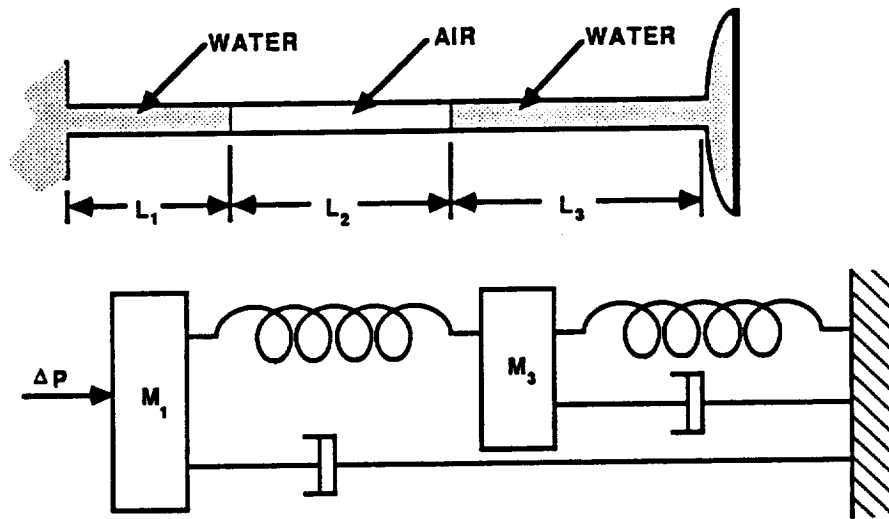
Figure H-4 Mass-spring model with bubble

In this model we assume that the pressure drop across the bubble due to viscous drag at the wall is negligible compared to the drag due to the liquid. We also neglect the surface tension drag of the gas-liquid interface. Both of these assumptions should be good for the anticipated application.

The spring constant of the bubble may be derived as follows:

$$\frac{1}{V_b} \frac{\Delta V_b}{\Delta p_b} = \frac{1}{\gamma p_b} \tag{H-20}$$

The displacement of the left slug of liquid is called x_1 and that of the right slug, x_3. Then, $\Delta V_b = \pi R^2 (x_1 - x_3)$ and the excess pressure in the bubble is:

$$\Delta p_b = \frac{\gamma P_b}{V_b} \pi R_b (x_1 - x_3) \qquad \text{(H-21)}$$

The right slug is displaced by the net pressure Δp and Δp_b while the right slug is driven by Δp_b and Δp_d. The equations analogous to (H-10) are:

$$\rho L_1 x_1 - \eta L_1 D x_1 + \frac{\pi R^2 \gamma P_b}{V_b}(x_1 - x_3) = \frac{L_1}{L_1 + L_3}\Delta p$$

$$\rho L_3 x_3 - \eta L_3 D x_3 + \frac{\pi R^2 \gamma P_b}{V_b}(x_3 - x_3) + \pi R^2 k x_3 = \frac{L_3}{L_1 + L_3}\Delta p \qquad \text{(H-22)}$$

where D and k have the same values as in equation (H-7). This is a 4th degree system and has two resonant frequencies. The system matrices of the system are:

$$A = \begin{bmatrix} 0 & 1 & 0 & \\ \frac{-\pi R^2}{\rho L_3}\left(\frac{\gamma P_b}{V_b} + k\right) & \nu D & \frac{\pi R^2 \gamma P_b}{\rho L_3 V_b} & 0 \\ 0 & 0 & 0 & 1 \\ \frac{\pi R^2 \gamma P_b}{\rho L_1 V_b} & \nu D & \frac{-\pi R^2 \gamma P_3}{\rho L_1 V_b} & 0 \end{bmatrix} \qquad \text{(H-23)}$$

$$B^T = \left[0, \frac{1}{\rho(L_1 + L_3)}, 0, \frac{1}{\rho(L_1 + L_3)}\right]; \qquad C^T = [1,0,0,0]$$

The poles of the system are at the values s = p which satisfy:

$$|sI - A| = 0 \qquad \text{(H-24)}$$

and the resonant frequencies are at $w_r = p/i$.

The model is easily extended to apply when the volume of the diaphragm chamber V_d is comparable to that of the lead-in tube, $\pi R^2 L$. The first term in (H-9) and (H-22b) is the total mass that moves. Replace L and L_3 in this term only by:

$$L' = L + V_d/2\pi R^2 \tag{4-25}$$

and this will increase the total mass to the required value. In the resonant frequency equation (H-12), L is replaced by L'.

Obstructions such as baffles do not change the mass that moves or the equivalent spring. The natural frequency is not changed. But the viscous drag is increased and the decay constant increases.

The model includes the spring constant of the diaphragm but omits the mass, m_d. When m_d is comparable to $2\pi R^2 L\rho$ (an unlikely occurrence) a further extension of the model is required. The equation of vibration of the diaphragm is coupled to the equation of the fluid motion through the driving pressure, Δp_d. The load term of the vibration equation is equated to the pressure term Δp_d of the fluid motion equation. For the diaphragm displacement w:

$$\rho_d h \frac{\partial^2 w}{\partial t^2} + D \, \nabla_2^2 \, \nabla_2^2 \, w = \Delta p_d(t) \tag{H-26}$$

where ρ_d is the density and h is the thickness of the diaphragm, $D = h^3 E/12(1-\alpha^2)$, E is Young's modulus, and α is the Poisson ratio. For a sinusoidal driving force we must solve:

$$D \, \nabla_2^2 \, \nabla_2^2 \, w - \rho_d h \omega^2 w = \Delta p_d \tag{H-27}$$

with Δp_d an unknown constant. The $w(r,\omega)$ is proportional to Δp_d. Now:

$$\Delta V_d = \int_u^R w \, 2\pi r dr = \int_o^t \int_o^R u \, 2\pi r dr = \pi R^2 \, \bar{x} \tag{H-28}$$

The integration of $w(r,\omega)$ results in $A(\omega)\Delta p_d = \pi R^2\bar{x}$. This shows that the form of equation (H-10) and the results that follow are modified only in that k is replaced by $A(\omega)$. The analysis used to derive equation (H-9) assumes zero frequency in evaluating the spring constant. For a plate, the spring constant is dependent on the frequency. Equation (H-27) can be reduced to a pair of Bessel equations and is not difficult to solve, if the need arises.

The following data was supplied by the vendor for the pressure transducer presently used for the breadboard apparatus:

V_d = 1.934 cc ΔV_d at 1000 torr = 0.27 cc

R_d = 2.559 cm   R = 0.3175 cm   L = 19.36 cm

When these values are inserted into equation (H-11) the natural frequency is predicted to be about 40 Hz when the gauge is immersed in water. The gauge should read about 4 percent high at the highest standard test frequency when the lead-in tube is full of water. For air, the natural frequency is more than 1 kHz.

The usual way to evaluate the correctness of a model for compression gauging is to fill the tank to a known volume V; measure p, Δp and ΔV; use the gauging formula,

$$V = \kappa\rho\,\Delta V/\Delta\rho \tag{H-29}$$

to calculate κ; correct κ for the acoustic boundary layer and find the inferred value of the ratio of specific heats, γ. Then, γ should be constant.

A set of data was taken with the pressure transducer first dry (filled with air) and then wet (immersed in water). The dry data show a variation of γ from 1.373 to 1.400 or about 0.7 percent over the frequency range 0.6 to 9 Hz with no discernible slope with frequency. The wet set varied over a range of about 5 percent with a definite slope toward higher frequencies. When the data are corrected using equation (H-1) with f_n = 40 Hz and the boundary layer correction is made after the resonance correction, the following values of γ result:

f (Hz)	γ
.6	1.3726
1.0	1.3725
2.0	1.3736
3.0	1.3757
4.0	1.3729
5.0	1.3753
6.0	1.3728
7.0	1.3704
8.0	1.3772
9.0	1.3769

that is, a range of 0.4 percent and random. The model therefore seems to fit the experimental data well.

For future applications equation (H-11) indicates that the lead-in tube should be as short as possible and the radius increased to that of the diaphragm. In the limit of a pressure diaphragm set in the side of the tank, the change in the frequency when it is dry vs. wet may be found as follows. The diaphragm displacement, w, is given by equation (H-26). The impedance of a radiating piston at low frequencies (wavelength long compared to the radius of the diaphragm) is $\Delta p = -i(16/6\pi)\rho_f \omega a\, dw/dt$ where ρ_f is the density of the fluid, and a is the radius of the diaphragm. When Δp_d in (H-26) is replaced by the radiation impedance and a sinusoidal driving force is assumed, (H-27) becomes:

$$D\, \nabla_2^2\, \nabla_2^2\, w - [\rho_d h + (16/6\pi)\, a\rho_f]\, \omega^2 w = 0 \tag{H-30}$$

When $\rho_f = 0$ the transducer is dry. The ratio of wet to dry resonant frequency is:

$$\frac{\omega_{wet}}{\omega_{dry}} = \left[1 + \frac{16 a\rho_f}{6\pi h \rho_d} \right]^{1/2} \tag{H-31}$$

Now, $\rho_f/\rho_d \simeq O(10^{-1})$ while $a/h \simeq O(10^3)$ so the reduction is of order 10. For the present commercial design with a long, narrow lead-in tube, the reduction is about 100.

It is therefore possible to avoid the problem of the resonance of the pressure transducer by proper design.

Appendix I

EFFECTS
of
TANK LEAKAGE

Appendix I

EFFECTS OF TANK LEAKAGE

The test data on compression gauging can be affected significantly by leakage of the tank. An on-orbit tank will not leak enough to confuse the analysis of the data, but bread-board test facilities are designed for rapid reconfiguration. These tanks may have leak rates that are appreciable. It is important to know how a leak modifies the data so that unexpected trends may be diagnosed.

The displacement of the compressor ΔV results in: compression of the ullage, ΔV_b; compression of the tank, ΔV_t and leakage ΔV_1. They are related as:

$$\frac{dV}{dt} = -\frac{dV_b}{dt} + \frac{dV_1}{dt} + \frac{dV_t}{dt}$$ (I-1)

Here, an inward motion of the piston is positive and an outward leak is positive. The correction for tank expansion has been calculated elsewhere. It is a small additive correction and will be ommitted here to simplify the analysis.

The compressor is moved sinusoidally and all variables have a time dependence of $\exp(i\omega t)$. Thus, equation (I-1) is a relation between the phasor of the variables.

$$\Delta V_o = -\Delta V_{bo} + Q_o/i\omega$$ (I-2)

Where Q is the flow rate in the leak. If we divide (I-2) by V_b and the phasor for pressure, Δp_o:

$$\frac{\Delta V_o}{V_b \Delta p_o} = \frac{-\Delta V_{bo}}{V_b \Delta p_o} + \frac{Q}{i \omega V_b \Delta p_o}$$ (I-3)

or, since the compressibility of an ideal gas is γp,

$$V_b = \gamma p \left[\frac{\Delta V_o}{\Delta p_o} - \frac{Q}{i \omega \Delta p_o} \right]$$ (I-4)

Next, we have to find $Q/\Delta p_o$ for the flow in a leak which is driven sinusoidally. The equation to be solved is:

$$i \, \omega \, u = \nu \, \nabla^2 u - \frac{1}{\rho_s} \frac{dp}{dx} \qquad (I-5)$$

where ν is the kinematic viscosity and the pressure gradient is in the flow direction. Actually, we only need the average value of u, $\bar{u}$. Since $Q = \bar{u} \, \bar{A}$ with $\bar{A}$ the average cross section of the leak. Without knowledge of the shape and dimensions of the leak, we cannot complete the analysis. However, a general characteristic of solutions of (I-5) is that:

$$Q/\Delta p = \frac{C(\omega,\nu)}{\rho L} \qquad (I-6)$$

where C is a complex constant that depends on the shape of the slit, the frequency, and the kinematic viscosity; and L is the length of the leak.

For a circular hole of radius R:

$$\frac{Q}{\Delta p} = \frac{i}{\omega\rho L} \left[1 - \frac{J_1(aR)}{a \, R \, J_o(aR)} \right] = \frac{C(\omega,\nu)}{\rho L} \qquad (I-7)$$

with

$$a = (-i \, \omega/\nu)^{1/2}$$

then,

$$V_b = \gamma p \left[\frac{\Delta V_o}{\Delta p} - \frac{C(\omega,\nu)}{i \, \omega \, \rho L} \right] \qquad (I-8)$$

The size of a leak can be estimated by increasing the pressure in a tank and recording the pressure decrease with time. In this case $\omega = 0$ and:

$$Q/\Delta p = \frac{C(0,\nu)}{\rho \, L} = \frac{B(0,\eta)}{L} = \frac{B}{L} \qquad (I-9)$$

where η is the viscosity. Then,

$$dQ = \frac{B}{L} \; d\Delta p \qquad\qquad (I\text{-}10)$$

and

$$\frac{d\rho}{dt} = - \frac{\rho Q}{V_o}$$

where ρ is the density of the bubble in the tank. For an ideal gas:

$$p = a \, \rho^\gamma = p_o + \Delta p; \qquad d\Delta p = a\gamma\rho^{\gamma-1}dp$$

$$\frac{d\Delta p}{dt} = \frac{a \, \gamma \, p^\gamma}{V_b} \frac{B}{L} \Delta p = \frac{\gamma \, p \, B}{V_b L} \Delta p \qquad\qquad (I\text{-}11)$$

$$\Delta p = \Delta p_o \, \exp \; -\left[\frac{\gamma p B}{L V_o}\right] t$$

Here, we assumed $p_o \gg \Delta p$ and $V_o \gg \int Q \, dt$, thus, the excess pressure decays exponentially. This equation can be used to find $C(\omega=0, \eta)$. However, (I-8) requires C evaluated at the compressor frequency. The decay rate can be used to compare leak rates, but not to correct the gauging formula.

Appendix J

EFFECTS

of

LARGE SURFACE TENSION

Appendix J
EFFECT OF LARGE SURFACE TENSION

Surface tension has two effects on compression gauging. First, the pressure inside a bubble, p_g, differs from that in the liquid, p_1, by:

$$p_g = p_1 + \frac{2\sigma}{R} \equiv p_1 (1 + \gamma) \qquad (J-1)$$

where σ is the surface tension and R is the radius of the bubble.

The second effect occurs when a bubble touches a solid surface. In that case the surface tension produces damping and a phase shift of the pressure signal as the three-phase interface line slides along the solid surface. Both of these effects are very small for all the liquids which are candidates for gaging.

The interest here is in ground simulation of a low-g bubble configuration. One way to simulate this situation is with balloons anchored to the bottom of the tank. Balloons have a surface tension several orders of magnitude larger than that for water. For this application only the first effect mentioned above is important. The purpose of this analysis is to show how surface tension modifies the measuring formula.

As the compressor changes the volume of bubbles by ΔV, the radius of the bubble and the pressure in both the gas and liquid vary. From equation (J-1):

$$\Delta p_g = \Delta p_1 - \frac{2\sigma \Delta R}{R_o^2} \qquad (J-2)$$

The gas in the bubble is nearly ideal and the compression is nearly adiabatic. Thus,

$$p_g V^\gamma = p_{go} V_o^\gamma = p_g (4\pi/3)^\gamma R^{3\gamma} = p_{go} (4\pi/3)^\gamma R_o^{3\gamma} \qquad (J-3)$$

$$\left(\frac{R}{R_o}\right)^{3\gamma} = \frac{p_{go}}{p_g}$$

Taking the derivative of (J-3):

$$\frac{\Delta R}{R_o} = - \frac{1}{3\gamma} \frac{\Delta p_g}{p_{go}} \tag{J-4}$$

and (J-2) becomes:

$$\Delta p_1 = \Delta p_g \left[1 - \frac{2\sigma}{3\gamma R_o p_{go}} \right] \equiv \Delta p_g (1 - x) \tag{J-5}$$

or:

$$\Delta p_g = \frac{\Delta p_1}{1 - \frac{2\sigma}{3\gamma \, R_o p_{1o}(1+\gamma)}} \equiv \frac{\Delta p_1}{1 - \frac{z}{1+\gamma}} \tag{J-6}$$

The measuring formula for gaging is:

$$V = \frac{-\Delta V}{\Delta p_g} \gamma p_{go} \tag{J-7}$$

If the mean pressure and the pressure variation are measured inside the bubble, surface tension does not modify the measuring formula. When the pressure transducer is in the liquid or in the gas outside the balloon, p_{go} and Δp_g must be replaced by p_{1o} and Δp_1 using formulas (J-1) and (J-6). Throughout:

$$x = \frac{2\sigma}{3\gamma R_o p_{go}}; \quad y = \frac{2\sigma}{R_o p_{1o}}; \quad z = \frac{2\sigma}{3\gamma R_o p_{1o}} \tag{J-8}$$

Then:

$$V = \frac{-\Delta V \, \gamma \, p_{go}(1+y) \left(1 - \frac{z}{1+y}\right)}{\Delta p_1} \approx \frac{-\Delta V \, \gamma p_{1o}}{\Delta p_1} (1+y-z) \tag{J-9}$$

This equation shows how the primary measuring formula (J-7) is modified by high values of σ when the pressures are measured in the liquid. The correction is a multiplicative factor. Most of the other secondary effects cause corrections which are also multiplicative factors. The most general formula for V is a product of all the correction factors.

Formula (J-9) may be used to find V when balloons are not used. However, the correction factor is so small in that case that it may be neglected. This shows that it is not necessary to know when the pressure transducers are exposed to bubbles or liquids.

Appendix K

GAGING HYDROGEN USING COMPRESSION

Appendix K

GAGING HYDROGEN USING COMPRESSION

The compression method of gaging has proven to be highly accurate for ordinary fluids at room temperature. The purpose of this analysis is to estimate the accuracy and predict the problems involved when measuring cryogens. Hydrogen is chosen as a test case since it is likely to be the most difficult of the commonly used cryogens to gage.

The measurement formula for the volume of the ullage V_b, when corrected for the compressibility of the tank, the compressibility of the liquid and the acoustic boundary layer, can be written as:

$$V_b = \frac{\left[\dfrac{\Delta V_c}{\Delta p} - \alpha - \dfrac{V_t}{\rho_1 c_1^2} \right]}{\left[1 + \dfrac{C}{\sqrt{f}} - \dfrac{\gamma p}{\rho_1 c_1^2} \right]} \qquad\qquad (K-1)$$

The symbols used here are:

γ Ratio of specific heats of the gas.

p   Mean operating pressure in the tank.

ΔV_c Volume displacement of the compressor.

Δp Measured pressure variation in the tank.

V_t Total volume of the tank.

α/V_t Compressibility of the tank.

ρ_1 Average density of the liquid.

c_1 Average speed of sound in the liquid.

f   Frequency of the compressor.

C   A constant, determined by measurements at 2 frequencies.

The only other significant correction to V_b for a cryogen is an implicit dependence of all the variables in formula (K-1) on the temperature.

The mass of the liquid M is related to V_b as:

$$M = \rho_1 (V_t - V_b) + \rho_g V_b \qquad\qquad (K-2)$$

where ρ_g is the density of the gas. For all practical applications the term in ρ_g can be neglected.

The accuracy of the method can be determined by combining the errors for all the items in equations (K-1) and (K-2). The large term in equation (K-1) is:

$$V_b = \gamma p \, \Delta V_c / \Delta p \qquad (K-3)$$

The other terms are corrections and contribute less than 10 percent to V_b. Consequently, it is not necessary to know the corrections very accurately. In equation (K-2) the term in ρ_g is a small term.

For ordinary liquids at room temperature an accuracy for M of better than 1 percent has been achieved. The accuracy for hydrogen should be of the same order of magnitude unless the error in some of the variables in equations (K-1) and (K-2) increase significantly because of the properties of the cryogen.

A comparative analysis of all the terms in equations (K-1) and (K-2) between water and hydrogen shows that there are two effects that may lead to larger error bars for hydrogen. First, the liquid compressibility of hydrogen is much larger and second, the properties of hydrogen vary more rapidly with temperature.

Equation (K-1) has a factor which is the addition of three compressibilities: that of the gas ullage, the tank, and the liquid. The correction for the compressibility of the liquid is part of the formula. If all quantities occurring in this term are known without error, the larger compressibility does not introduce an error. However, when the error in V_b is calculated, it is seen that if the liquid compressibility becomes comparable to that of the bubble, the error in V_b can be dominated by the error in the liquid compressibility. The three compressibilities are compared in Table K-1 for three storage temperatures.

Table K-1
COMPRESSIBILITIES OF THE GAS, LIQUID AND TANK

T	P	GAS	LIQUID	TANK
13.9 K	0.05 atmos	100×10^{-2}/psi	0.77×10^{-4}/psi	1×10^{-4}/psi
22.8	2.0	4.2×10^{-2}	1.9×10^{-4}	1×10^{-4}
27.2	4.0	2.1×10^{-2}	4.2×10^{-4}	1×10^{-4}

The compressibility of the tank is estimated from a standard design of a cryogenic space storage tank. The liquid compressibility is only 2 percent that of the gas in the worst case. This means that an error in the liquid compressibility of 10 percent will contribute only a 0.2 percent error to V_b. Since the compressibility of liquid hydrogen is known to within 1 percent, this effect is not an issue.

We may encounter significant thermal stratification in hydrogen during long periods of storage. The factors in equation (K-1) and (K-2) which depend on temperature and are not measured directly are: γ, ρ_1, c_1^2 and V_t. Since the liquid compressibility produces a correction of 0.5 percent in V_b at the most likely storage pressure and is a function mainly of pressure, a temperature variation of 5 K will lead to a negligible error in V_b.

The remaining variables which depend on temperature are γ in equation (K-1) and ρ_1 in equation (K-2). For a liquid which is stored at saturation, as most cryogens are, the bubble interface must be on the saturation line. Since the pressure in the tank in space is uniform, even when the temperature of the liquid is stratified, the temperature at the bubble surface is known because the pressure p is measured. The bubble is surrounded by an isothermal surface and is unlikely to have a large thermal stratification. The value of γ along a constant pressure line is constant to about 0.1 percent for a temperature variation of 5 K. See Table K-2. If the pressure in the tank is controlled by venting, the variation of γ with temperature is negligible.

If the pressure is allowed to drift, γ should be corrected to the saturation value according to the data in Table K-3.

Table K-2
γ OF HYDROGEN GAS AT 0.1 ATMOS.

T(K)	γ
20	1.667
30	1.667
40	1.666

Table K-3
γ OF HYDROGEN GAS ALONG THE SATURATION LINE

T (K)	γ	T (K)	γ
13.9	1.695	22.8	2.031
16.1	1.731	25.0	2.276
18.3	1.790	27.2	2.730
20.6	1.883		

The largest source of error for the gaging of hydrogen is the variation of ρ_1 with temperature. ρ_1 occurs in equation (K-2). The density of liquid hydrogen is shown in Table K-4.

Table K-4
DENSITY OF LIQUID HYDROGEN

T (K)	ρ_1(g/cc)	T (K)	ρ_1(g/cc)
13.9	0.0769	22.8	0.0676
16.1	0.0749	25.0	0.0644
18.3	0.0728	27.2	0.0605
20.6	0.0704		

The change of density with temperature is about -1.5 percent per degree. At present it is not known how much thermal stratification will occur in a storage tank with estimated 10^{-3} g random background acceleration.

This analysis indicates that the volume of the ullage of hydrogen can be found with about the same accuracy as water--better than 1 percent. The major difficulty is converting the volume to mass when strong thermal stratification exists. If it is necessary to know the mass, an array of thermometers can be used to determine a volume averaged temperature of the liquid.